Electrical Transport, Filtering and NMR of GaAs/AlGaAs Quantum Wires

Bram Evert

November 7, 2013

Contents

1 Introduction **7**

2 Motivation and Theory **12**

2.1 Landauer-Büttiker formalism 12

2.2 Luttinger liquids 18

2.3 Nuclear Spin-ordering 22

2.4 Resistively Detected NMR 24

2.4.1 Theory 24

2.4.2 Resistively Detected NMR (RDNMR) 31

2.5 Possible Applications 33

2.5.1 Majorana fermions

33

2.5.2 Topological Quantum Computation 34

3 Methodology **46**

3.1 Samples 46

3.1.1 GaAs Heterostructures and Quantum Wells 46

3.1.2 Device Structure 50

3.1.3 Parameters 53

3.2 Description of Fridges 54

3.2.1 VTI 54

3.2.2 Helium-3 Cryostat 57

3.2.3 Dilution Refrigerator 59

3.3 Electronic Transport Measurements 61

3.3.1 Theory of electronic transport measurement 61

3.3.2 Measurement Circuit 63
3.4 Cold Filter design and fabrication 66
3.4.1 Π filters 67
3.4.2 RC Filters 73
3.4.3 PCB Sample Holders 75

4 Results **85**
4.1 Characterization of filters 88
4.2 Quantization of Conductance 96
4.3 Resistively-detected NMR 101

5 Conclusion **110**
5.1 Future Work 110

Acknowledgements

I would like to thank the many people whose efforts have made this work possible. First those who I have shared the lab with who generously donated their time and expertise to teach the techniques or low temperature physics. In particular I would like to thank Phd candidates Benjamin Schmidt and Michel Savard, who were always available and willing to teach or help me with experiments. Their knowledge and guidance has been instrumental to this work.

Significant gratitude goes to Dr. Keyan Bennaceur, who has guided my project and make extraordinary efforts to assist with experiments. He has been a invaluable presence in the lab for his vast knowledge of experiments, but also for his universally optimistic outlook and powers of motivation. I also extend thanks to the many other students who have shared the lab with me, especially Sam Neale who has been a good friend on a similar path and our various summer students.

The operation of our lab is made possible by the staff members of the department who provide their formidable technical skills to meet our bizarre and demanding requirements for experiments. Richard Talbot, who seems to have a solution to every problem has provided incredible support and Pascal Bourseguin, who has constructed so many parts and taken the time to provide excellent training to a novice machinist. John Smeros has been of great help, managing our ever shifting helium requirements with grace.

Finally, I would like to thank my Dr. Guillaume Gervais, my supervisor for his incredible ability and tireless efforts in running this lab. How he is able to juggle the requirements of securing funding, teaching, presenting our findings and still managing to provide superb guidance to students is beyond me. He has given me the freedom and support to pursue my projects within his lab and introduced me to the methods of scientific research. I thank him for giving me the amazing opportunity to work in his lab, and for his efforts in seeing my Master's to completion. The lessons learned under his supervision and the example he sets will be of great value in my future endeavors.

Abstract

The study of electrons in low dimensions is a field which has yielded incredible insights in the past decades from the Fractional Quantum Hall Effect to Wigner Crystallization. In recent years, interest has grown from studying the fundamental physics of two dimensional conductors to engineering experimental new states using nanotechnology techniques. We now have the capability to create high quality one and zero dimensional devices, that is, quantum wires and quantum dots. At very low temperatures, quantum physics dominates the behavior of these devices causing new properties to emerge, due to enhanced electron-electron interactions, spin-orbit interactions and many other effects. These new properties are the result of the interaction of ensembles of quantum particles and cannot be understood by classical intuition. Not only are there exciting new physics to be discovered at low dimensions, but there are promising applications on the horizon.

Electrons constrained to one dimension are predicted to enter a state known as the Luttinger liquid. While there exists strong evidence for the observation of the Luttinger liquid already, it is still an area of highly active study. Furthermore, it has been predicted that interactions between helically ordered nuclear spins in GaAs and a Luttinger liquid state could results in a nuclear spin feedback effect which would result in distinct experimental observations. Not only would this state provide clear evidence of Luttinger liquid behavior, but it has potential to support sought-after Majorana fermions which have applications in quantum information processing.

This project consisted of the fabrication of GaAs/AlGaAs quantum wires samples in collaboration with Sandia National Laboratories with varying parameters such as length and well-depth. We then performed detailed electronic transport measurements at low temperature to identify promising quantum wire samples. Good samples were cooled further to 300 mK where some quantization of conductance was observed. It was determined that to reach lower electronic temperatures, filtering was required. To this end, low temperature filtered samples holders were designed, constructed and characterized. The filtered sample holders resulted in superior observations to unfiltered samples, likely reflecting a lower electron temperature. Using our best sample with filters, we then performed resistively-detected nuclear magnetic resonance experiments, probing the interaction between the electrons and the nuclear spins in quantum wires. While the predicted state was not observed, the groundwork for such an experiment is complete and its expected that a sufficiently high quality sample will display the signature behavior with current methodology.

Abrégé

L'étude des électrons dans de faibles dimensions est un domaine qui a donné un aperçu incroyable dans les dernières décennies du Effet Hall quantique fractionnaire de Wigner cristallisation . Au cours des dernières années, l'intérêt s'est développé à partir de l'étude de la physique fondamentale des deux conducteurs dimensions à l'ingénierie expérimentale nouveaux Etats à l'aide de techniques de la nanotechnologie . Nous avons maintenant la possibilité de créer de haute qualité et un zéro dispositifs dimensions , c'est- fils quantiques et boîtes quantiques . A des températures très basses , la physique quantique domine le comportement de ces dispositifs provoquant de nouvelles propriétés émergent , en raison des interactions entre électrons améliorées , les interactions spin-orbite et de nombreux autres effets. Ces nouvelles propriétés sont le résultat de l'interaction des ensembles de particules quantiques et ne peuvent être compris par intuition classique. Non seulement la nouvelle physique y passionnants à découvrir à basse dimensions , mais il ya des applications prometteuses à l'horizon.

Les électrons contraints à une dimension sont prévus pour entrer dans un état connu comme le liquide de Luttinger . Bien qu'il existe des preuves solides pour l'observation du liquide de Luttinger déjà , il est encore un domaine d'étude très active. En outre, il a été prévu que les interactions entre les spins nucléaires hélice commandés en GaAs et un état liquide de Luttinger pourraient se traduit par un effet de rétroaction des spins nucléaires qui se traduiraient par des observations expérimentales distinctes. Non seulement cet état de fournir des preuves claires de comportement de type liquide de Luttinger , mais il a le potentiel pour soutenir convoités fermions de Majorana qui ont des applications dans le traitement de l'information quantique .

Ce projet consistait en la fabrication de GaAs / AlGaAs quantum fils échantillons en collaboration avec Sandia National Laboratories avec des paramètres tels que la longueur et le bien- profondeur variable. Nous avons ensuite effectué des mesures détaillées de transport électronique à basse température pour identifier les échantillons de fils quantiques prometteurs. Bonne échantillons ont été refroidis à la suite de 300 mK où on a observé une certaine quantification de la conductance . Il a été déterminé que, pour atteindre des températures inférieures électroniques , le filtrage est nécessaire. À cette fin , à basse température filtrées porte-échantillons ont été conçus, construits et caractérisé. Les porte-échantillons filtrés ont donné lieu à des observations supérieures aux échantillons non filtrés , ce qui reflète probablement une température d'électrons inférieure. Grâce à

notre meilleur échantillon de filtres , puis nous avons effectué des expériences de résonance magnétique nucléaire résistivement - détectés , sonder l'interaction entre les électrons et les spins nucléaires dans les fils quantiques. Alors que l'état prédit n'a pas été observée , les bases d' une telle expérience est complète et sa s'attend à ce qu'un échantillon suffisamment haute qualité affichera le comportement de signature avec la méthodologie actuelle .

Chapter 1

Introduction

In 1959, Richard Feynman gave his famous lecture "There's Plenty of Room at the Bottom", a remarkably clairvoyant talk which encouraged scientists to explore the science of the very small[1]. This lecture is considered a seminal event in the history of nanotechnology. With the realization in the 1960s that very small circuits could be fabricated in Silicon, a 40 year project of relentless progress in semiconductor technology began. Since the 1960s, feature sizes have decreased from the millimeter scale to the state-of-the-art 14nm process used by Intel. However the set of tools developed for the semiconductor industry has proven adaptable and useful to a great many fields, including physics. While physics is highly intertwined with the design of micro-electronics, nanotechnology has opened the door to studying more exotic phenomena as well. One avenue of research now accessible thanks to advanced fabrication technologies is the study of lower dimensional systems; that is, systems in which the electrons are effectively reduced to two, one or zero dimensions.

Lower dimensional physics are essentially the result of a single consideration —length scale. In the classical theories of conductivity there is an assumption that the dimensions of the conductor are much larger than three key length scales: the electron *wavelength* (λ), the *Mean free path* (L_m) and the *Phase-relaxation length* (L_φ). These assumptions allow for many averages and approximations, however as the dimensions of the conductor approach these scales, the approximations break down and we must consider new effects. With the decrease in size and density, and the increase in characteristic lengths, quantum mechanics will play an important role in determining the energy levels of the electrons and electron-electron interactions are greatly enhanced. With some very interesting theoretical predictions to test, scientists began to pursue the study of lower dimensional electron sys-

tems, leading to a number of major discoveries such as the Quantum Hall Effect (QHE)[2] and Fractional Quantum Hall Effect (FQHE)[3], Wigner Crystallization[4] and Radiation-induced magneto-resistance oscillations[5]. What made possible these notable discoveries was the use of two dimensional electron gases, and in particular the use of GaAs/AlGaAs heterostructures. The devices used in these experiments reduced the dimensions of the conductor, but they also increased mobility and decreased the density, allowing for longer characteristic lengths. The study of two-dimensional electron systems in itself is a fascinating topic; however it was quickly realized that heterostructures which could create such perfect systems of electrons in a quantum state could also be used to make quantum devices. Such devices are made by patterning electrical gates on the surface of the 2-Dimensional Electron Gas (2DEG) and applying a potential which depletes the electrons below. This technique has allowed for the creation of many interesting devices which often involve reducing the number of dimensions from two to one dimension (quantum wire) or zero dimensions (quantum dot). While many interesting quantum devices have been created, this thesis is on the study of a one-dimensional system —quantum wires.

The history of one dimensional devices begins with successful fabrication and characterization of quantum point contacts, devices which create a point-like constriction in a two-dimensional conductor. These were simultaneously discovered in 1988 by Wees *et al[6]* and Wharam *et al[7].* The devices showed the unique behavior of reducing conduction to a single quantum electron channel. A flurry of activity followed, with many groups duplicating the effort and studying the behavior of the quantum point contacts, varying length, temperature, magnetic field and sample parameters. While some observations still require theoretical explanation, such as the so-called 0.7 feature, study on quantum point contacts has not been on the forefront in recent years. Rather, they are typically used as components in more complex devices, such as qubits made from quantum dots.

That said, there is still possible new physics lurking in one-dimensional conductors. While two and three-dimensional conductors are well explained by Fermi Liquid theory, condensed matter theory predicts the electron will be in a Luttinger liquid State, which has the unique effect of spin-charge separation. At the moment, there is good evidence of Luttinger liquid behavior, and it remains a highly active area of study. Recently, the possibility of creating quasiparticles which are Majorana fermions in one-dimensional systems has attracted much interest. Such a device would require a one-dimensional, spin-polarized conductor in close proximity to a superconductor and could have applications in a type of fault-tolerant quantum information processing known as non-abelian quantum computa-

tion. Much of the work in this thesis is in the direction of creating Majorana fermions using a system of GaAs quantum wires where a theorized nuclear-spin interaction could create a one-dimensional state which could be a ripe hunting ground for Majorana's. While creating such a device is outside the scope of this work, and it remains unknown if the spin-orbit interaction is strong enough, it's hoped that it could be achieved in following experiments.

The outline of this thesis is as followed. First brief overviews of relevant physical theories will be given along with a discussion of the experimental results that accompany them. Chapter 3 will consist of a in depth discussion of the methodology of the experiments. It's hoped that this thesis will provide all the information needed to replicate and extend this work as well as related endeavors. The challenges encountered in measurements will also be discussed with suggested improvements and solutions. Lastly, chapter 4 will present the results of experiments, in particular the results of a resistively detected nuclear magnetic resonance experiment.

References

[1] RP Feynman. "There's plenty of room at the bottom". In: *Engineering and Science* (1960). URL: http://calteches.library.caltech.edu/1976/1/1960Bottom.pdf.

[2] K Klitzing, G Dorda, and M Pepper. "New method for high-accuracy determination of the fine-structure constant based on quantized Hall resistance". In: *Physical Review Letters* (1980), pp. 11–14. URL: http://link.aps.org/doi/10.1103/PhysRevLett.45.494.

[3] D.C. Tsui, H.L. Stormer, and A.C. Gossard. "Two-Dimensional Magnetotransport in the Extreme Quantum Limit". In: *Physical Review Letters* 48.22 (1982), pp. 1559–1562. URL: http://onlinelibrary.wiley.com/doi/10.1002/cbdv.200490137/abstracthttp://link.aps.org/doi/10.1103/PhysRevLett.48.1559.

[4] VJ Goldman, M Santos, M Shayegan, and JE Cunningham. "Evidence for two-dimentional quantum Wigner crystal". In: *Physical review letters* 65.17 (1990), pp. 2189–2192. URL: http://link.aps.org/doi/10.1103/PhysRevLett.65.2189.

[5] Adam C. Durst, Subir Sachdev, N. Read, and S.M. Girvin. "Radiation-induced magnetoresistance oscillations in a 2D electron gas". In: *Physica E: Low-dimensional Systems and Nanostructures* 20.1-2 (Dec. 2003), pp. 117–122. ISSN: 13869477. DOI: 10.1016/j.physe.2003.09.028. URL: http://linkinghub.elsevier.com/retrieve/pii/S1386947703005083.

[6] BJ Van Wees, H Van Houten, CWJ Beenakker, JG Williamson, LP Kouwenhoven, D Van der Marel, and CT Foxon. "Quantized conductance of point contacts in a two-dimensional electron gas". In: *Physical Review Letters* 60.9 (1988), pp. 848–850. URL: http://link.aps.org/doi/10.1103/PhysRevLett.60.848.

[7] DA Wharam and TJ Thornton. "One-dimensional transport and the quantisation of the ballistic resistance". In: *Journal of Physics C: ...* 209 (1988). URL: http://iopscience.iop.org/0022-3719/21/8/002.

Chapter 2

Motivation and Theory

2.1 Landauer-Büttiker formalism

For the vast majority of electrical conductors encountered in day-to-day life, the classical theory of conduction serves us very well. The typical picture of a conducting electron is a particle which is accelerated by the electric field until it collides with an defect and is deflected in a random direction, similar to the theory of gases. This is a useful picture for most conductors, but it relies on some basic assumptions of length scales. But what happens when the mean free path is on a similar scale to the size of the conductor? Does this imply that the resistance is zero? This situation requires an new, more subtle theory of conduction.

The Landauer-Büttiker formalism is a theory of conductance which, unlike other theories of conductance, considers current based transmission probabilities. This approach is particularly useful for mesoscopic conductors because it deals well with ballistic conduction, in which the source of resistance is more exotic phenomena than random collisions. In the framework of the Landauer-Büttiker formalism, the question of a conductor's behavior when the mean free path is long becomes, what happens when the transmission probability is close to unity? As we will see, this is a far more useful way to look at the problem.

In the case of a ballistic conductor, the only source of resistance is the contact resistance. In the electrical contact the current is carried by infinitely many transverse modes, however in the semiconductor only a few modes carry the current, thus requiring a redistribution of the current. We assume that contacts in this case are reflectionless, meaning that transmission is near perfect for electrons coming into the contact (as it is no trouble to enter

the conductor with infinite k-states), however for electrons leaving the contact transmission is rather low. Thus all the resistance will occur from entering the conductor. This brings us the theoretical model of a Quantum Point Contact (QPC), which can be considered a perfect, narrow conductor with contacts on either side. Inside this narrow conductor, there will be sub-bands, each with its own dispersion relation, $E(N,k)$, where E is the energy, N is the band number and k is the momentum. Each band has a minimum allowable energy $\varepsilon_N = E(N, k = 0)$, as shown in figure 2.1.1.

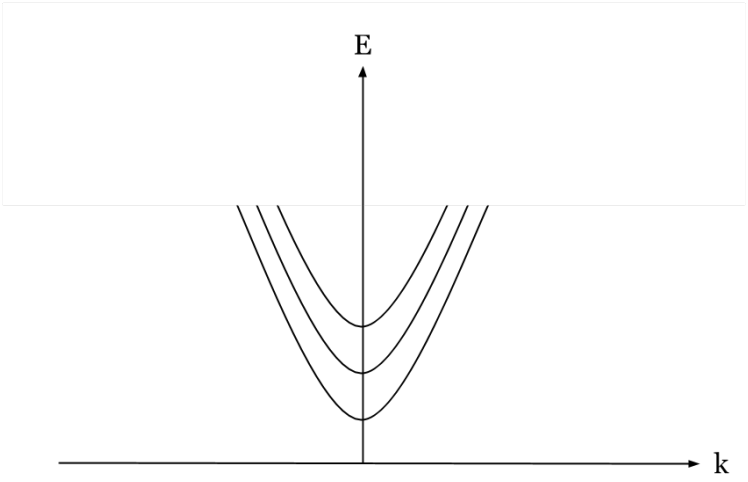

Figure 2.1.1: Dispersion relation of transverse modes in a narrow conductor

We count the number of conducting modes at energy E by counting those modes with cut-off energies which are lower than E using,

$$M(E) = \sum_N \vartheta(E - \varepsilon_N) \tag{2.1.1}$$

where $M(E)$ is the number of conducting modes lower than E and ϑ is the Heaviside function. Knowing the number of transverse modes, we can then determine the current in each one and add them up to find the total. In one dimension the current of a single mode is given by the adding up all the electrons over their k-states, multiplying by velocity, given by $\frac{1}{\hbar}\frac{\partial E}{\partial k}$, and dividing by length, L.

$$I^+ = \frac{e}{L}\sum_k v f^+(E) = \frac{e}{L}\sum_k \frac{1}{\hbar}\frac{\partial E}{\partial k} f^+(E). \tag{2.1.2}$$

If we make the assume a large number of particles and apply periodic boundary conditions we can convert the sum to an integral and arrive at the following expression. Additionally we have multiplied by 2 to account for spin,

$$I^+ = \frac{2e}{h}\int_{\varepsilon}^{\infty} f^+(E)dE. \tag{2.1.3}$$

This result is simply to extend to multiple modes by using the function $M(E)$ which tells us how many modes are above the cut-off energy but lower than E.

$$I^+ = \frac{2e}{h}\int_{-\infty}^{\infty} f^+(E)M(E)dE. \tag{2.1.4}$$

From this formula we get a general result: each mode carries $\frac{2|e|}{h}$ current per unit energy. If we assume the number of modes is constant over the range of the applied potential, represented by $\mu_1 - \mu_2$, then,

$$I = \frac{2e^2}{h}M\frac{(\mu_1 - \mu_2)}{e}] \rightarrow G_C = \frac{2e^2}{h}M, \tag{2.1.5}$$

where G_C is the conductance. This is an important result because it tells us that in a narrow conductor, the conduction actually takes on fixed, quantized values based on the number of allowed modes. In fact, if we assume periodic boundary conditions, the values of the modes, k_y must be spaced by $2\pi/W$, where W is the width of the constriction. We can therefore write the number of modes for a given width.

$$M = Int\left[\frac{k_f W}{\pi}\right] = Int\left[\frac{W}{\lambda_f/2}\right]. \tag{2.1.6}$$

where k_f is the Fermi wavevector and λ_f the Fermi wavelength. For a experimentally realistic system based on a 2DEG, this suggests conductor width on the scale of 100s of nanometers per mode. The above theory is sufficient to explain the conductance of a Quantum Point Contact, however with a bit more work, its possible to derive the Landauer formula, the cardinal formula of the Landauer-Büttiker formalism. To derive the formula, we imagine a conductor with two contacts and two leads as pictured in figure 2.1.2.

As previously mentioned, its assumed the contacts are reflectionless and the electrons can effortlessly exit the conductor. This means the $+k_x$ states in the first lead are occupied only by electrons from the left contact and the $-k_x$ states are occupied by electrons from the right contact, and these electrons will have energies μ_1 and μ_2, respectively. All the

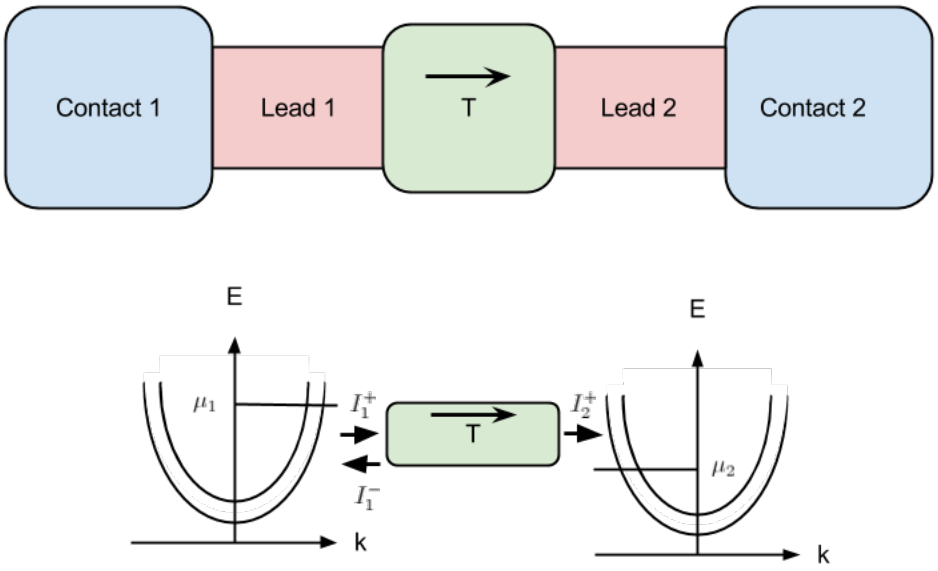

Figure 2.1.2: A Ballistic Conductor with contacts and its transverse modes.

current flow takes place between these two energies. We can then write the three currents fluxes as follows.

The current from the left lead is given by,

$$I_1^+ = (2e/h)M[\mu_1 - \mu_2], \tag{2.1.7}$$

and the current into the right lead is the same, but multiplied by the transmission probability, T,

$$I_2^+ = (2e/h)MT[\mu_1 - \mu_2]. \tag{2.1.8}$$

The current reflected back to the left contact is then,

$$I_1^- = (2e/h)M(1-T)[\mu_1 - \mu_2], \tag{2.1.9}$$

resulting in a net current of,

$$I = I_1^+ - I_1^- = I_2^+ = (2e/h)MT[\mu_1 - \mu_2]. \tag{2.1.10}$$

Finally, we obtain a conductance given by,

$$G = \frac{I}{(\mu_1 - \mu_2)/|e|} = \frac{2e^2}{h}MT, \tag{2.1.11}$$

equation 2.1.11. This is known as the Landauer Formula and is used to describe conductance of several mesoscopic phenomena. Furthermore, it can be simply shown that this equation is consistent with the more familiar Einstein relation shown in equation 2.1.12, where σ is the conductivity, N_S is the density of states and D is the diffusion coefficient,

$$\sigma = e^2 N_s D. \tag{2.1.12}$$

If we replace the conductivity with conductance, the density of states with the transverse modes and the diffusion constant with the transmission probability, the two formulas appear the same.

Experimental results

While the Landauer Formula provides an elegant way to determine the conductance of a ballistic conductor, any theory will ultimately require hard experimental proof. Ballistic transport was first studied by Sharvin[1], but was limited to classical ballistic transport due to the extremely small Fermi wavelength in metals. It was only with the advancements in technology that a quantum system became available to study. The crucial technique was the use of 2-Dimensional Electron Gases (2DEGs). Rather than physically make a narrow contact, split gates are placed above the 2DEG and the point contact is electrostatically defined by depleting the area below the gates as shown in figure 2.1.3.

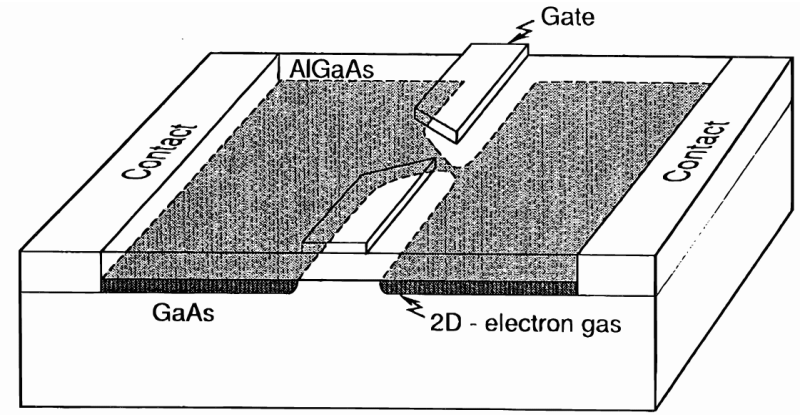

Figure 2.1.3: Quantum Point Contact Structure[2].

Using this method, two groups in 1988 independently managed to fabricate and measure quantum point contacts which displayed the signature effect predicted by the Landauer formula, i.e., the quantization of conductance at values of $\frac{2e^2}{h}$ [3, 4].

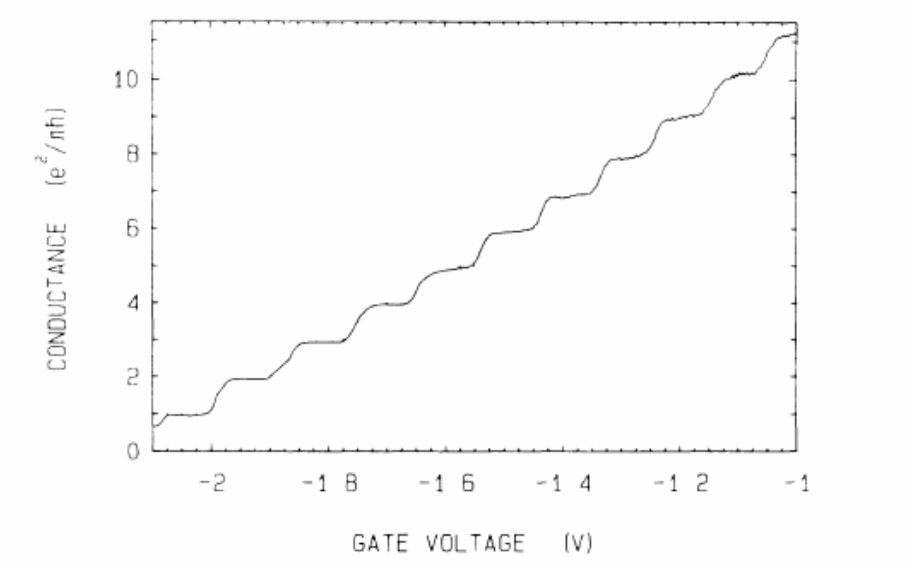

Figure 2.1.4: The conductance of a quantum point contact, showing the signature effect of Landauer theory [3].

When corrected for the ohmic contact resistance it is possible to observe quantization within 1% [3], however the accuracy and shape of the plateaus varies between devices of

the same design, indicating that local fluctuations in the electrostatic environment have significant effects on the conductance. Thus, its thought impossible to reach quantization accuracy comparable to say, the Quantum Hall Effect which is the modern standard of resistance.

Additionally, the QPCs show interesting temperature dependence. The plateaus are best defined at a finite temperature of around 0.5K, rather than at absolute zero. At higher temperatures, thermal averaging broadens the plateaus until it becomes a straight line. Somewhat unexpectedly however, lower temperatures superimpose an oscillatory shape on the plateaus in some devices, probably due to resonances and reflections at the contacts [5].

The length of QPCs has also been shown to have significant effects on their characteristics. At low temperatures and in longer wires, oscillations in conductance near the edge of the plateaus appears, however this has not been observed in all devices. It remains unclear what the exact cause of this phenomenon is [6].

Of more note is the well known '0.7 anomaly', a feature which often appears below the first plateau at roughly 0.7 quantized conductance. The features has been observed to be highly dependent on length and temperature, however achieving consistency between experiments has proven difficult. Theoretical explanations for the 0.7 feature are still a matter of debate and active experiments are ongoing [7, 8, 9, 10].

QPCs have also been studied in magnetic fields. The most dramatic result of the magnetic field is the addition of 0.5 ($2e^2/h$) step in the conductance. This step is the result of the Zeeman interaction lifting the spin degeneracy in the wire [11]. However, it has also been observed that the 0.5 step smoothly transitions to the 0.7 feature as shown in figure 2.1.5.

Additionally a variety of other, possibly related effects have been observed. A 1.7 feature, although not as pronounced as the 0.7 feature has been observed as well as 0.5 and 0.25 feature in some samples. These effects are largely suspected to be spin related however no clear theoretical picture has emerged [11].

2.2 Luttinger liquids

Landauer-Büttiker theory covers the basic conductance of electrons in a single dimension, however, it neglects the effects of interactions. In two and three dimensional systems, taking into account the interactions leads to Landau's Fermi Liquid Theory [12], which

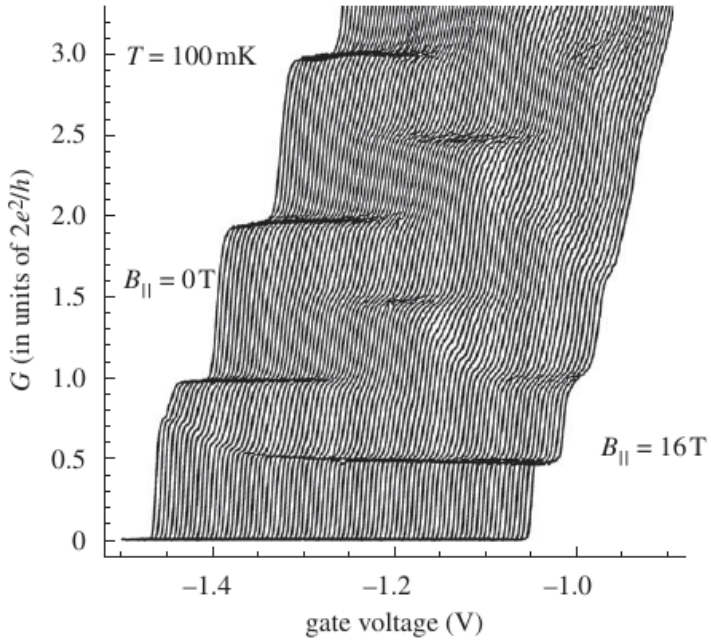

Figure 2.1.5: The 0.7 feature for increasing magnetic field. The feature is seen at $0.7(2e^2/h)$ when the field is at $0T$, but as the field is increased it smoothly transitions to become the 0.5 conductance plateau [11].

produces quasi-particles with similar characteristics to weakly interacting fermions. In one dimension however, the consequences of interactions are much more dramatic. Because, the electrons can only move left or right, a perturbation will significantly affect a large number of electrons. This sort of dependence encourages highly cooperative behavior of electrons in the 1D system. As an illustration, a particle attempting to tunnel into the wire may create a short-wavelength density perturbation, pushing the liquid of interacting electrons away from the incoming particle. To accommodate the particle all the electrons to the left of the particle must ultimately shift by one-half of the average inter-particle distance, as must the particles to the right. This is an appreciably different picture to the higher dimensional case where the electrons are free to reorder in all directions; ultimately the new electron makes much less of a disturbance in three dimensions. This simple picture actually leads to the suppression of the tunneling rate to the wire at zero bias, one of the basic experimental observations associated with Luttinger liquids.

Specifically, the zero-bias anomaly refers to the suppression of the tunneling rate for

particles entering a 1D wire around the zero bias point, in contrast to the featureless tunneling rate around zero-bias for a 3D metal [13]. The signature zero-bias anomaly is a deep minimum at zero-bias with $dI/dV \approx V^{\alpha}$. The power-law dependency was specifically predicted for [14, 15] and measured in carbon nanotubes [16, 17]. Despite some difficulties in interpreting the results, these results are considered clear evidence of Luttinger liquid physics. Further experiments have also discovered the zero-bias anomaly in gallium-arsenide quantum wire dots [18], nanotube dots [19] and other systems [20]. Despite the agreement of these results with theory, there is some uncertainty regarding the interpretation. Because some higher dimensional systems can produce similar behavior it has been suggested that these effects in the leads could be responsible for the observations. Experiments in multi-walled nanotubes with a wide range of biases producing very similar power-law results [21] has cast doubts and makes it difficult to conclusively state that the aforementioned systems are Luttinger liquids.

Fortunately, the zero-bias anomaly is one of the more conventional results of the exotic Luttinger liquid state and there are a few other paths to experimental verification. One of the most interesting phenomena resulting from Luttinger liquids is spin-charge separation. In Fermi Liquid theory, quasi-particles which behave similarly to electrons are formed. They are highly localized, spin 1/2 and carry both spin and charge. Conversely in a Luttinger liquid, there are no such localized states and the basic excitations in the system are waves. More remarkable, charge and spin are carried by charge and spin density waves with different velocities. This phenomenon creates some unique physics which can be detected through experiments such as so-called momentum-resolved tunneling. In the experiment, an electron is extracted from the wire with a momentum, p. However, in the liquid such an electron would not be associated with a unique energy, $\varepsilon(p)$, and would therefore leave behind multiple excitations defined by the spectral function $A(p, \varepsilon)$. This information can be obtained through momentum-conserving tunneling between two parallel 1D electron channels. In the experiment (pictured in 2.2.1), the momentum of a tunneling electron is tuned using a magnetic field, B, applied perpendicular to the wires while the energy resolution is controlled by the interwire bias, V. This provides information about the spectral function, $A(p, \varepsilon)$, through the interwire current, $I(B, V)$.

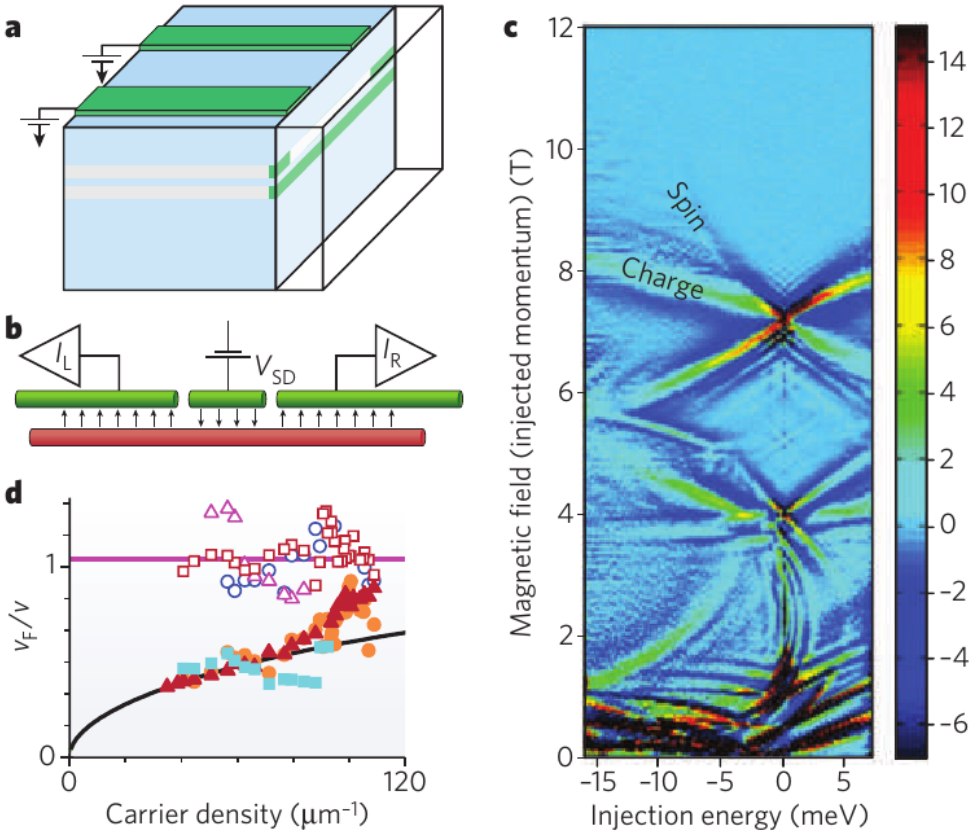

Figure 2.2.1: Probing spin-charge separation and charge fractionalization using momentum-resolved tunneling spectroscopy. Figure a) shows the schematic of the double wire geometry used and b) shows the circuit used to measure the current. Figure c) shows the spectral function, $\partial I(V,B)/\partial V$, indicating the spin and charge excitation branches. Figure d) shows the measure spin and charge velocities (the open and filled symbols, respectively) for different carrier densities (colours), plotted as the Fermi velocity over measured velocity [22].

The measurements reveal clear maxima of $\partial I(V,B)/\partial V$ along a system of lines in the plane, as predicted by theory. Two of the lines cross at a point which can be identified as the tunneling electrons with a momentum near p_F. The velocity of the excitations can be extracted from the slopes at the crossing point and the results are consistent with theoretical estimates for charge and spin wave velocities. This experiment provides some of the best evidence for detection of the Luttinger liquid, although they do raise some question of what happens to spin-charge separation at higher energies. Further understanding of Luttinger liquids at higher energies is an active topic and progress has been made in

theoretical understanding in recent years [23].

2.3 Nuclear Spin-ordering

Interactions between localized magnetic moments and the delocalized electrons contain the essential physics of many condensed matter systems, including nuclear magnets [24], heavy fermion materials of the Kondo-lattice type [25] and ferromagnetic semiconductors [26, 27, 28]. This suggests that these interactions may have a significant role to play other states. Of interest are states with strong electron-electron interactions, where the effects of interplay between the localized magnetic moments and strong interactions has not been studied. Low-dimensional systems are an ideal case for these effects to manifest since the nuclear spins of the ions couple to the electron spin, and the low dimensionality of the electrons enhances interactions. The study of these interactions in low dimensional systems has been pursued by theorists B. Braunecker, P. Simon and D. Loss in several papers [29, 30, 31, 32], resulting in some testable predictions. A brief summary of the results and predictions will be given here.

The first assumption made by the theorists is that the electrons are in a Luttinger liquid state as a result of their interactions. It is in this state that the coupling between the nuclear spins and the electrons results has notable consequences. It is suggested that below a crossover temperature, T^*, the Ruderman-Kittel-Kasya-Toshida (RKKY) interaction will cause the nuclear spins to form a helimagnet.

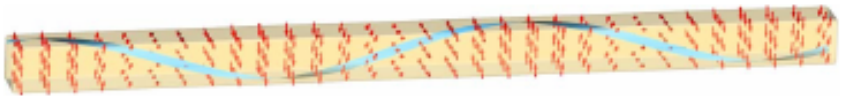

Figure 2.3.1: Illustration of the Helimagnet. The red arrows represent the nuclear spins while the blue ribbon illustrates the helix.[29]

The ordering of the nuclear spins results in an Overhauser field, a magnetic field created by the nuclear spins, which acts back on the electron spins, creates a feedback loop. The feedback enhances the instability of the electron conductor towards a density wave order, resulting in a restructuring of the electronic states. Specifically, a partial gap appears for half of the electron modes, and these modes become spin-polarized, following the helimagnet. The remaining gapless electron modes, on the other hand, will strengthen the RKKY

coupling between the nuclear spins. This feedback means that the system is unstable and the aforementioned critical temperature could lie much higher than without the feedback.

Furthermore, when the model is investigated using physical parameters from GaAs quantum wires, the crossover temperature is predicted to be within 10-100mK, an experimentally reachable temperature. Thus, this unique physical effect is expected to be present in devices which can be fabricated and measured using current technology. Additionally, the theory makes several verifiable experimental predictions. First, the helical magnetization resulting from the nuclear spin ordering follows the modified Bloch law in 2.3.1, where m_{2k_F} is the magnetization, T is the temperature, T^* is the crossover temperature and g' is determined from the RKKY interaction.

$$m_{2k_F} = 1 - \left(\frac{T}{T^*}\right)^{3-2g'}. \tag{2.3.1}$$

This effect could theoretically be detected by using magnetic sensors smaller than the helix, as in magnetic resonance force microscopy[33, 34]. Another possible route to detection is measuring the electronic excitation gap. The gap is expected to be related to m_{2k_F}(depending on the Luttinger liquid Parameters) and therefore measuring the gap provides a direct way to measure m_{2k_F}. A third signature effect is the strong binding of the nuclear helimagnet to the electron modes results in anisotropy in the electron spin susceptibility.

The most obvious and easiest to measure effect, however, is caused by the pinning of one half the electron conduction modes. This results in the conductance of the wire dropping by a factor of 2 to e^2/h when cooling through the crossover temperature, T^*. This effect should be quite clear in experiment and can be interpreted as a signature effect of the theory. Furthermore, the effect should disappear with the application of radiation at the Larmour frequency as it would destroy the nuclear spin ordering. For this reason, this is the primary observation we have chosen to pursue, although measuring multiple predicted effects would be ideal.

While the state is interesting in itself, and could potentially provide sought-after proof of a Luttinger liquid state in these systems, it was shortly realized that it had potential applications in other areas of physics. Specifically, the pursuit of Majorana fermions has become a active topic in recent years and it happens that this state provides a potential platform for observing them. This aspect will be further discussed in section 2.4.

2.4 Resistively Detected NMR

Resistively-detected Nuclear Magnetic Resonance is a technique which allows us to probe the nuclear spin polarization of a state using transport measurements. While conventional NMR is a well known technique, it is limited in application to large systems, requiring $\gtrapprox 10^{16}$ nuclear spins to obtain measurable signals. Quantum systems typically involve fewer spins by at least a few orders or magnitude, meaning conventional techniques cannot be applied. RDNMR works around this problem by utilizing the interaction between transport electrons and the surrounding nuclei. When the resonance condition is reached, the interaction will affect transport, resulting in a signal in the measured electron resistivity. A brief overview of the theory will be given here, as well as some of the previous results.

2.4.1 Theory

The Nuclear Zeeman Interaction

All nucleons have the intrinsic quantum property of spin. As a result, all nuclei also have the property, determined by their quantum spin number, S. When a particle with non-zero spin is in a magnetic field, it interacts with the field according to the Zeeman interaction,

$$\hat{H} = -\mu \cdot \mathbf{B}, \tag{2.4.1}$$

where μ is the magnetic moment, determined by the gyromagnetic ratio, γ and the total quantum spin number, $\mathbf{J}$,

$$\mu = \gamma \mathbf{J}. \tag{2.4.2}$$

The gyromagnetic ratio is generally defined as a system's ratio of the magnetic dipole moment to its angular momentum. For a quantum particle, we take the angular momentum to be that associated with its spin. In the case of the nucleus, this is,

$$\gamma_n = \frac{e}{2m_p} g_n = g_n \frac{\mu_n}{\hbar}, \tag{2.4.3}$$

where e is the electron charge, m_p the mass of a proton, g_n is the g-factor of the nucleus, and $\mu_n$the nuclear magneton ($\mu_n = e\hbar/2m_p$) . Using this definition of the gyromagnetic ratio, we can calculate the Zeeman energy to be,

$$E_{Z_n} = -\gamma_n \hbar B m_J = -g_n \mu_n B m_J, \tag{2.4.4}$$

where m_J is the magnetic quantum number, representing the spin-projection along the direction of the applied magnetic field, B. m_J is quantized to values $m_J = -J, -J+1, ..., J-1, J$, meaning the Zeeman energy is quantized in units of $\hbar m_J$. An illustration of the phenomenon is shown in 2.4.1.

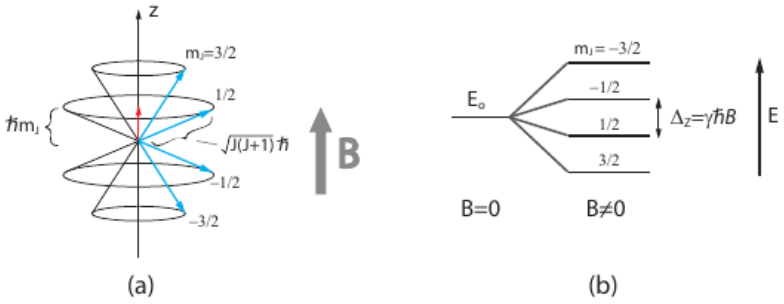

Figure 2.4.1: (a)A quantum particle in a magnetic field is restricted to 2J+1 allowed states, corresponding to projections of the spin along the direction of the field. This is an example of a J=3/2 particle. (b) The field results in Zeeman splitting of the energy level [35].

The energy gap between each state is easily calculated using 2.4.4,

$$\Delta z_n = \gamma_n \hbar B, \tag{2.4.5}$$

and is equal between each level and depends only on the gyromagnetic ratio and B. Going back to our $J = 3/2$ example, clearly the lowest energy state is the spin aligned to the magnetic field: the $m_j = 3/2$ state. This would lead us to believe that all the nuclei would align in the $m_j = 3/2$ state and indeed this is correct, but only at the zero temperature limit. When considering finite temperature, thermal excitations can cause some nuclei to occupy other states, with a probability determined by the Boltzmann distribution,

$$p(E_j) = \frac{e^{-E_j/k_B T}}{\sum_i^n e^{-E_i/k_B T}}. \tag{2.4.6}$$

Applying this to a large number of spins, we can determine the overall polarization of the spins. The overall net polarization is calculated from the expectation value of the Boltzmann distribution. This can be calculated from the Boltzmann distribution,

$$P(m) = e^{-E_{Z_n}/(k_B T)}/Z = e^{xm/J}/Z, \tag{2.4.7}$$

where $x = \frac{g_n \mu_n JB}{k_B T}$, Z is the partition function and m is the spin quantum number,

$$P(m) = e^{xm/J}/(\sum_{m'=-J}^{J} e^{xm'/J}). \tag{2.4.8}$$

It follows that the expectation value is then,

$$\langle m \rangle = (-J) \times P(-J) + ... + J \times P(J) = (\sum_{m=-J}^{J} m e^{xm/J})/(\sum_{m=-J}^{J} e^{xm/J}), \tag{2.4.9}$$

which nicely reduces to,

$$\langle m \rangle = J B_J(x) = \frac{(2J+1)}{2J} coth(x\frac{(2J+1)}{2J}) - \frac{1}{2J} coth(x\frac{1}{2J}), \tag{2.4.10}$$

where x is defined as above, B_J is the Brillouin function and J is the total nuclear spin. The Brillouin function is the result of summing the arithmetic-geometric series in the numerator by the geometric series in the denominator. The Brillouin function ranges from 1, when $B/T \to \infty$, to 0, when $B/T \to 0$. The polarization, $P = \langle m \rangle$, relates to the measurable quantity of magnetization through,

$$M = M_S P, \tag{2.4.11}$$

where $M_S = n g_n \mu_n J$. The implications of this are that at zero temperature, M is maximized as only the lowest energy state is occupied, while at high temperature there is no magnetization as the energy states are equally populated.

For typical temperatures where $\mu B << k_B T$, the magnetization given by the Brillouin function simplifies to Curie's Law given by,

$$M = \frac{n \mu_n^2 g_n^2 J(J+1)}{3 k_B} \frac{B}{T} = \frac{n \mu_n^2}{3 k_B} \frac{B}{T} \tag{2.4.12}$$

Because the nuclear magneton is so small, the condition is nearly always met. In fact percent polarization only reaches >10% for temperatures below 50 mK. The percent polarization at 10T is shown in 2.4.2 as function of temperature.

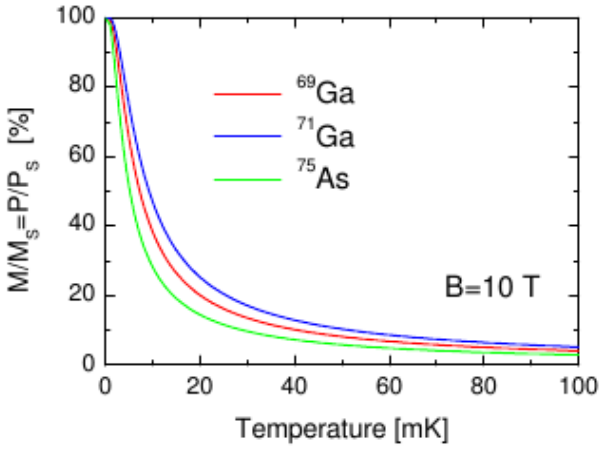

Figure 2.4.2: Percent Nuclear Polarization for ^{69}Ga, ^{71}Ga and ^{75}As, the isotopes found in GaAs[35].

Nuclear Magnetic Resonance

Nuclear magnetic resonance is the phenomenon of nuclei in a magnetic field absorbing and re-emitting radiation. By applying electromagnetic radiation with a frequency, f, the sample is irradiated with photons of energy hf. If the photon energy matches the Zeeman splitting energy,

$$hf = -\gamma_n \hbar B, \tag{2.4.13}$$

then transitions between the two states will be induced by the inbound photons. Using the above equation, we can determine the frequency of light which will cause these transitions,

$$f = \frac{\gamma}{2\pi} B. \tag{2.4.14}$$

Remarkably, the frequency of radiation which induces transitions is linear proportional to the magnetic field, with the relationship being determined only by the gyromagnetic ratio.

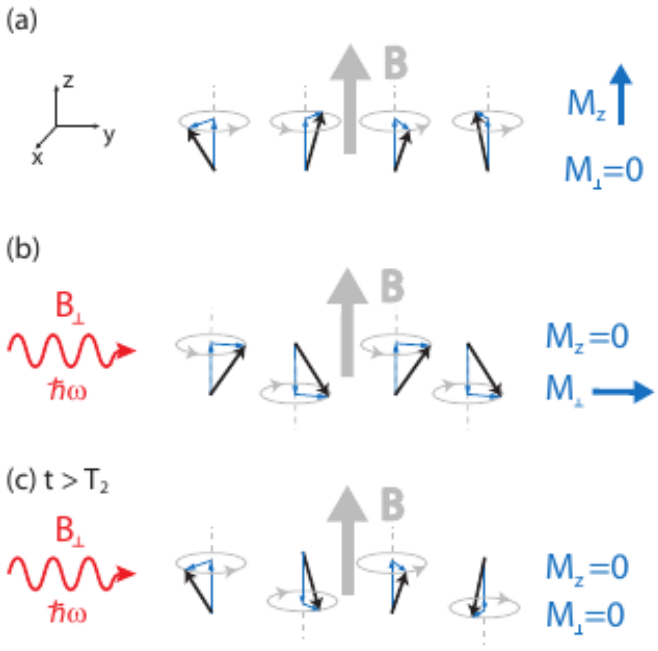

Figure 2.4.3: Illustration of the NMR process showing four spins. a) The spins are aligned to the field and spinning at the Larmour frequency. As shown, the spins are generally out of phase, resulting in the average $M_z = M$ and $M_\perp = 0$. b) A continuous transverse field, oscillating at the Larmour frequency is applied causing the spins to randomize and evenly distribute between the available states and reducing the magnetization to zero, $M_z = 0$. However, the spins form a coherent phase from the applied field meaning that $M_\perp$is no longer zero. c) The spins which were momentarily coherent quickly dephase from interactions, causing $M_\perp$ to also reduce to zero [35].

Applying radiation of this frequency to the sample causes transitions which disturb the equilibrium Boltzmann distribution. This means that even if the temperature or other effects suggest that most of the nuclei will be polarized, the the radiation will cause many energy transitions, completely randomizing the polarization. If the radiation is removed, over time the nuclear spins will revert to their original behavior, according to the formula

$$M_z(t) = M_o - [M_o - M_z(0)]e^{-t/T_1}, \tag{2.4.15}$$

where M_o is the equilibrium state, and T_1 the spin-lattice relaxation time. T_1 is interpreted as the mean time for an individual nucleus to return to its thermal equilibrium state of spin. At low temperatures where few phonons are present, spin relaxation relies entirely on photon emission, meaning relaxation times can be minutes or even hours.

However, despite the fact that the nuclei all precess at the same Lamour frequency, they are not typically in phase with one another meaning there is no net magnetization in the transverse direction. The application of the transverse radiation can impart a phase coherence among the nuclear spins causing a component of the net polarization to point in the x-y direction (the B-field points in the z direction). This effect quickly decays, according to the spin-spin relaxation time, T_2. The relaxation is described by,

$$M_{\perp}(t) = M_{\perp}(t=0)e^{-t/T_2}. \tag{2.4.16}$$

The spin-spin relaxation time is generally much quicker than the spin-lattice relaxation time as it results from interactions with local atoms and inhomogeneities in the magnetic field. The description of spin relaxations are derived from the Bloch equations, a set of macroscopic phenomenological equations used to calculate nuclear magnetization on relaxation times.

In some cases it is easier to apply a classical view of NMR to understand results. Of course, we are dealing with quantum particles so applying a classical theory will produce incorrect results for a single particle, however averaged over a large number of particles the classical view holds. In this view, each atom is considered a magnetic moment, precessing about the magnetic field at the Larmour frequency. The difference between this and the quantum view is the quantization of the energy levels; in the classical view we ignore this and allow the atom to be oriented in any direction. Again, while false for any individual atom, for the ensemble this view will produce correct results and in typical NMR experiments, we probe the ensemble rather than an individual particle. Thus, the classical theory is helpful in simplifying our theory and understanding of experimental results. The Zeeman energy which we calculated for the quantum case, then reduces to,

$$E_{Z_n} = -\gamma_n \hbar B I_Z = -\mu B cos(\theta), \tag{2.4.17}$$

where the spin projection along the B-field, $I_Z = Icos(\theta)$. Similar to the quantum view, applying transverse radiation at the Larmour frequency can tip the spins away from the B-field axis through an angle θ as illustrated in 2.4.4. The magnitude of this angle depends on how long the radiation is applied, according to the the pulse time, transverse B-field,

$$\theta = 2\pi\gamma_N \tau B_{\perp}. \tag{2.4.18}$$

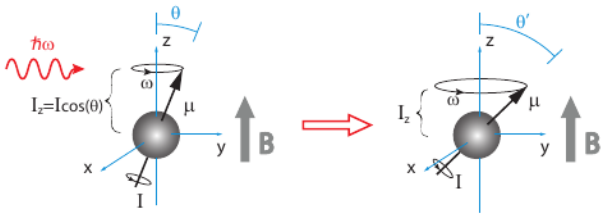

Figure 2.4.4: The transverse radiation tips the spin away from the equilibrium axis in the classical view of NMR [35].

Similarly to the quantum scenario, the characteristic times, $T_1$and T_2 determine the time for magnetization to return to equilibrium in the z-direction and the x-y direction respectively.

Electrons in a magnetic field

It would be remiss to not mention that the same analysis can generally be applied to the electrons in a magnetic field with a key difference. For electrons, the spin magnetic moment is opposite to the direction of the spin, resulting in the relation,

$$\gamma_e = -g_e \frac{\mu_B}{\hbar}, \tag{2.4.19}$$

whereμ_B is the Bohr Magneton, $\frac{e\hbar}{2m_e}$. This results in a Zeeman energy for electrons in a magnetic field which is

$$E_Z = g^* \mu_B B S_Z. \tag{2.4.20}$$

As usual, S_Z is the spin projection and $g^*$is the effective g-factor. For electrons, the g-factor is positive meaning that the lowest energy state is with the electrons anti-aligned to the field. However, in a semiconductor, spin-orbit interactions can modify the g-factor in a significant way. In GaAs, the g-factor is affected so much it becomes -0.44 (compared to ~ 2 in vacuum) meaning the electrons actually do align with the field. Electrons can be probed in the same fashion as the nuclei in NMR in a less commonly known technique called Electron Spin Resonance (ESR).

2.4.2 Resistively Detected NMR (RDNMR)

There are many techniques for observing NMR, including Continuous Wave Spectroscopy, Fourier Transform Spectroscopy and Multi-dimensional NMR Spectroscopy. Generally, all these methods involve placing the sample in a magnetic field, bombarding it with radiation and analyzing the radiation which returns. Resistively detected NMR, differs from all these methods, however, in that it does not observe the light which is affected by the NMR. Rather, it detects the effects of NMR on electronic transport.

In the sample, electrons can couple to the nuclear spins of the surrounding atoms thought the hyperfine spin interaction. In the case of a solid placed in a magnetic field where the nuclear spins exhibit an average overall polarization, the hyperfine interaction energy is,

$$E_{HF} = A\langle I_Z\rangle S_Z, \tag{2.4.21}$$

with S_Z being the projection of the electron spin in the field direction and $\langle I_Z\rangle$representing the average nuclear spin polarization. A is the hyperfine coupling constant, defined as,

$$A = \frac{2\mu_o}{3}(g_e\mu_B)(g_n\mu_n)|\psi(0)|^2, \tag{2.4.22}$$

where $|\psi(0)|$ is the electron probability density at the lattice site. We must include the effect of the hyperfine interaction in the calculation of the Zeeman energy, meaning that the Zeeman Energy for electrons becomes,

$$E_Z = g^*\mu_B B S_Z + A\langle I_Z\rangle S_Z, \tag{2.4.23}$$

or, more lucidly,

$$E_Z = g^*\mu_B(B + B_n)S_Z, \tag{2.4.24}$$

with $B_n = A\langle I_Z\rangle/g^*\mu_B$ representing an effective shift in the nuclear magnetic field called the Overhauser shift. To see how this affects the longitudinal resistance, we consider the thermally activated regime, in which the magnetoresistance is determined by,

$$R_{xx} \propto e^{-\Delta/2k_BT} \tag{2.4.25}$$

where Δ is the gap. The gap is determined by the gap of the quantum state in addition

to the gap induced by the Zeeman interaction. So, we can rewrite the equation 2.4.25 including the effect of the Zeeman interaction as,

$$R_{xx} \propto e^{-g^*\mu_B(B+B_n)/2k_BT}. \tag{2.4.26}$$

In this form, its possible to see that the longitudinal resistance is determined in part by B_n, which is dependent on the hyperfine coupling and therefore the nuclear polarization. Thus the nuclear polarization has a direct effect on the longitudinal resistance of a sample. The details of the response to radiation are dependent on the detailed behavior of the state, which in some cases is not well understood, but its clear that in general there should be a response.

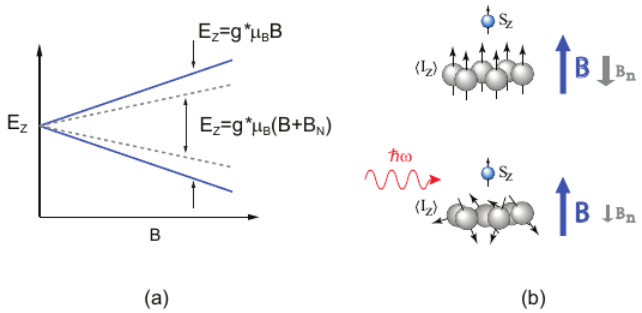

Figure 2.4.5: (a) The effective magnetic field, B_n, influences the Zeeman energy (b) Destroying the nuclear polarization with radiation at the Larmour frequency reduces the effective nuclear field, thus increasing the Zeeman energy[35].

The technique was first demonstrated by Dobers *et al* [36], who observed that interactions between the electrons and nuclear spins could be detected in R_{xx} measurements. This study was performed at the relatively high temperature of 4K and thus required dynamic nuclear polarization via electron spin resonance. This work was followed up by Kronmüller *et al.* in the study of the huge magnetoresistance peak that appears around $\nu = 2/3$ in thin quantum well samples[37]. Using much lower temperatures where nuclear polarization is significantly stronger than previous experiments, Desrat *et al* [38] found that NMR could be performed without the use of Dynamic Nuclear Polarization. This result opened the door for using RDNMR to study exotic states such as FQHE which occur only at very low temperatures and several experiments have followed in recent years. An experiment

performed by Keane *et al* [39] used RDNMR to study both electron and hole QPCs and was successful in comparing the hyperfine coupling of the two systems.

2.5 Possible Applications

2.5.1 Majorana fermions

Majorana fermions are spin 1/2 particles proposed by Ettore Majorana in a seminal 1937 paper[40], resulting from a modification to the Dirac equation which would admit purely real-solutions. These solutions are Majorana fermions; fermions which are their own antiparticles. Supersymmetric theories suggest that bosonic particles may have Majorana 'superpartners' which could be a key to explaining dark matter. Its possible the Large Hadron Collider will test some of these predictions, however, it happens there is another path towards detecting Majoranas in the field of condensed matter physics. Its routine in condensed matter systems for ensembles of quantum mechanical particles to form quasi-particles, occasionally with dramatically different properties than their constituents of electrons and ions. Superconductivity is a common realization of this as the electrons condense into Cooper-Pairs which carry the current in superconductor. Cooper-pairs provide a natural place to look for Majorana-like particles, since they violate charge conservation symmetry by consisting of a superposition of an electron and hole. However, this is not sufficient to result in Majoranas; nearly all superconductors are s-wave paired. This means they take the form $d = uc_{\uparrow}^{\dagger} + vc_{\downarrow}$which is physically distinct from its antiparticle, $d^{\dagger} = u^{*}c_{\uparrow} + v^{*}c_{\downarrow}^{\dagger}$. Thus, a conditions for the existence of Majorana fermions is a 'spinless superconductor', a system with paired fermions and only one spin type. Such superconductors are known as $p + ip$ and are very special, specifically to realize a Majorana we require a 1D p-wave superconductor in proximity to a 2D $p + ip$ superconductor: in this system the Majorana's will appear at the ends of the wire and bind to vortices in the 2D conductor.

While theoretically such a system would support Majorana's, it involves many exotic components and would be experimentally difficult. Thus, despite theoretical interest, experiments were basically unfeasible. This took a dramatic turn in 2008 with the work of Fu and Kane [41], who realized that Majorana fermions could be realized in a system combining a conventional superconductor and a topological insulator. Their crucial insight was that the proximity effect would result in a state which could support Majo-

rana excitations. A flurry of theoretical and experimental work has followed, proposing several similar structures which could support Majorana fermions. Possible experimental evidence was achieved in April 2012 by Mourik *et al.* [42] in indium antimonide nanowires. While further verification is ongoing, efforts to isolate Majorana fermions in other systems continue.

One such system that could support Majoranas is the previously discussed nuclear-spin ordered state proposed by Braunecker and Loss [29, 31]. The nuclear spin-ordering creates a gap for half of the modes, resulting in a Luttinger liquid state with a single fermionic species. This satisfies the requirement that the 1D conductor be 'spinless'. Calculations in [31] indicate that Majorana Edge States (MES) could be formed in a similar fashion to other proposals -by placing the wire in proximity to an s-wave superconductor. This platform provides a compelling path towards the realization of Majorana fermions due to its simplicity. While other fabrication schemes are complicated and difficult to scale, the architecture of this device is remarkably simple and could be scaled to support networks for Majorana wires which have applications in the area of quantum computing.

2.5.2 Topological Quantum Computation

Much of the recent interest in Majorana fermions is driven not out of pure physical interest, but by applications to quantum computing. Specifically, Majoranas have properties which make them useful in Topological Quantum Computing schemes. We will briefly discuss these properties and how they might apply to a quantum computer.

For this we will consider a system of just four Majoranas, labeled $\gamma_{1,2,3,4}$ as shown in figure 2.5.1

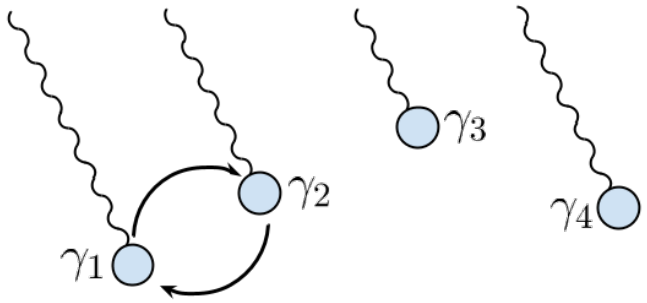

Figure 2.5.1: A 2D topological superconductor with four vortices binding Majorana modes. $\gamma_1$and $\gamma_2$are undergoing a clockwise braid. This picture generalizes to all Majorana systems including quantum wire systems, although the practical implementation is a bit more complex.

Additionally, we will define conventional fermion and number operators,

$$f_j = (\gamma_{2j-1} + i\gamma_{2j})/2 \tag{2.5.1}$$

$$n_j = f_j^\dagger f_j \tag{2.5.2}$$

The two Majoranas on the right are pinned by an applied potential, while the two on the left are adiabatically changed positions (in the clockwise direction). Majoranas have the important property that crossing the particles will result in a fundamentally different ground state than it began. The proof of this is non-trivial, for a rigorous approach see reference [43]. For our purposes however, all we need to understand is how the Majorana operators transform under exchange. When the particles are exchanged or "braided" $\gamma_1$crosses a branch cut and thus picks up a minus sign. The transformation is represented,

$$\gamma_1 \to -\gamma_2 \tag{2.5.3}$$

$$\gamma_2 \to \gamma_1. \tag{2.5.4}$$

The unitary operator corresponding to this transformation is,

$$U_{12} = (1 + \gamma_1\gamma_2)/\sqrt{2}, \tag{2.5.5}$$

and more generally,

$$U_{j,j+1} = (1 + \gamma_j \gamma_{j+1})/\sqrt{2}. \tag{2.5.6}$$

Thus, up to a general overall phase factor, the ground state wavefunction evolves as

$$|n_1, n_2\rangle \to U_{j,j+1}|n_1, n_2\rangle. \tag{2.5.7}$$

Applying this result to the three clockwise exchanges available in our system, the ground state wavefunction evolves as,

$$|n_1, n_2\rangle \to U_{12}|n_1, n_2\rangle \to e^{i\frac{\pi}{4}(1-2n_1)}|n_1, n_2\rangle \tag{2.5.8}$$

$$|n_1, n_2\rangle \to U_{23}|n_1, n_2\rangle \to \frac{1}{\sqrt{2}}[|n_1, n_2\rangle + i(-1)^{n_1}|1 - n_1, 1 - n_2\rangle] \tag{2.5.9}$$

$$|n_1, n_2\rangle \to U_{34}|n_1, n_2\rangle \to e^{i\frac{\pi}{4}(1-2n_2)}|n_1, n_2\rangle. \tag{2.5.10}$$

As we can see, adiabatically exchanging $\gamma_{1,2}$ or $\gamma_{3,4}$ internally rotates the ordinary fermion operators, causing the ground state to pick up non-trivial phase factors. Even more interestingly, exchanging $\gamma_{2,3}$ swaps half of $f_1$with half of f_2 resulting in another non-trivial rotation within the ground state manifold.

This sort of odd behavior, where exchanging particles results in non-trivial rotations within a ground state manifold, is known as non-Abelian statistics. Stated plainly, if sequential exchanges are performed, the final state depends on the order in which they are carried out. This is a result of the non-trivial commutation relations of the operators $U_{j,j+1}$and thus generalizes to arbitrarily many particles.

This brief analysis is done in reference to a 2D topological superconductor and it turns out there is two problems when trying to extend this to 1D quantum wires. First, exchange statistics are never well-defined in 1D systems. If we attempted to adiabatically exchange Majorana zero-modes from the ends of a wire, first they would have to cross each other, necessarily lifting the ground state degeneracy, and additionally the final state would be indistinguishable from the initial. Fortunately this obstacle can be surmounted by using networks of wires, which do allow for meaningful exchanges as in figure 2.5.2. The other issue is that the vortices which make non-Abelian statistics possible in 2D topological

superconductors are absent in the 1D systems, so there is some question of whether the statistics would even emerge. Fortunately, theoretical work indicates that this turns out not to be an issue. A detailed discussion of both these issues can be found in references [44, 45]. While the simple structures discussed here are not actually capable of quantum computation, more complex proposals exist to provide the necessary building blocks[46, 47]. Based on the theoretical work, it appears that quantum-wire based Majoranas provide a clear path to building a topological quantum computer, provided they can be successfully produced in experiments.

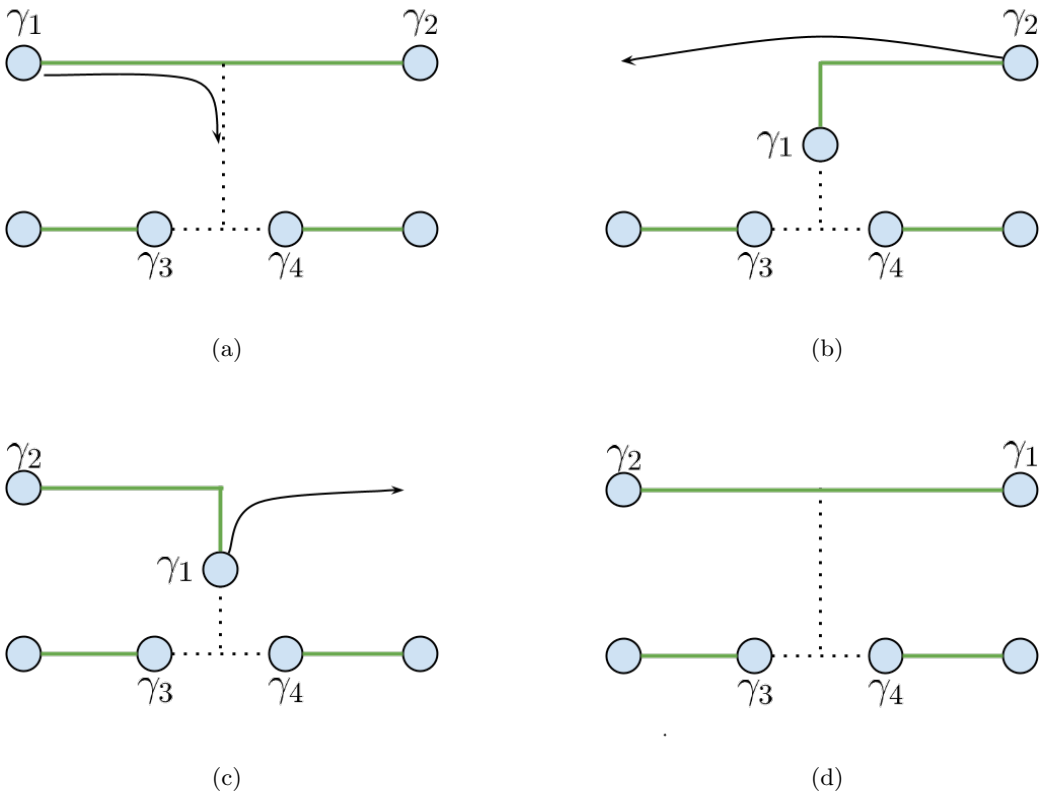

Figure 2.5.2: A demonstration of a simple particle exchange using a quantum wire network.

While the non-Abelian statistics discussed are certainly fascinating new physics, it should be briefly mentioned why the concept of a topological quantum computer is so appealing. The operation of exchanging non-Abelian anyons is the 'braid' operation which

is a unitary transformation within a degenerate ground state. Furthermore, the only way to perform operations on the ground state is through braiding particles. If we pause to reflect on this statement for a moment, the implication is that the state of the system is entirely non-local - it cannot be changed by a local perturbation. This is why topological computing is considered 'fault-tolerant'.

Current quantum computing platforms tend to encounter two main types of errors. First, local perturbations such as electron-phonon interactions or electron-nuclear interactions can change a qubit state. Second, unitary errors can occur, for example a rotation which is 90.01 degrees rather than 90. As of yet, no system has been able to address both of these difficulties. However, a topological quantum computer is naturally immune to both types of error. In a topological system, the computation is performed in the ground state, which is separated from higher energy states by a gap. As long as the temperature is lower than the gap size, the probability of an excitation out of the ground state is exponentially suppressed and the state must evolve within the ground state subspace. However, within the degenerate subspace, local operations have no non-zero matrix elements; the only way to change the state is by braiding particles. This can be understood by noting that the qubits themselves are construction of widely separated particles. A local perturbation is irrelevant to what is a topological phenomena. Similarly, unitary errors (such as the imprecise rotation) aren't a problem, since we can't very well partly cross two particles.

So, by design, a topological quantum computer addresses the most common types of error encountered in conventional quantum computing schemes. This makes it an extremely interesting possibility for practical implementations. Of course, until recently, the search for non-Abelian anyons was limited to a few exotic materials, most notably the fractional quantum hall states. With the realization that Majorana fermions could be realized in quantum wire systems using relatively conventional ingredients, there has been an immense amount of interest in fabricating systems in the laboratory.

References

[1] Yu V Sharvin. "On the possible method for studying fermi surfaces". In: *Zh. Eksperim. i Teor. Fiz.* 48 (1965).

[2] Henk Van Houten and Carlo Beenakker. "Quantum point contacts". In: *Physics Today* July (1996). arXiv:0512609v1 [arXiv:cond-mat]. URL: http://link.aip.org/link/phtoad/v49/i7/p22/s1.

[3] BJ Van Wees, H Van Houten, CWJ Beenakker, JG Williamson, LP Kouwenhoven, D Van der Marel, and CT Foxon. "Quantized conductance of point contacts in a two-dimensional electron gas". In: *Physical Review Letters* 60.9 (1988), pp. 848–850. URL: http://link.aps.org/doi/10.1103/PhysRevLett.60.848.

[4] DA Wharam and TJ Thornton. "One-dimensional transport and the quantisation of the ballistic resistance". In: *Journal of Physics C: ...* 209 (1988). URL: http://iopscience.iop.org/0022-3719/21/8/002.

[5] Aaron Szafer and AD Stone. "Theory of quantum conduction through a constriction". In: *Physical review letters* 62.3 (1989), pp. 300–303. URL: http://link.aps.org/doi/10.1103/PhysRevLett.62.300.

[6] CWJ Beenakker and H Van Houten. "Quantum transport in semiconductor nanostructures". In: *Solid state physics* 228 (1991), pp. 1–111. arXiv:0412664v1 [arXiv:cond-mat]. URL: http://www.sciencedirect.com/science/article/pii/S0081194708600910.

[7] Y. Komijani, M. Csontos, I. Shorubalko, T. Ihn, K. Ensslin, Y. Meir, D. Reuter, and a. D. Wieck. "Evidence for localization and 0.7 anomaly in hole quantum point contacts". In: *EPL (Europhysics Letters)* 91.6 (Sept. 2010), p. 67010. ISSN: 0295-5075. DOI: 10.1209/0295-5075/91/67010. URL: http://stacks.iop.org/0295-5075/91/i=6/a=67010?key=crossref.20c100def7f0a26181e6d02d978c6169.

[8] Yigal Meir. "The theory of the 0.7 anomaly in quantum point contacts". In: *Journal of Physics: Condensed Matter* 20.16 (Apr. 2008), p. 164208. ISSN: 0953-8984. DOI: 10.1088/0953-8984/20/16/164208. URL: http://stacks.iop.org/0953-8984/20/i=16/a=164208?key=crossref.6bc8dd8fd78337cb8dae4a7b5846d1c9.

[9] Pepper Michael and Jonathan Bird. "The 0.7 feature and interactions in one-dimensional systems". In: *Journal of Physics: Condensed Matter* 20.16 (Apr. 2008), p. 160301. ISSN: 0953-8984. DOI: 10.1088/0953-8984/20/16/160301. URL: http://stacks.iop.org/0953-8984/20/i=16/a=160301?key=crossref.11e08c0f22acf3f75fe466e53fb6f654.

[10] V Tripathi and N R Cooper. "Nuclear magnetic resonance probes for the Kondo scenario for the 0.7 feature in semiconductor quantum point contact devices". In: *Journal of Physics: Condensed Matter* 20.16 (Apr. 2008), p. 164215. ISSN: 0953-8984. DOI: 10.1088/0953-8984/20/16/164215. URL: http://stacks.iop.org/0953-8984/20/i=16/a=164215?key=crossref.ca40123c95798739551fd8a4fffb0068.

[11] K-F Berggren and M Pepper. "Electrons in one dimension." In: *Philosophical transactions. Series A, Mathematical, physical, and engineering sciences* 368.1914 (Mar. 2010), pp. 1141–62. ISSN: 1364-503X. DOI: 10.1098/rsta.2009.0226. URL: http://www.pubmedcentral.nih.gov/articlerender.fcgi?artid=3263805\&tool=pmcentrez\&rendertype=abstract.

[12] Philip Phillips. *Advanced Solid State Physics*. Cambridge University Press, 2012, p. 402. ISBN: 0521194903. URL: http://books.google.com/books?id=5n02cBeJSj0C\&pgis=1.

[13] CL Kane and MPA Fisher. "Transport in a one-channel Luttinger liquid". In: *Physical review letters* (1992). URL: http://link.aps.org/doi/10.1103/PhysRevLett.68.1220.

[14] Reinhold Egger and Alexander Gogolin. "Effective Low-Energy Theory for Correlated Carbon Nanotubes". In: *Physical Review Letters* 79.25 (Dec. 1997), pp. 5082–5085. ISSN: 0031-9007. DOI: 10.1103/PhysRevLett.79.5082. URL: http://link.aps.org/doi/10.1103/PhysRevLett.79.5082.

[15] Charles Kane, Leon Balents, and Matthew Fisher. "Coulomb Interactions and Mesoscopic Effects in Carbon Nanotubes". In: *Physical Review Letters* 79.25 (Dec. 1997), pp. 5086–5089. ISSN: 0031-9007. DOI: 10.1103/PhysRevLett.79.5086. URL: http://link.aps.org/doi/10.1103/PhysRevLett.79.5086.

[16] Henk Postma, Mark de Jonge, Zhen Yao, and Cees Dekker. "Electrical transport through carbon nanotube junctions created by mechanical manipulation". In: *Physical Review B* 62.16 (Oct. 2000), R10653–R10656. ISSN: 0163-1829. DOI: 10.1103/PhysRevB.62.R10653. URL: http://link.aps.org/doi/10.1103/PhysRevB.62.R10653.

[17] Zhen Yao, HWC Postma, Leon Balents, and Cees Dekker. "Carbon nanotube intramolecular junctions". In: *Nature* 402.November (1999), pp. 273–276. URL: http://www.nature.com/nature/journal/v402/n6759/abs/402273a0.html.

[18] Om Auslaender, a Yacoby, de Picciotto R, Kw Baldwin, Ln Pfeiffer, and Kw West. "Experimental evidence for resonant tunneling in a luttinger liquid". In: *Physical review letters* 84.8 (Feb. 2000), pp. 1764–7. ISSN: 1079-7114. URL: http://www.ncbi.nlm.nih.gov/pubmed/11017620.

[19] H W Postma, T Teepen, Z Yao, M Grifoni, and C Dekker. "Carbon nanotube single-electron transistors at room temperature." In: *Science (New York, N.Y.)* 293.5527 (July 2001), pp. 76–9. ISSN: 0036-8075. DOI: 10.1126/science.1061797. URL: http://www.ncbi.nlm.nih.gov/pubmed/11441175.

[20] Latha Venkataraman, Yeon Hong, and Philip Kim. "Electron Transport in a Multichannel One-Dimensional Conductor: Molybdenum Selenide Nanowires". In: *Physical Review Letters* 96.7 (Feb. 2006), p. 076601. ISSN: 0031-9007. DOI: 10.1103/PhysRevLett.96.076601. URL: http://link.aps.org/doi/10.1103/PhysRevLett.96.076601.

[21] Bernhard Stojetz, C Miko, L Forró, and Christoph Strunk. "Effect of band structure on quantum interference in multiwall carbon nanotubes". In: *Physical review letters* (2005), pp. 1–5. arXiv:0410764v1 [arXiv:cond-mat]. URL: http://link.aps.org/doi/10.1103/PhysRevLett.94.186802.

[22] Vikram V Deshpande, Marc Bockrath, Leonid I Glazman, and Amir Yacoby. "Electron liquids and solids in one dimension." In: *Nature* 464.7286 (Mar. 2010), pp. 209–16. ISSN: 1476-4687. DOI: 10.1038/nature08918. URL: http://www.ncbi.nlm.nih.gov/pubmed/20220839.

[23] Adilet Imambekov and Leonid I Glazman. "Universal theory of nonlinear Luttinger liquids." In: *Science (New York, N.Y.)* 323.5911 (Jan. 2009), pp. 228–31. ISSN: 1095-

9203. DOI: 10.1126/science.1165403. URL: http://www.ncbi.nlm.nih.gov/pubmed/19039106.

[24] H Frohlich and FRN Nabarro. "Orientation of nuclear spins in metals". In: *... of the Royal ...* (1940). URL: http://rspa.royalsocietypublishing.org/content/175/962/382.full.pdf.

[25] Hirokazu Tsunetsugu, Manfred Sigrist, and Kazuo Ueda. "The ground-state phase diagram of the one-dimensional Kondo lattice model". In: *Reviews of Modern Physics* 69.3 (July 1997), pp. 809–864. ISSN: 0034-6861. DOI: 10.1103/RevModPhys.69.809. URL: http://link.aps.org/doi/10.1103/RevModPhys.69.809.

[26] T. Dietl, a. Haury, and Y. Merle d'Aubigné. "Free carrier-induced ferromagnetism in structures of diluted magnetic semiconductors". In: *Physical Review B* 55.6 (Feb. 1997), R3347–R3350. ISSN: 0163-1829. DOI: 10.1103/PhysRevB.55.R3347. URL: http://link.aps.org/doi/10.1103/PhysRevB.55.R3347.

[27] H. Ohno. "Making Nonmagnetic Semiconductors Ferromagnetic". In: *Science* 281.5379 (Aug. 1998), pp. 951–956. DOI: 10.1126/science.281.5379.951. URL: http://www.sciencemag.org/cgi/doi/10.1126/science.281.5379.951.

[28] H Ohno, H Munekata, and T Penney. "Magnetotransport properties of p-type (In, Mn) As diluted magnetic III-V semiconductors". In: *Physical Review Letters* 68.17 (1992), pp. 6–9. URL: http://link.aps.org/doi/10.1103/PhysRevLett.68.2664.

[29] Bernd Braunecker, Pascal Simon, and Daniel Loss. "Nuclear magnetism and electron order in interacting one-dimensional conductors". In: *Physical Review B* 80.16 (Oct. 2009), pp. 1–28. ISSN: 1098-0121. DOI: 10.1103/PhysRevB.80.165119. URL: http://link.aps.org/doi/10.1103/PhysRevB.80.165119.

[30] Bernd Braunecker, Pascal Simon, and Daniel Loss. "Nuclear Magnetism and Electronic Order in C13 Nanotubes". In: *Physical Review Letters* 102.11 (Mar. 2009), p. 116403. ISSN: 0031-9007. DOI: 10.1103/PhysRevLett.102.116403. URL: http://link.aps.org/doi/10.1103/PhysRevLett.102.116403.

[31] Suhas Gangadharaiah, Bernd Braunecker, Pascal Simon, and Daniel Loss. "Majorana Edge States in Interacting One-Dimensional Systems". In: *Physical Review Letters* 107.3 (July 2011), pp. 1–4. ISSN: 0031-9007. DOI: 10.1103/PhysRevLett.107.036801. URL: http://link.aps.org/doi/10.1103/PhysRevLett.107.036801.

[32] Bernd Braunecker, George Japaridze, Jelena Klinovaja, and Daniel Loss. "Spin-selective Peierls transition in interacting one-dimensional conductors with spin-orbit interaction". In: *Physical Review B* 82.4 (July 2010), pp. 1–5. ISSN: 1098-0121. DOI: 10.1103/PhysRevB.82.045127. URL: http://link.aps.org/doi/10.1103/PhysRevB.82.045127.

[33] C L Degen, M Poggio, H J Mamin, C T Rettner, and D Rugar. "Nanoscale magnetic resonance imaging." In: *Proceedings of the National Academy of Sciences of the United States of America* 106.5 (Feb. 2009), pp. 1313–7. ISSN: 1091-6490. DOI: 10.1073/pnas.0812068106. URL: http://www.pubmedcentral.nih.gov/articlerender.fcgi?artid=2628306\&tool=pmcentrez\&rendertype=abstract.

[34] H J Mamin, M Poggio, C L Degen, and D Rugar. "Nuclear magnetic resonance imaging with 90-nm resolution." In: *Nature nanotechnology* 2.5 (May 2007), pp. 301–6. ISSN: 1748-3395. DOI: 10.1038/nnano.2007.105. URL: http://www.ncbi.nlm.nih.gov/pubmed/18654288.

[35] Cory R Dean. "A Study of the Fractional Quantum Hall Energy Gap at Half Filling". PhD thesis. 2008.

[36] M Dobers and K Klitzing. "Electrical Detection of Nuclear Magnetic Resonance in Ga As-Al* Gai-* As Heterostructures". In: *Physical review ...* 61.14 (1988). URL: http://140.120.11.121/~vincent/reference/QHE/2DESandQHE/NMR/p1650_1.pdf.

[37] S. Kronmüller, W. Dietsche, K. v. Klitzing, G. Denninger, W. Wegscheider, and M. Bichler. "New Type of Electron Nuclear-Spin Interaction from Resistively Detected NMR in the Fractional Quantum Hall Effect Regime". In: *Physical Review Letters* 82.20 (May 1999), pp. 4070–4073. ISSN: 0031-9007. DOI: 10.1103/PhysRevLett.82.4070. URL: http://link.aps.org/doi/10.1103/PhysRevLett.82.4070.

[38] W. Desrat, D. Maude, M. Potemski, J. Portal, Z. Wasilewski, and G. Hill. "Resistively Detected Nuclear Magnetic Resonance in the Quantum Hall Regime: Possible Evidence for a Skyrme Crystal". In: *Physical Review Letters* 88.25 (June 2002), pp. 1–4. ISSN: 0031-9007. DOI: 10.1103/PhysRevLett.88.256807. URL: http://link.aps.org/doi/10.1103/PhysRevLett.88.256807.

[39] Z K Keane, M C Godfrey, J C H Chen, S Fricke, O Klochan, A M Burke, A P Micolich, H E Beere, D A Ritchie, K V Trunov, D Reuter, A D Wieck, and A R Hamilton. "Resistively detected nuclear magnetic resonance in n- and p-type GaAs quantum

point contacts." In: *Nano letters* 11.8 (Aug. 2011), pp. 3147–50. ISSN: 1530-6992. DOI: 10.1021/nl201211d. URL: http://www.ncbi.nlm.nih.gov/pubmed/21714512.

[40] E Majorana. "Teoria simmetrica dell'elettrone e del positrone". In: *Il Nuovo Cimento* (1937). URL: http://link.springer.com/article/10.1007/BF02961314.

[41] Liang Fu and C. CL Kane. "Superconducting proximity effect and Majorana fermions at the surface of a topological insulator". In: *Physical review letters* 100.3 (Mar. 2008), pp. 1–4. ISSN: 0031-9007. DOI: 10.1103/PhysRevLett.100.096407. arXiv:arXiv:0707.1692v3. URL: http://link.aps.org/doi/10.1103/PhysRevLett.100.096407.

[42] V Mourik, K Zuo, S M Frolov, S R Plissard, E P a M Bakkers, and L P Kouwenhoven. "Signatures of Majorana fermions in hybrid superconductor-semiconductor nanowire devices." In: *Science (New York, N.Y.)* 336.6084 (May 2012), pp. 1003–7. ISSN: 1095-9203. DOI: 10.1126/science.1222360. URL: http://www.ncbi.nlm.nih.gov/pubmed/22499805.

[43] Ady Stern, Felix von Oppen, and Eros Mariani. "Geometric phases and quantum entanglement as building blocks for non-Abelian quasiparticle statistics". In: *Physical Review B* 70.20 (Nov. 2004), p. 205338. ISSN: 1098-0121. DOI: 10.1103/PhysRevB.70.205338. URL: http://link.aps.org/doi/10.1103/PhysRevB.70.205338.

[44] David J. Clarke, Jay D. Sau, and Sumanta Tewari. "Majorana fermion exchange in quasi-one-dimensional networks". In: *Physical Review B* 84.3 (July 2011), p. 035120. ISSN: 1098-0121. DOI: 10.1103/PhysRevB.84.035120. URL: http://link.aps.org/doi/10.1103/PhysRevB.84.035120.

[45] Jay D. Sau, David J. Clarke, and Sumanta Tewari. "Controlling non-Abelian statistics of Majorana fermions in semiconductor nanowires". In: *Physical Review B* 84.9 (Sept. 2011), p. 094505. ISSN: 1098-0121. DOI: 10.1103/PhysRevB.84.094505. URL: http://link.aps.org/doi/10.1103/PhysRevB.84.094505.

[46] Karsten Flensberg. "Non-Abelian Operations on Majorana Fermions via Single-Charge Control". In: *Physical Review Letters* 106.9 (Mar. 2011), p. 090503. ISSN: 0031-9007. DOI: 10.1103/PhysRevLett.106.090503. URL: http://link.aps.org/doi/10.1103/PhysRevLett.106.090503.

[47] B van Heck, a R Akhmerov, F Hassler, M Burrello, and C W J Beenakker. "Coulomb-assisted braiding of Majorana fermions in a Josephson junction array". In: *New Journal of Physics* 14.3 (Mar. 2012), p. 035019. ISSN: 1367-2630. DOI: 10.1088/1367-2630/14/3/035019. URL: http://stacks.iop.org/1367-2630/14/i=3/a=035019?key=crossref.dd6993fc88e0e4d06efa10ff7cdd33af.

Chapter 3

Methodology

3.1 Samples

3.1.1 GaAs Heterostructures and Quantum Wells

While 2DEGs can be created in wide variety of semiconductor systems and even in graphene, the best 2DEGs continue to be provided by GaAs/AlGaAs heterostructures. These heterostructures are grown by molecular beam epitaxy (MBE) and demonstrate the high mobility available in any material.

The heterostructure is formed by epitaxially growing AlGaAs onto a GaAs crystal. Due to the extremely similar lattice constants between GaAs ($565.35pm$) and AlAs ($566.2pm$), GaAs and AlGaAs create a nearly perfect, strain-free and defect-free interface. To create the 2DEG however, we require some free electrons which are provided by doping the AlGaAs layer with Silicon in a process called modulation doping. Unlike normal doping processes such a diffusion or implantation, modulation doping uses in single atomic layer of Si atoms deposited in the MBE process. This has the unique effect of concentrating all the immobile donors in a single layer far from the interface. GaAs has a larger electron affinity than AlGaAs though, meaning the free electrons tend to migrate to the GaAs layer.

The separation of charge between the positive Si donors which are stuck in place far from the interface and the negative electrons which migrate to the GaAs region, results in an electric field between the two regions of charge. Since the donors are stuck in a thin layer far from the interface, the field across the AlGaAs is constant. However, the mobile electrons, although preferring to remain in the GaAs due to the lower band energy, are free

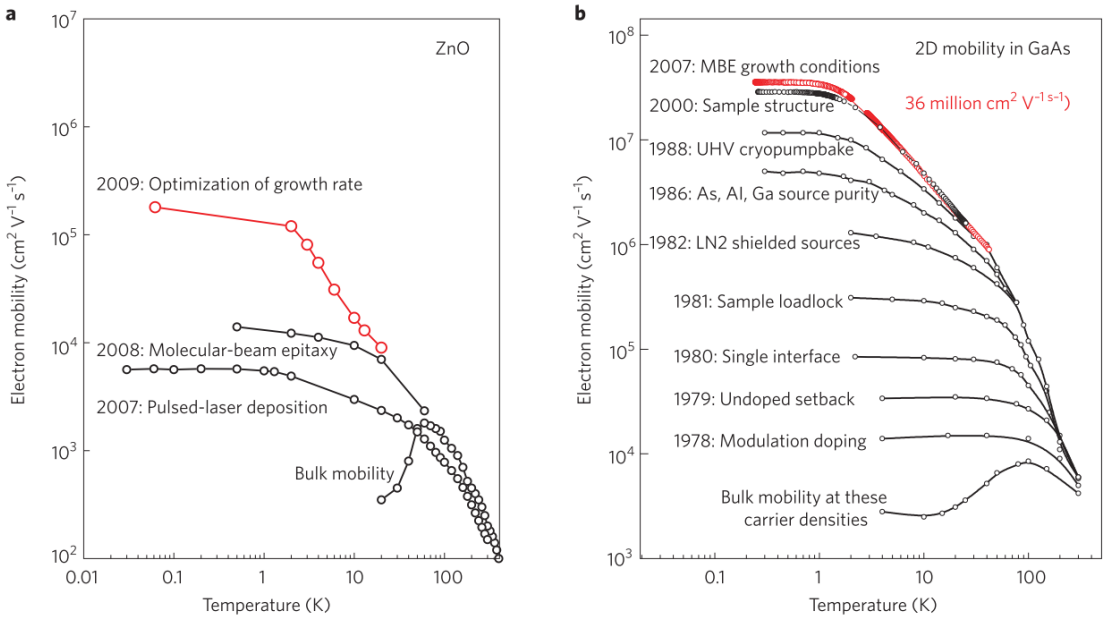

Figure 3.1.1: The progress of mobility in Gallium Arsenide 2DEGs over the years is shown in b) to its current peak of $3.6 \times 10^7 cm^2/V \cdot s$. For comparison, the mobility of ZnO structures is shown in a)[1].

to move within this structure. The result can be seen in 3.1.2 as they will naturally tend to stick as close to the interface as possible. The gradient in the electric field causes the band to bend, showing the energy well which the electrons will reside in. This is the 2DEG, the well created this way is a very thin layer, which at low temperatures will become a quantum well. The actual thickness of the well in the $\hat{z}$ direction is determined by electron density and the details of the confining potential.

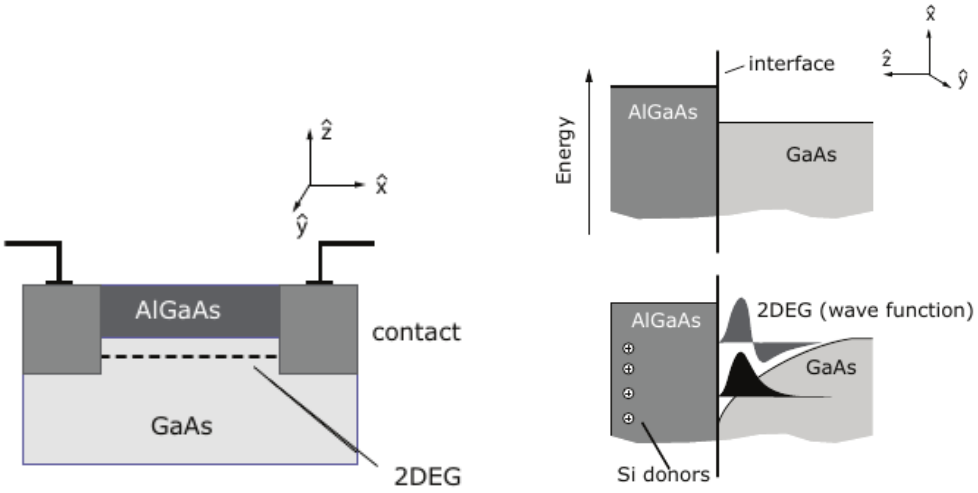

(a) Schematic of a typical GaAs/AlGaAs heterostructure configuration

(b) The conductance band in GaAs is slightly lower than in AlGaAs so the free electrons from Si donors congregate in the GaAs region. This charge creates and electric field causing band-bending in the GaAs region, creating a triangular shaped well.

Figure 3.1.2: Figures showing the basic principle of a GaAs/AlGaAs heterostructure [2].

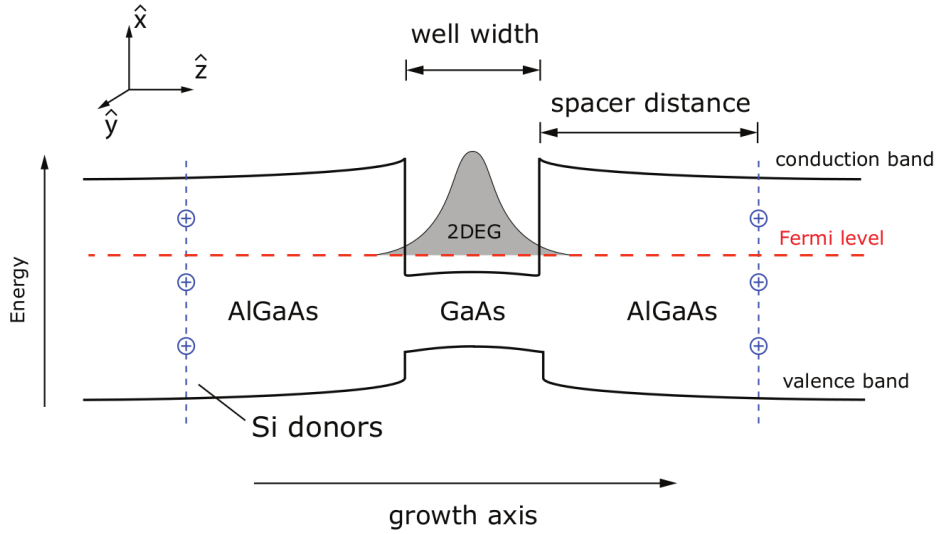

Figure 3.1.3: Schematic of the AlGaAs/GaAs/AlGaAs well structure. The device is constructed symmetrically to achieve a square well structure [2].

Thanks to the clean interface, electrons in this well also experience extremely little scattering. The modulation doping technique also is important here, as it keeps the donor impurities far from the interface. It is these features which allow the GaAs/AlGaAs heterostructure to achieve unprecedented electron mobilities and observe new physics.

Further optimizations are also available as shown in figure 3.1.3. To achieve greater control over the shape of the wavefunction, it is usual to create a square well using a thin GaAs layer and symmetric heterostructures. In this case, the shape of the square well is illustrated as very box like, and the wavefunction is well approximated by the classic 'particle-in-a-box' exercise. More complex structures such as double wells are also commonly used in experiments, although are outside the scope of this work.

In this experiment we used 14 different samples from two different wafers. The wafers were grown at The Center of Integrated Nanotechnologies (CINT) at Sandia National Laboratories by Dr. John Reno, and are known as VA142 and VA150. The structure and growth parameters of each wafer are summarized in the tables below.

Layer	Material	Thickness	Dopant	Density	Temp	Comment
1	GaAs	10.0 nm	undoped		630°C	Cap
2	AlGaAs	10.0 nm	undoped		630°C	24%
3	delta-dope	0.0 nm	Si (n)	2.00E+12	630°C	
4	AlGaAs	10.0 nm	undoped		630°C	24%
5	delta-dope	0.0 nm	Si (n)	2.00E+12	630°C	
6	AlGaAs	55.0 nm	undoped		630°C	Upper Setback 24%
7	GaAs	30.0 nm	undoped		630°C	Quantum Well
8	AlGaAs	55.0 nm	undoped		630°C	Lower Setback 24%
9	delta-dope	0.0 nm	Si (n)	2.00E+12	630°C	
10	AlGaAs	10.0 nm	undoped		630°C	24%
11	delta-dope	0.0 nm	Si (n)	2.00E+12	630°C	
12	AlGaAs	88.0 nm	undoped		630°C	24%
13	AlGaAs	10.0 nm	undoped		630°C	x35 55.2%
14	GaAs	3.0 nm	undoped		630°C	
15	GaAs	100.0 nm	undoped		630°C	

Table 3.1: The growth sheet for VA142. The most important parameters from this table are the well depth (100nm) and the location and density of the two delta-dopes (55 and 65 nm from the interface in both directions, all $2 \times 10^{12}/cm^2$)

Layer	Material	Thickness	Dopant	Density	Temp	Comment
1	GaAs	10.0 nm	undoped		630°C	Cap
2	AlGaAs	98.0 nm	undoped		630°C	24.1%
3	delta-dope	0.0 nm	Si (n)	1.00E+12	630°C	
4	AlGaAs	75.0 nm	undoped		630°C	Upper Setback 24.1%
7	GaAs	30.0 nm	undoped		630°C	Quantum Well
8	AlGaAs	95.0 nm	undoped		630°C	Lower Setback 24.1%
9	delta-dope	0.0 nm	Si (n)	1.00E+12	630°C	
12	AlGaAs	98.0 nm	undoped		630°C	24.1%
13	AlGaAs	10.0 nm	undoped		630°C	x35 54.1%
14	GaAs	3.0 nm	undoped		630°C	
15	GaAs	100.0 nm	undoped		630°C	

Table 3.2: The growth sheet for VA150. The most important parameters from this table are the well depth (198nm) and the location and density of the two delta-dopes (75nm from the interface on top and 95 nm on the bottom, both $1 \times 10^{12}/cm^2$)

As evident from the growth sheets, there are a few differences between the wafers. Firstly, VA142 has a much shallower well. This is significant as when the gates are placed on top, the distance between the 2DEG and the applied potential will greatly affect the electrostatic environment. The other differences are the level of doping, VA142 has four delta-dopes to VA150's two, and each is twice as strong. This should result in more electrons in the system, although it is uncertain how this affects the density of the 2DEG.

3.1.2 Device Structure

While the wafers by themselves are excellent high mobility samples which can show interesting quantum states, for this work we are interested in making one-dimensional devices. We start with the 2DEG as they are well understood and straightforward to fabricate, thus leaving only the challenge of eliminating one further degree of freedom for the electrons. To do this, metal gates were patterned on the surface, as in figure 3.1.4. The devices were fabricated at CINT by McGill Ph.D student Dominique Laroche and then shipped to McGill for testing.

When a negative potential is applied on these gates, the areas directly below will have their conduction band energy raised beyond the fermi level, resulting in the depletion of electrons. As the potential is gradually increased, the $\sim 1\mu m$ region between the gates will be depleted, until it becomes wide enough for only a single electron mode. For a sense of

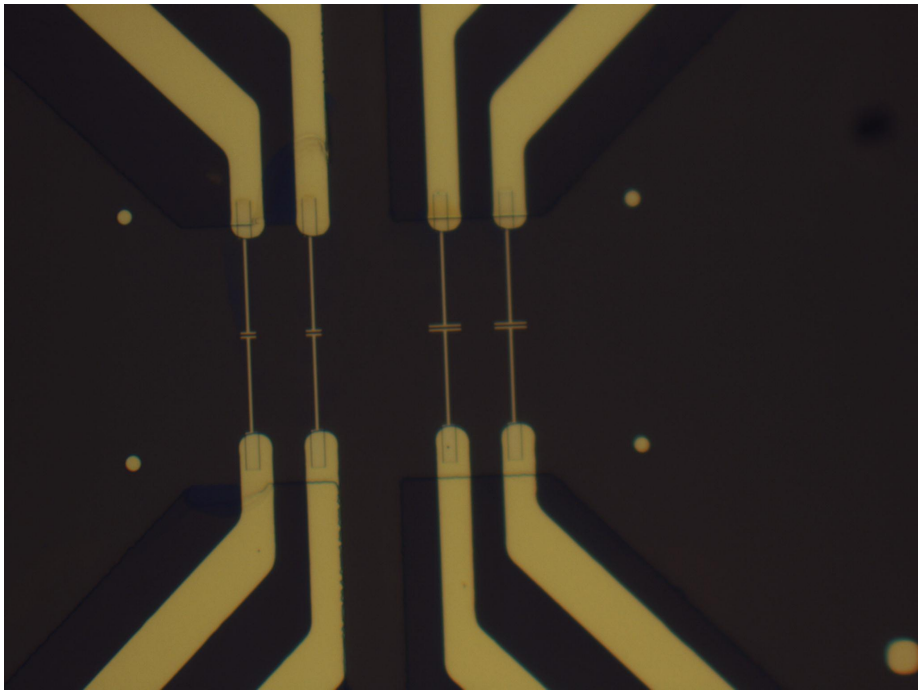

Figure 3.1.4: VA142-3. A set of four quantum wires patterned on the surface of wafer VA142. Wires are $1\mu m$ and $5\mu m$ in size

scale, this occurs on the order of 100nm. Thus we end up with a situation like that shown in figure 3.1.5

Contacting the 2DEG and the surface of the chip is a non-trivial task. It is desirable for the contact to be as non-invasive as possible and have high efficiency. Contact is made by diffusing indium from the surface to the 2DEG. This method preserves the 2DEG mobility, but is liable to create finicky contacts which couple to the 2DEG in unpredictable ways. Figure 3.1.6 illustrates the ohmic contacting method.

While typically these sorts of devices are Quantum Point Contacts on the order of $0.5\mu m$ to $1.5\mu m$, our devices are quantum wires, $5\mu m$ and over. This means we are attempting to create a uniform constriction, rather than simply a point constriction and this will be extremely dependent on the electrostatic environment and the accuracy of the lithography. Superior 2DEGs also play a significant role in creating longer constrictions [3].

Additionally, it should be mentioned that although the wafers are extremely high mobility, on the order of $10^6 cm^2/V \cdot s$, this is significantly reduced by the use of lithography. The reason for the defects is not exactly clear, however in general any processing introduces

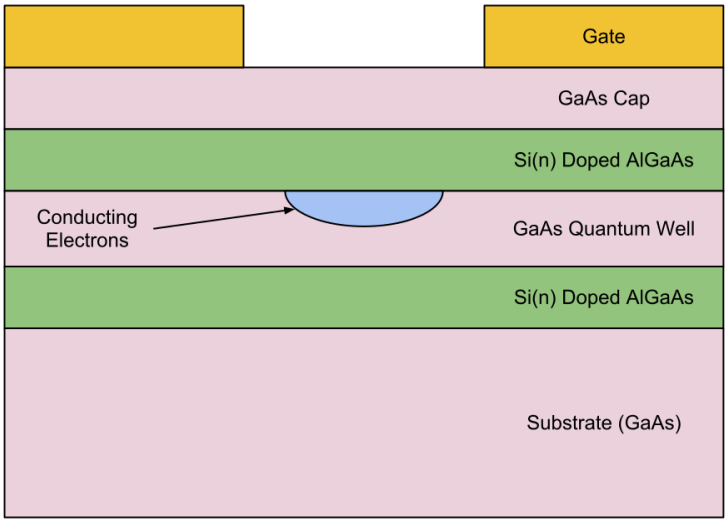

Figure 3.1.5: Schematic of a quantum wire which is formed by split metallic gates on the surface of the 2DEG.

defects which increase scattering in the 2DEG. While this sort of processing makes it very difficult to observe fragile states such as the 5/2 FQHE, the requirements for quantum wires are less strict.

Figure 3.1.6: Ohmic Contact Schematic

3.1.3 Parameters

All the devices used in experiments will be listed in table 3.3, with their varying characteristics.

Sample	Contact	Depth	ALD	Gate	Wires
VA142-1	Ge-Au-Ni-Au	100nm	No	Ti-Au	1um (x4), 5um (x4)
VA142-2	Ge-Au-Ni-Au	100nm	No	Ti-Au	1um (x4), 5um (x4)
VA150ALD2	Ge-Au-Ni-Au	198nm	30nm	Ti-Au	1um (x4), 5um (x4)
VA150InSn1	In	198nm	No	Ti-Au	1um (x4), 5um (x4)
VA150InSn2	In	198nm	No	Ti-Au	1um (x4), 5um (x4)
VA161	Ge-Au-Ni-Au	100nm	No	Ti-Au	1um (x4), 5um (x4)
Second Batch	-	-	-	-	-
VA142-1	Ge-Au-Ni-Au	100nm	75nm	Ti-Au	5um (x2), 10um (x2), 15um (x2), 20um (x2)
VA142-2	Ge-Au-Ni-Au	100nm	75nm	Ti-Au	5um (x2), 10um (x2), 15um (x2), 20um (x2)
VA142-3	Ge-Au-Ni-Au	100nm	75nm	Ti-Au	5um (x2), 10um (x2), 15um (x2), 20um (x2)
VA142-4	Ge-Au-Ni-Au	100nm	75nm	Ti-Au	5um (x2), 10um (x2), 15um (x2), 20um (x2)
VA142-5	Ge-Au-Ni-Au	100nm	No	Ti-Au	5um (x2), 10um (x2), 15um (x2), 20um (x2)
VA142-6	Ge-Au-Ni-Au	100nm	No	Ti-Au	5um (x2), 10um (x2), 15um (x2), 20um (x2)
VA142-7	Ge-Au-Ni-Au	100nm	No	Ti-Au	5um (x2), 10um (x2), 15um (x2), 20um (x2)
VA142-9	Ge-Au-Ni-Au	100nm	No	Ti-Au	Variable Length Design (5um x8)

Table 3.3: Details of the quantum wire devices. Two batches were fabricated, the first on a variety of wafers, the second only on VA142. The ohmic contact material was a stack of Ge-Au-Ni-Au and some samples had an Atomic Layer Deposition (ALD) layer separating the contacts from the wafer surface. The ALD layer is intended to reduce tunneling from the contacts. The contacts were annealed to diffuse into the sample and create good ohmic characteristics. All the gates were created using a Ti-Au stack. Wire lengths ranged from 1-5μm in the first batch to 20μm in the second batch. VA142-9 (Second Batch) was created with four 5μm wires close together in series, so that a wire of variable length could be created.

3.2 Description of Fridges

To perform experiments in this work, we used three low temperature systems, each with uniquely suited capabilities. Given the large number of samples to test, it was determined to by most practical to test wires very quickly at relatively high temperatures. This allowed us to screen samples and find the wires which performed the best. By 'best' we mean wires which first of all, had working gates, but also displayed consistent pinch-off points, small hysteresis and minor fluctuations in conductivity. It was found that many wires did not meet these criteria, likely indicating local defects in the wires and thus unlikely to display interesting physics. This strategy called for a fridge which is capable of quickly cooling samples to cryogenic temperatures as well as quickly warming them up. Preferably this fridge would have a large sample holder to allow for more samples to be cooled at once as well. For this purpose, a Variable Temperature Insert (VTI) from Janis Systems was used.

Once the samples were screened in the VTI system, it was desirable to test them at lower temperatures. For this purpose, two fridges were available, a 300mK helium-3 system and a 17mK dilution refrigerator. Both systems were used to characterize the quantum wires, with some samples being tested first on the ^{3}He system and then the dilution fridge, while others were put directly in the dilution fridge. The ^{3}He system's temperature of 300mK was useful for both prototyping and testing in which wires successfully displayed quantum behavior, however was not sufficient for the observation of unique physics. Only the dilution refrigerator with its ultra-low temperature was capable of that. Due to its impressive capabilities though, the dilution refrigerator is both difficult to operate and in high demand. This led to limited opportunities for use and in some cases samples had to be tested at higher temperatures than desired.

3.2.1 VTI

The Variable Temperature Insert (VTI) is a low temperature system designed for rapid testing. It has a temperature range of 1.5-300K and is unique among the available systems due to the removable insert. This allows the fridge to remain at the liquid helium temperature of 4K, while the insert which holds the samples is removed and samples are added or removed. This ability gives the VTI significantly higher throughput than any other fridge. While other systems take multiple days to cool samples, multiple samples can be tested in the VTI in a single day.

Once the insert is placed and sealing in the VTI cooling is done through flowing helium

gas in the chamber. This means the sample is directly in contact with the cooling interface which eliminates a source of many problems in cooler fridges. The cooling power in the fridge comes from evaporative cooling. Briefly, the sample tube is constantly pumped, meaning it is generally under vacuum and a small amount of liquid helium is leaked into the sample tube. As the liquid evaporates into the vacuum, the high energy particles are removed, resulting in the temperature of the liquid dropping. On a more macroscopic level, we can look at the liquid requiring energy from the environment to achieve the liquid-to-gas transition, resulting in the temperature of the environment reducing. While this method is sufficient to reduce the temperature of a sample below 4K, it is ultimately limited. Commercially available systems, like the VTI, struggle to get below 1.6K using evaporative cooling of helium. While this temperature is generally not sufficient to observe new phenomena, it is extremely effective for testing a prototyping purposes. A drawing of the VTI is included in figure 3.2.2.

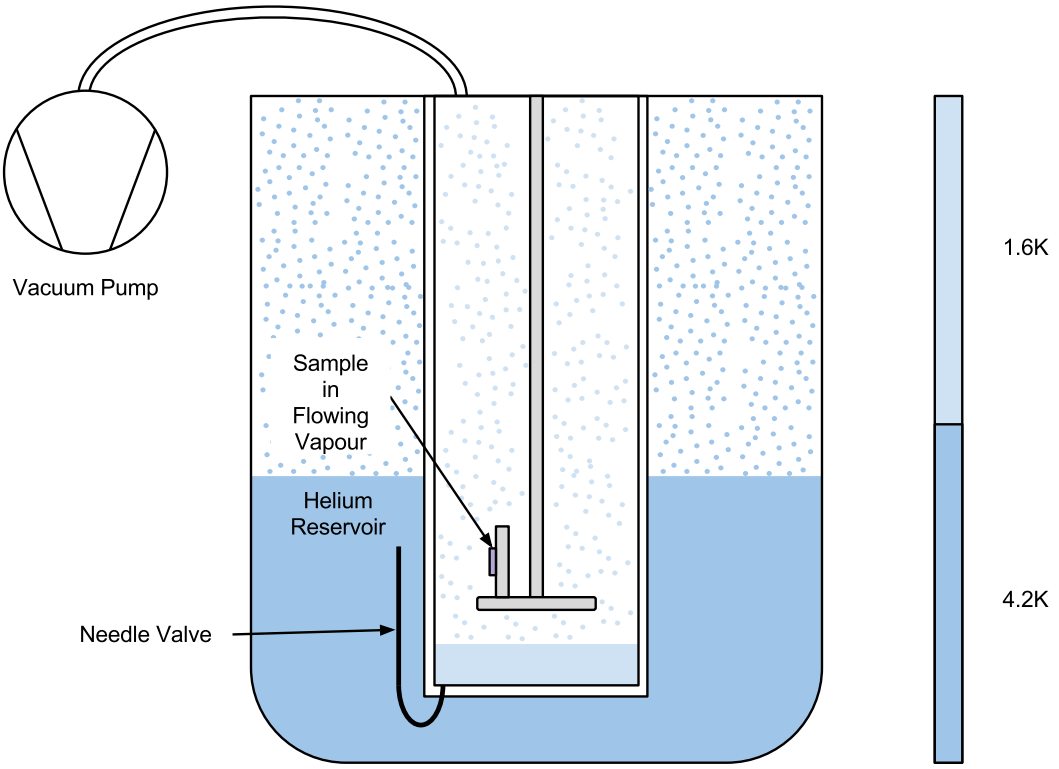

Figure 3.2.1: Cartoon Schematic of the VTI Cryostat.

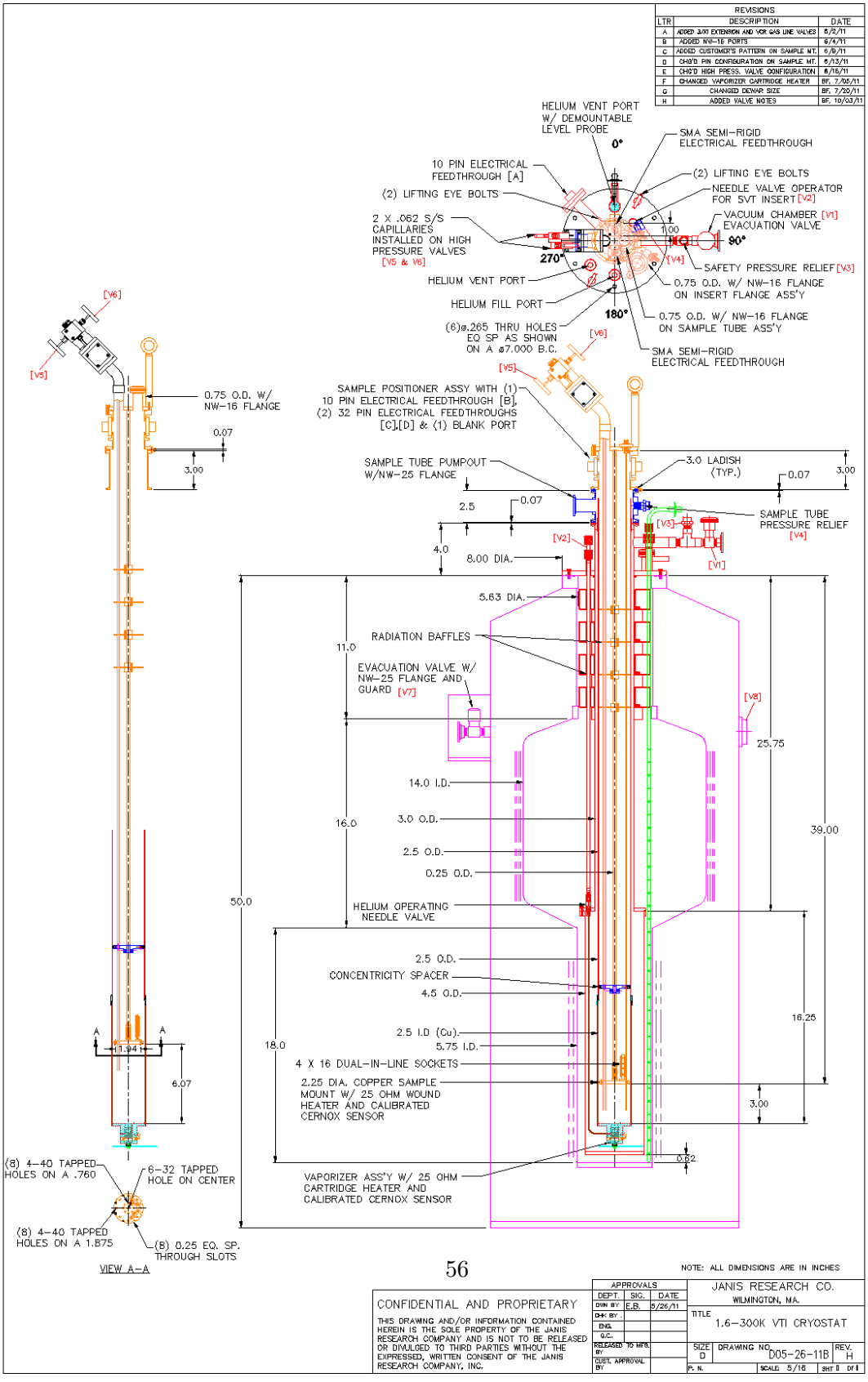

Figure 3.2.2: Schematic of the VTI Fridge

3.2.2 Helium-3 Cryostat

The helium-3 (^{3}He) cryostat is a fridge that works on similar principles to the VTI, but is capable of reaching 300mK. While the 300mK temperature is more conducive to quantum behavior, such as the quantization of conductance, is visible, it requires two days to cool down and samples cannot be easily switched. For this reason, the ^{3}He fridge is better suited to cooling samples which have already shown to have been good candidates in the VTI.

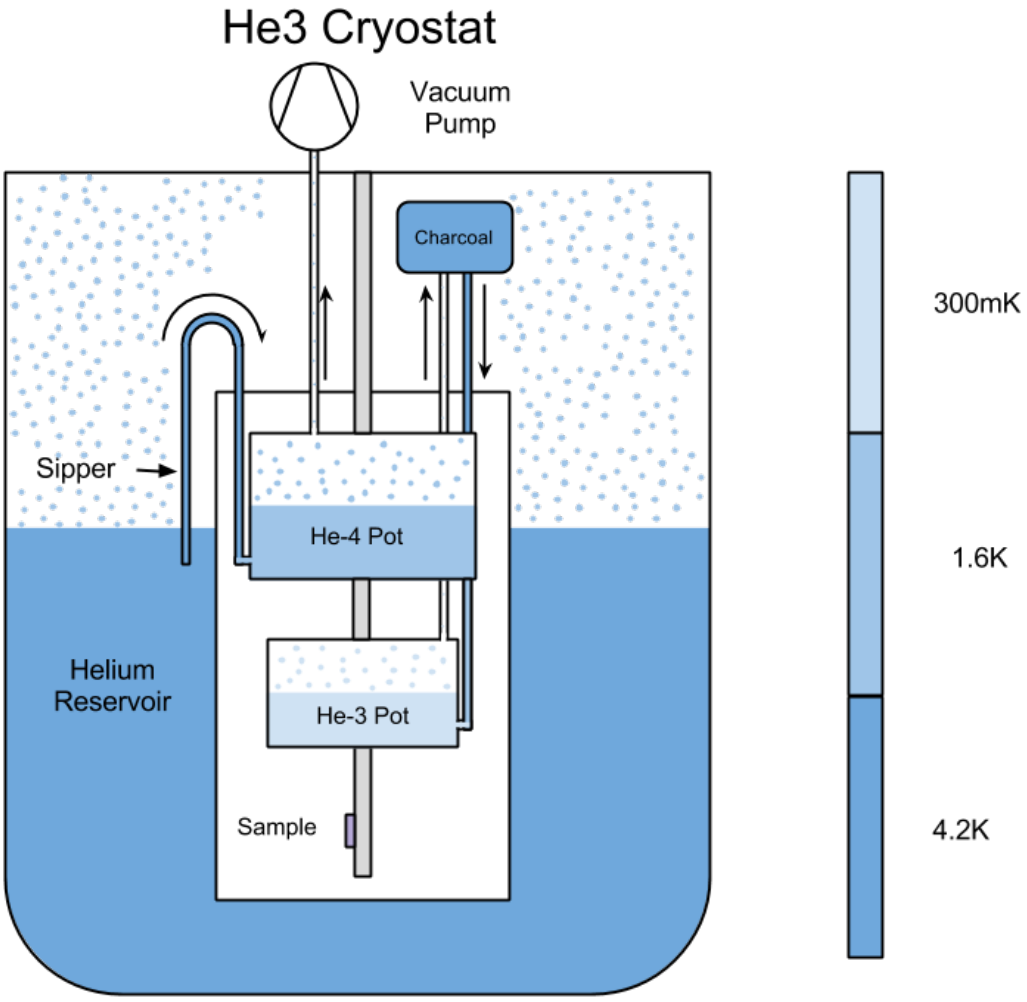

Figure 3.2.3: Cartoon Schematic of the He3 Cryostat.

The ^{3}He fridge works on the same principle as the VTI, through evaporative cooling, however rather than using ^{4}He, by far the most common isotope, it uses evaporative cooling of rare ^{3}He to achieve its low temperature. Because the ^{3}He isotope is significantly lighter than the ^{4}He isotope, it requires less energy to vaporize and evaporation can occur at much lower temperature than ^{4}He. Commercially available ^{3}He fridges like ours from Janis Systems typically reach about 300 mk. Because ^{3}He is extremely expensive however, it cannot be used inside an open system such as the VTI. Instead it is used in a closed system where the return line goes back to the helium reservoir. Rather than a typical vacuum pump, a charcoal which absorbs ^{3}He gas is used to pump the ^{3}He pot. Additionally, it is much more efficient to use ^{3}He to do only the last stage of cooling, since its possible to reach 1.6K using much more abundant ^{4}He. Thus the system is staged, with each stage reaching a lower temperature.

This fridge has a liquid nitrogen jacket which reduces the heat load on the helium bath, reducing the fridge's helium consumption. The first cooling stage is the liquid helium bath, which cools the the fridge to 4.2K. Unlike the VTI where everything is placed in flowing gas, in the ^{3}He fridge the sample and tail are under high vacuum to prevent heating. The evaporative cooling is contained to small pots along the tail. There is two pots, the "1K pot" and the ^{3}He pot. The 1K pot is on top and provides most of the cooling power, condensing the ^{3}He as it comes from the reservoir. The 1K pot is not thermally anchored to the tail or the ^{3}He pot, as it would cause heating. The second stage is the ^{3}He pot, which contains ^{3}He undergoing evaporative cooling. This pot gets below 300 mK and is in thermal contact with the tail and the samples.

During these experiments a new coin-silver tail was installed on the system to ensure excellent thermal contact for all the samples below the ^{3}He pot. While this fridge is significantly colder than the VTI, it is more difficult to use and takes a long time to cool down. However, it is useful for observing quantum phenomena in a way which the VTI is not, and can be used for some experiments. In addition to its significantly lower temperature, the ^{3}He fridge features a 8T superconducting magnet. This allows for many experiments which the VTI does not, primarily Hall Effect measurements which can provide information about the samples such as mobility and density.

3.2.3 Dilution Refrigerator

The dilution refrigerator can reach temperatures below 23 mK with significant cooling power. Achieving such low temperatures requires several cooling stages, including the previously discussed evaporative cooling of ^{3}He and ^{4}He. Cooling below 300mK is achieved by exploiting the entropy of mixing between the two isotopes of helium in the liquid phase.

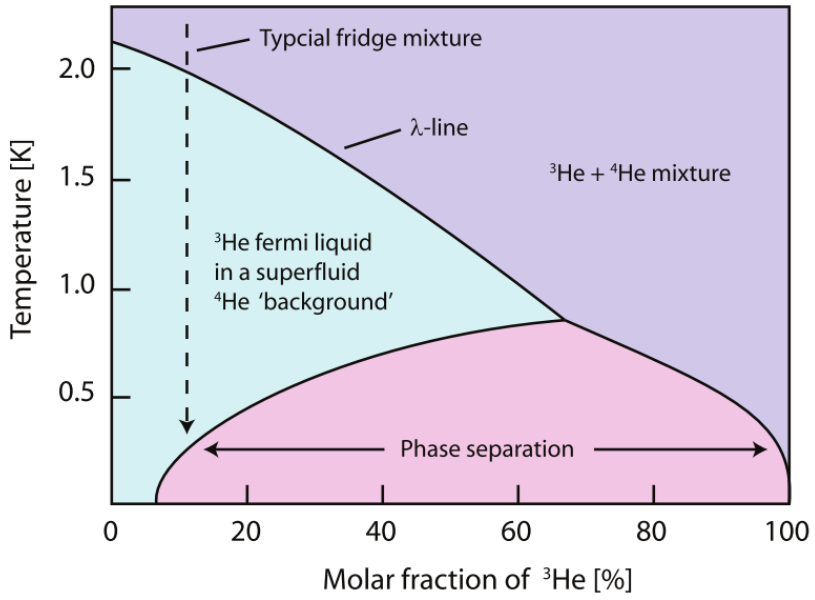

Figure 3.2.4: Phase Diagram for liquid helium mixtures. Dashed line shows a cooling curve for a mixture of 10% ^{3}He [2].

A mixture of ^{4}He and ^{3}He at low temperature will abruptly separate into two phases — a ^{3}He-rich phase "concentrated" phase floating on top and a ^{3}He-poor "dilute" phase on the bottom. As the mixture is cooled, the concentrated phase approaches 100% ^{3}He while the dilute phase reaches a steady-state concentration of 6.6% ^{3}He. Similar to the evaporative cooling process, when ^{3}He molecules cross the boundary from the dilute phase to the concentrated phase, some energy is absorbed. Unlike the evaporative cooling process however, this process depends on the quantum properties of the ^{3}He fermi-liquid and the ^{4}He bose-liquid [4]. The cooling power is easily determined however using the temperature of the mixture, T, and the molar flow rate across the boundary, $\dot{n}$.

$$\dot{Q} = 84\dot{n}T^2 \tag{3.2.1}$$

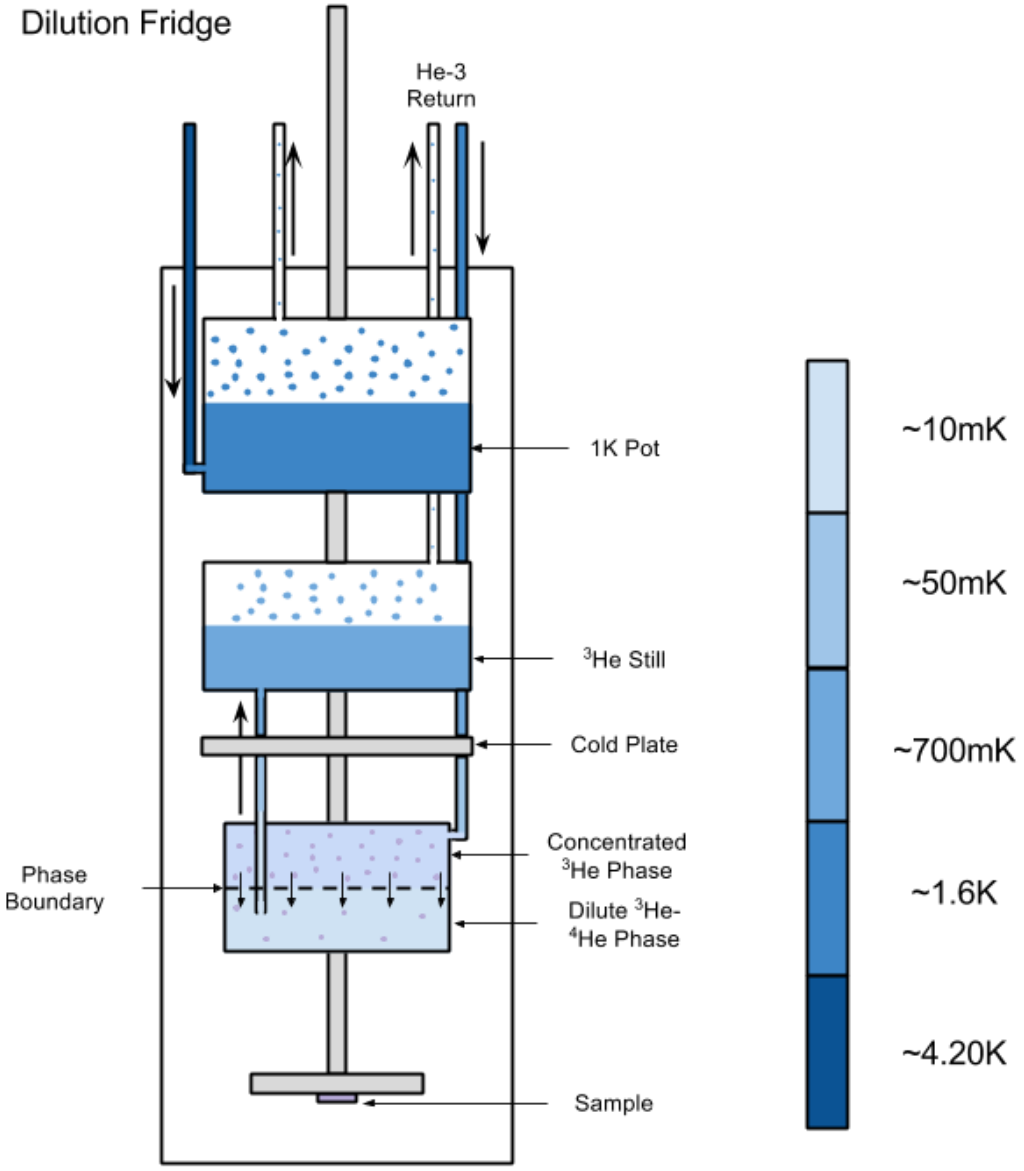

Figure 3.2.5: Schematic of the Dilution Fridge cooling process. Stages above 1.6K are not shown.

In addition to being able to reach extremely low temperatures, the dilution refrigerator features a 9T magnet, making the fridge capable of exploring many fascinating magnetic states. While the 1D state we are observing does not require an external magnetic field, it is nonetheless useful for characterization and necessary for NMR experiments. The field is applied perpendicular to the samples, all of which are exposed to a relatively uniform field. Although the field is most accurate for the bottom sample, deviations are minor according to the field map provided with the fridge.

3.3 Electronic Transport Measurements

Electronic transport measurements are the staple measurement of low temperature physics, particularly where quantum electronic states are concerned. Most cryogenic systems in our lab is equipped with electrical sample holders which connect the low temperature sample to the outside world for testing. Wiring also plays a key role in the thermalization of the sample and especially the electrons. Because the wires go all the way to room temperature, it is necessary to heat sink them at various cooling stages and ensure excessive heating is not directed to the sample. Since the wires are heat sunk at the lowest stage of cooling, they are one of the primary ways to ensure the sample is in thermal contact with the cooling stage. Often a dedicated heat sink wire is also connected the sample, but ensuring good thermal contact of the wires is very important as they are directly connected to the 2DEG, which has an incredibly low heat capacity. Typically, the wires are used to make electronic transport measurements. These measurements vary widely in frequency, voltage and current and will depend on the specific set up of the measurement.

3.3.1 Theory of electronic transport measurement

Making electronic transport measurements is a problem of surprising depth. While a resistor may be measured so easily with a multimeter, measuring the precise conductance of mesoscopic conductors with often bizarre behavior increases the complexity considerably.

A typical four point measurement has the current entering through one terminal, and leaving through another, while two additional terminals along the current path measure the local potential.

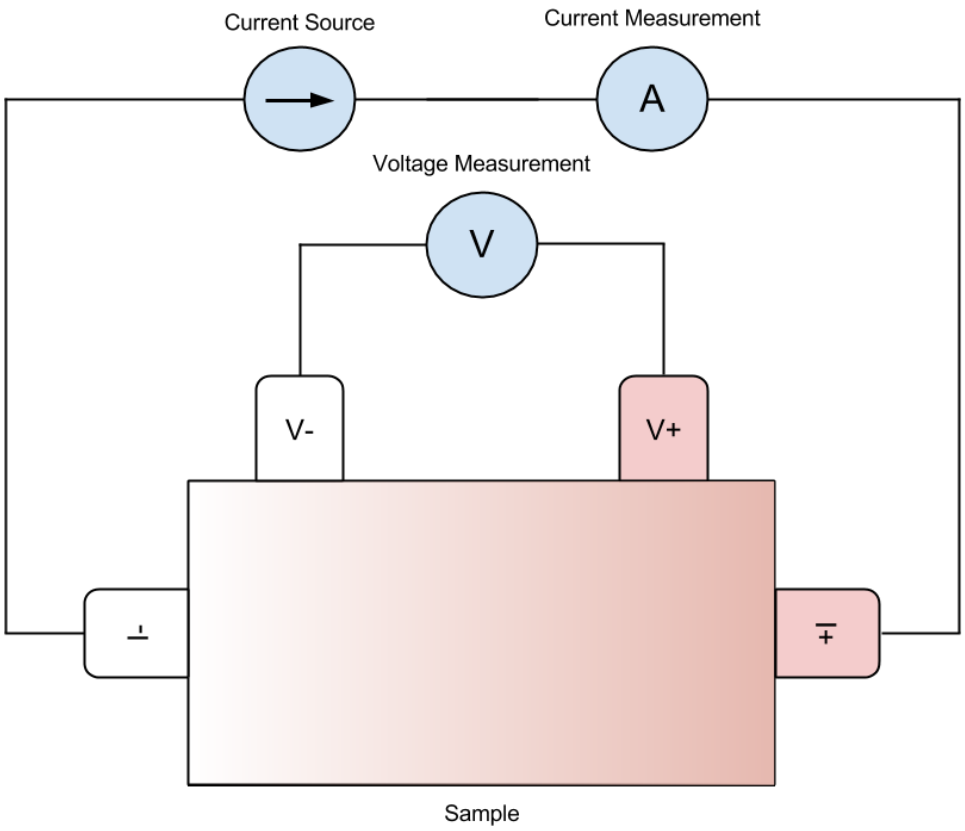

Figure 3.3.1: Classic Four Point measurement. The current enters through the I+ contact and travels through the contact resistance into the sample and out the I- contact. Both these contacts have some contact resistance which affects the real potential on the sample. The voltage is measured at V+ and V-. The contact resistance doesn't affect the voltage measurement, because the impedance of the voltmeter is incredibly high relative to the contact resistance.

Taking the approach of Landauer, the current should be equal to,

$$I = (2e/h)MT\Delta\mu \tag{3.3.1}$$

where M is the number of modes, T is the transmission probability and $\Delta\mu$ is the difference in potential. Thus the four-terminal resistance should be,

$$R_{4t} = \frac{(\mu_{P1} - \mu_{P2})/e}{I} = \frac{h}{2e^2 M}\frac{1-T}{T} \tag{3.3.2}$$

In practice however, probes are not identical and do not couple identically to the states.

The microscopic profiles of the contacts will typically vary greatly by contact and will affect the potential experienced by the probe. For this reason, different configurations of contacts must be tested to discover the best one. Additionally it leads to small deviations in the measurement, for example in measuring the quantized conductance of QPCs.

Mesoscopic transport measurements are also highly sensitive to quantum interference. A scatterer near a probe could easily result in destructive quantum inference causing a probe to measure a different potential. This is a potent reminder that we are not dealing with simple conductors here, but quantum conductors. Like other effects, this sort of problem must be dealt with mainly through trial and error.

3.3.2 Measurement Circuit

Quantum Wires and Quantum Point Contacts offer additional challenges to those previously discussed. This arises mainly from the fact that the resistance of a quantum wire varies over a massive range as the gates create the constriction.

To avoid issues with Schottky barriers and similar mismatches in energy levels which would distort measurements, it is standard to perform conductivity measurements on mesoscopic samples using AC signals at very low frequencies and lock-in amplifiers. The lock-in applies a fixed frequency voltage signal to the circuit and then makes a voltage measurement at only that frequency, using filtering and the analog multiplication of sine waves. This technique allows lock-ins to make very accurate measurements in noisy environments — since a very narrow bandwidth is measured and the technique is phase-sensitive, virtually all the noise which would appear in a simple oscilloscope-type measurements is absent.

Virtually any semiconductor device can be destroyed by a large voltage or current and this is doubly true for mesoscopic devices at low temperature. Because the number of electrons in the system is extremely low and the 2DEG is virtually a perfect conductor, large current and voltages can very easily destroy the sample. 1D quantum wires are particularly vulnerable as they are capable of conducting an extremely small amount of current. Avoiding large currents and voltages is paramount and is made more difficult by the huge variability in a quantum wire. If the circuit was created to ensure a small constant current, the voltage would become extremely high as the wire pinches off. Conversely, a circuit designed to maintain a small constant voltage would cause very high current when the sample is at low resistances.

To overcome this, a measurement circuit was designed which would avoid both these

problems.

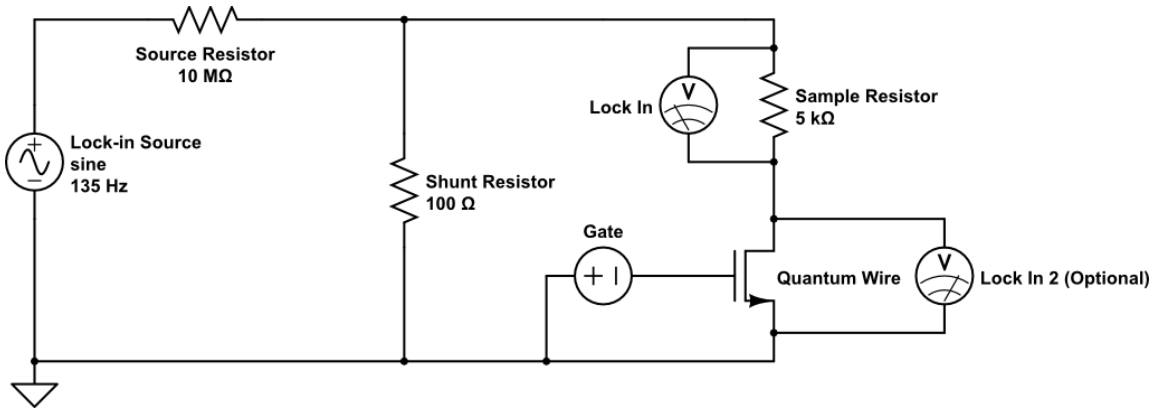

Figure 3.3.2: The circuit used to measure the conductance of quantum wires

The first circuit element is a source resistor, which severely limits the current to the sample. Typically the lock-in was operated at 5V, which meant with the $10\,M\Omega$ resistor, the current to the circuit was 500 nA. The sample was placed in series with a $5\,k\Omega$ resistor and then in parallel with a $100\,\Omega$ resistor. The effect of this is that the resistance of the right half of the circuit is determined by,

$$R = \left(\frac{1}{100\Omega} + \frac{1}{5000\Omega + R_S}\right)^{-1} \approx 100\,\Omega. \tag{3.3.3}$$

The $5\,k\Omega$ resistor is quite large compared to $100\,\Omega$ so in parallel the resistance is nearly exactly $100\,\Omega$, especially when R_s is large. This means that the voltage at that node is never greater than $50\,mV$, regardless of how large the sample resistance becomes. Thus we have solved the issue of avoiding large voltages on the sample.

As for avoiding high currents, the $100\,\Omega$ resistor and $5\,k\Omega$ resistors both address this. When the sample resistance is very low, the $5\,k\Omega$ resistor protects the sample, causing $\sim 98\%$ of the current to flow though the shunt resistor. Thus the current in the sample never exceeds $10\,nA$ and it will helpfully reduce as the resistance increases. For example a single conductance channel ($2e^2/h \rightarrow 12.9\,k\Omega$) would only conduct about $3\,nA$ in this circuit arrangement.

To make a two point measurement in this circuit, we measure the current going into the sample. Since we know that the voltage at the node is always $50\,mV$ or so, we can get a reasonable estimate of the sample resistance by measuring the voltage across the sample

resistor and treating it as a voltage divider.

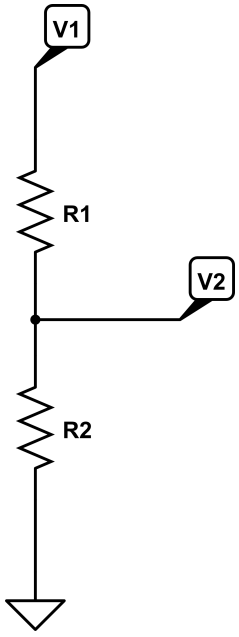

Figure 3.3.3: Voltage divider circuit. A voltage (V1) is applied at the top and V2 is measured at the centre

In our case, what we actually measure is $\Delta V = V_1 - V_2$ and we can solve for the sample conductance, which is G_2 in this case.

$$G_s = \frac{1}{R_2} = \left(\frac{V_1}{(V_1 - \Delta V)} - 1 \right) \cdot \frac{1}{R_1}. \tag{3.3.4}$$

This formula does not account for the 100Ω resistor however that causes only a small error. The larger problem is that it is a two point measurement which does not account for contact resistance. Using a second lock-in, we can perform a four point measurement which will avoid both this issues.

The four point measurement measures both the voltage over the $5k\Omega$ resistor and directly probes the voltage on the sample. In this case, no assumptions are necessary, the voltage drop over the $5k\Omega$ resistor directly provides the current going into the sample while the voltage probes measure the potential drop over the sample. Using the four point technique, the sample resistance is determined to be,

$$G_s = \frac{V_1/5k\Omega}{V_2}, \tag{3.3.5}$$

where V_1 and V_2 now refer to the measured values of the two lock-ins. In general, the four point technique is superior, but requires more equipment. Thus in some cases, a two-point measurement was made when quantitative accuracy was deemed not to be crucial.

3.4 Cold Filter design and fabrication

To observe quantum states in electronic systems, it is critical that the actual electrons in the system are isolated from possible sources of heat. This means any thermal coupling to the hot environment must be removed and the sample should be heat-sunk to the lowest temperature stage of the fridge. The one unavoidable source of heat however, is the electrical contacts and wires themselves. Generally the wires are extremely well thermalized to the lowest temperature stage, however this cannot control for radiation which propagates through the wires. While the wires themselves inevitably have some capacitance which filters out radiation in the GHz range and above, the VHF to VLF (300MHz to 3kHz) can slip through to the sample. In typical applications this sort of radiation would never cause any sort of heating. However in the ultra-low temperature regime, far less energy is required to cause heating. Even more concerning, not only are we at ultra-low temperatures, but we are searching for fragile quantum states with slight energy gaps. All of these factors make experiments vulnerable to heating by radiation which would not normally be a concern.

For these reasons most low temperature experiments require the use of filtered wiring[5]. Additionally, the filters must be at low temperature so that they do not introduce an excessive amount of thermal radiation themselves. While some of the wires on the dilution fridge include filters, however the sample position which we had access to did not. All other fridges have no such filtering and thus do not prevent this sort of heating of the electrons. This proved to be a major difficulty in achieving the low electron temperatures required.

Given the requirement of using all three fridges, it was concluded that a project of developing effective filters, rewiring and installing them on each fridge and then troubleshooting the newly wired fridges would be an inefficient approach. Instead, we chose to build filters which could be integrated into sample holders. Thus the filters could be moved from fridge

to fridge with the sample, a more elegant approach. The downside of this approach was the arguably more difficult engineering challenge of constructing sample holders which can fit in the extremely constrained space, be compatible with the sockets and work at extremely low temperature. Several designs were tried in search of the best characteristics including ease of construction. The designs and results will be discussed here.

3.4.1 Π filters

The first filters used were room-temperature Π filters. These filters were places between the equipment and the fridge as an easy plug-in solution. The filter design is shown in figure 3.4.1

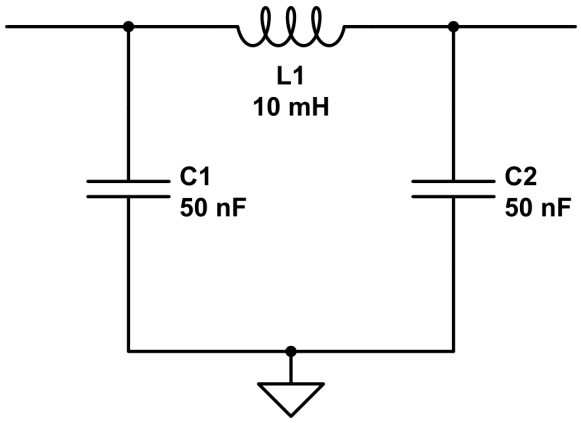

Figure 3.4.1: Pi-filters used at room temperature.

These filters have a theoretical frequency response as shown in figure 3.4.2

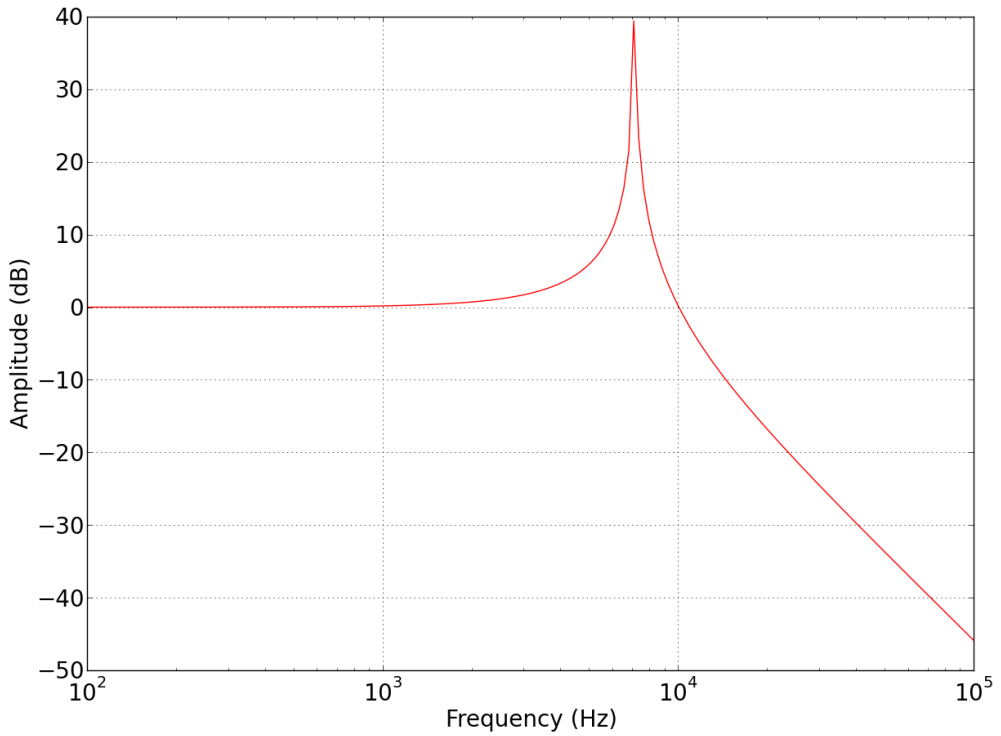

Figure 3.4.2: Theoretical Frequency Response of Room Temperature Pi-filter

The filters have a resonance at $\sim 7.2kHz$ and a $-3dB$ point at $\sim 11kHz$. As a relatively low frequency filter, they should filter out all the frequencies of concern. However, this characterization is not necessary representative of the actual performance in circuit. We have to account for the measurement circuit, as well as the fact that our probes are filtered. Thus, the real measurement circuit is going to appear as in figure 3.4.3.

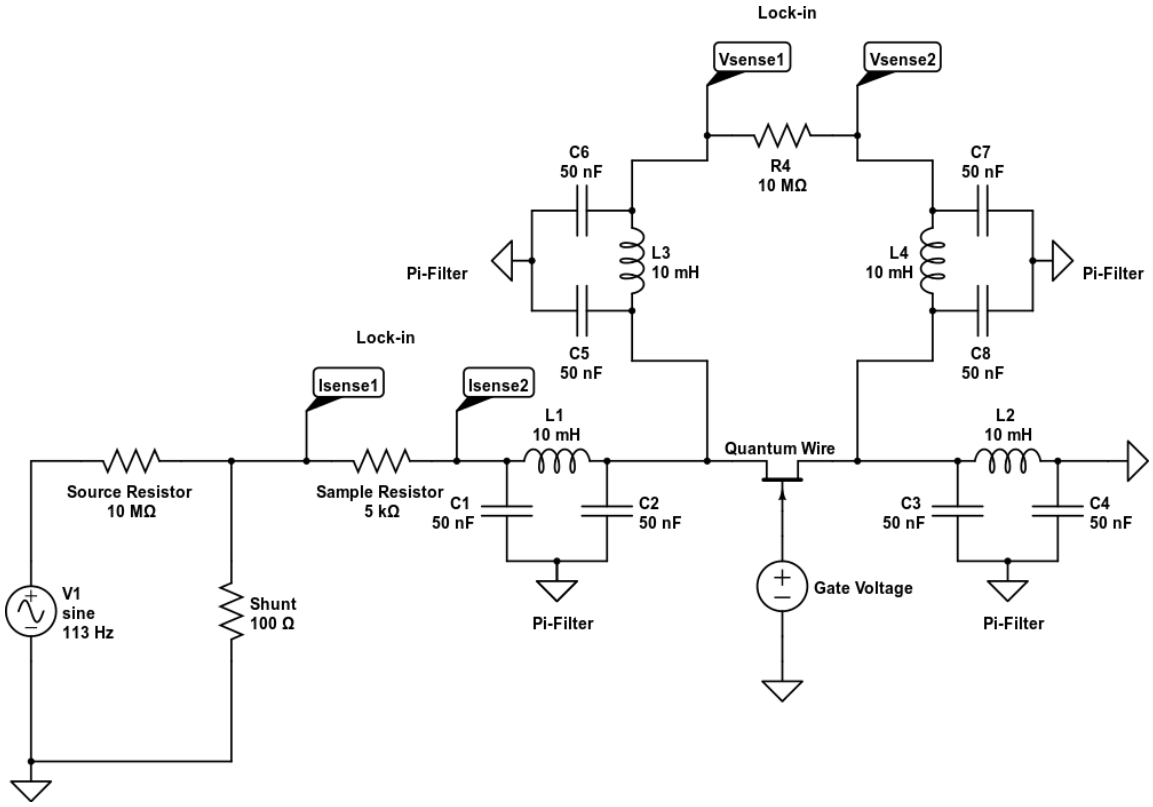

Figure 3.4.3: Measurement Circuit with Π Filters

As shown, the filters make the circuit very complicated. Additionally, our measurements become more difficult to interpret as we must account for the effect of the filters. This circuit is far too difficult to solve by hand, so we must resort to circuit simulation software. The approach taken was to simulate the the circuit at various values of resistance, corresponding to fractions of a quantized conductance, eg. $0.2\left(\frac{e^2}{h}\right), 0.4\left(\frac{e^2}{h}\right), 0.6\left(\frac{e^2}{h}\right), ...$ This resulted in a series of data points, showing the relationship between the measured values on our instruments and the actual conductance of the sample. To make things more straightforward, this relationship can be presented as a relationship between the measured conductance and the real conductance it corresponds to. The relationship is shown in figure 3.4.4.

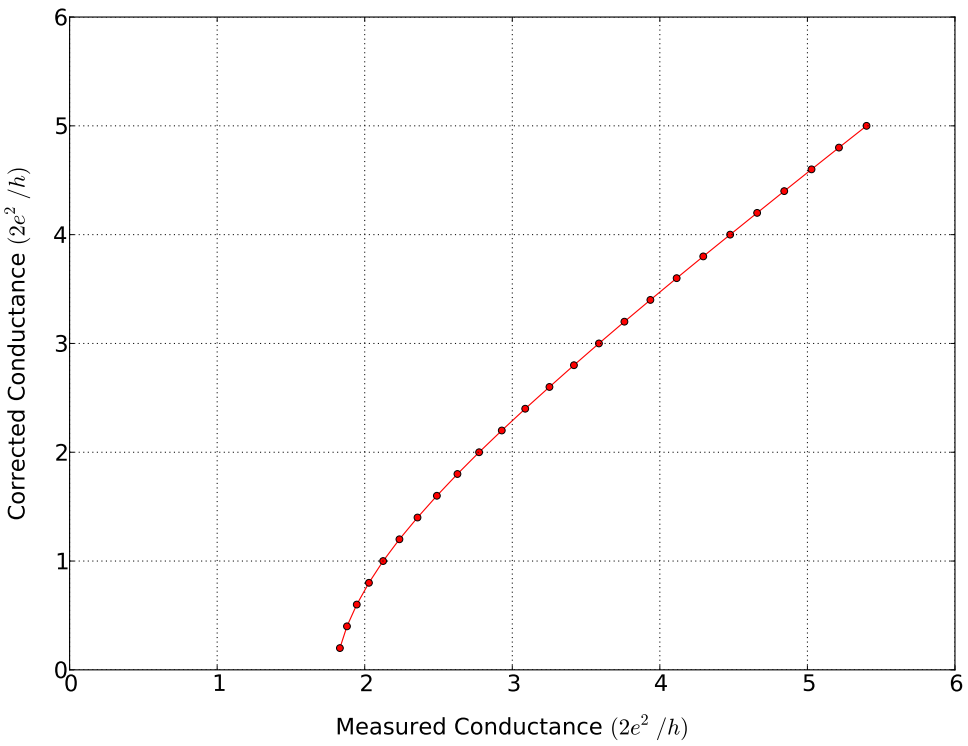

Figure 3.4.4: Mapping from measured conductance to corrected conductance

While the graph serves a good indication of how the measured conductances relates to the actual sample conductance, the question remains of how to apply this knowledge to actual data. For this task, a matlab script creates a cubic interpolation between the points of the curve. Using this cubic interpolation, we can calculate to reasonable accuracy the correction for any arbitrary conductance. This method results in a very accurate correction to the plots as shown by the corrections to quantized conductance plots. QPC conductance plateaus are accurate to within a few percent of the fundamental value and the resulting correction brings the plateaus nearly exactly in line with this value. This can be seen in figure 4.2.3 and we take this as experimental proof of this correction method.

Cold Π Filters

While the Π filters which were placed outside the fridge at room temperature showed good filtering characteristics, they do not protect against thermal noise produced closer to the sample. Thus, its desirable to have filters which are very cold, preferably at the temperature of the sample. Given the good filtering characteristics of the Π filters, it was determined that they would be miniaturized and attached to the sample holders, thus providing filtering as close the sample as possible. Additionally, this would allow the samples to be moved between systems with the filters still attached.

Fitting three component Π filters into such a small space however is a difficult engineering challenge. It was determined that the dilution refrigerator allowed for a maximum sample holder size of about $10mm$ x $15mm$, but virtually unlimited height, while the rest of the fridges were more generous with space. To fit the filters into this space, a stacked design was used. This design created a three-level sample holder, with components on each level as seen in figure 3.4.5

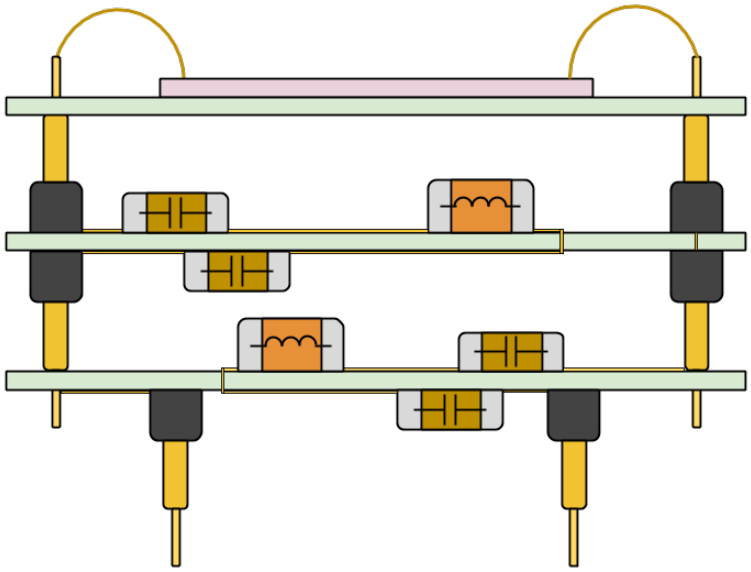

Figure 3.4.5: Schematic of Π Filtered Sample Holder. Each level filters four pins.

To create this sample holder, PCB boards were designed and ordered along with surface mount components. The PCB layout was done in eagle and the schematics are shown below.

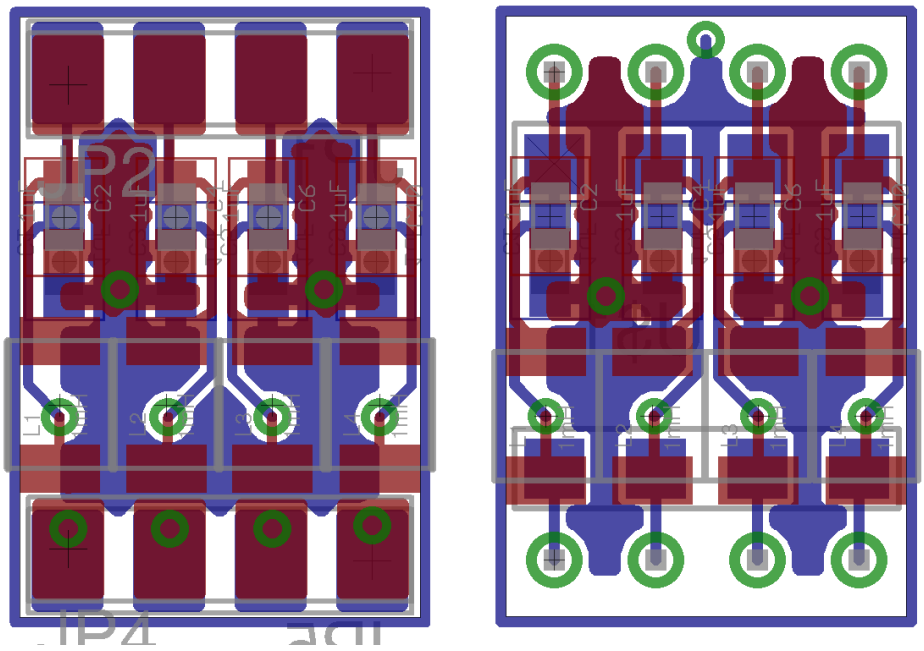

(a) The layout of the middle board of the sample holder. Contains four Π filters which filter the bottom four pins

(b) The bottom board of the sample holder. Contains four Π filters which filter the top four pins.

Figure 3.4.6: Eagle Schematics of the filtering boards. Blue corresponds to metal on the bottom layer and red is metal on the top layer. Green is vias which connect the bottom to the top. Each board has 4 complete Π filters.

While these cold filters share the same design principles as the warm Π filters, they use smaller, surface mount components due to space constraints. The size limits also affect the values of components available. The inductors are $1mH$, the largest available value, while the capacitors are selected to be $1uF$. This gives the filter a theoretical frequency response which is shown in figure 3.4.7. The resonance of this filter should be at $5kHz$ and the $-3dB$ point at $7.8kHz$.

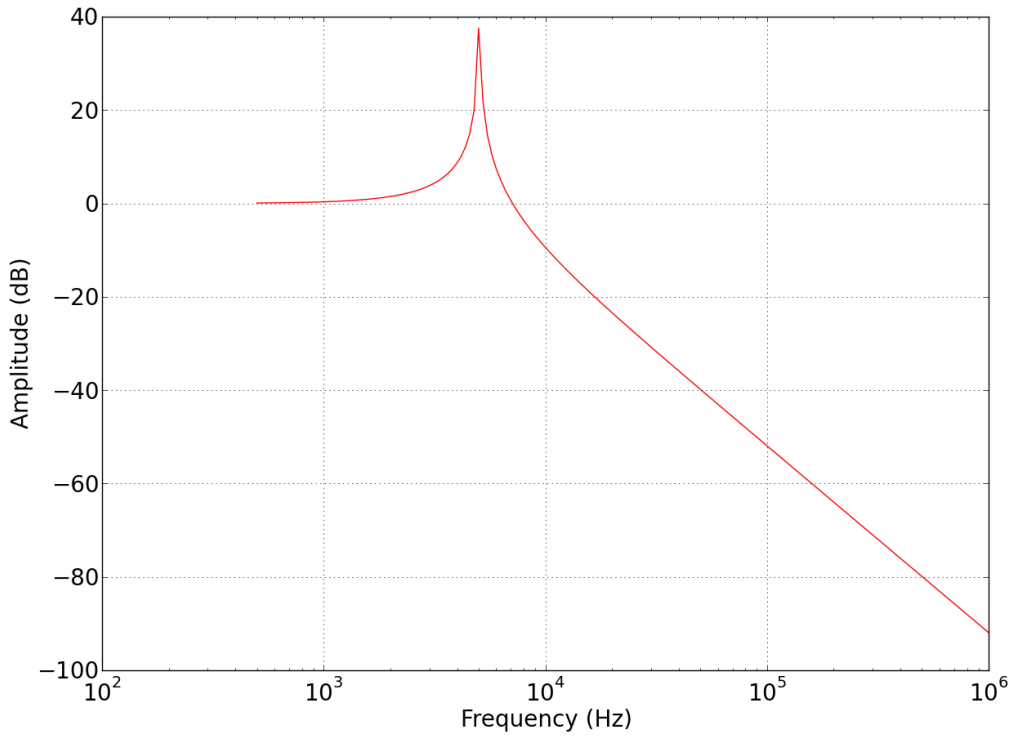

Figure 3.4.7: The theoretical frequency response of the cold Π filter

However, this makes a the unrealistic assumption that the components will not be affected by the extremely low temperature. While manufacturers do give temperature coefficients for component values, these are often unreliable and only valid to at most -55^oC in any case. Thus a component's value at low temperature is a matter of experiment.

3.4.2 RC Filters

The second filter design used was a significantly simpler RC filter. This has the advantage of requiring much less space than the Π filter design as only two levels are needed. It also reduces the complexity of the sample holder considerably, avoiding issues such as contraction and broken solder joints. Surprisingly, these advantages do not necessarily result in worse performance. While LC filters are second order filters and can have much steeper roll off than first order RC filters, in this particular application we are limited

by component size. In this case its impossible to acquire inductors which are both small enough and with enough inductance to provide good filtering.

An RC filter on the other hand, is not limited in this way. Although capacitor values are severely affected by temperature, resistors are much easier to deal with and come in virtually any value. This allows RC filters to be designed for virtually any level of capacitance. Even more conveniently, the measurement circuit already provides significant resistance — or more importantly, very low currents. Because of this, it turns out only a capacitor is required to make an effective RC filter. Thus, a bottom board with all 8 pins connected to $1uF$ capacitors is provides filtering to samples in this design. This design also addresses problems with the sample holders at low temperature. With the more complex boards, contact problems relating to thermal contraction were frequently experienced. These sample holders were designed to be more robust, to account for the thermal contraction and maintain electrical contact.

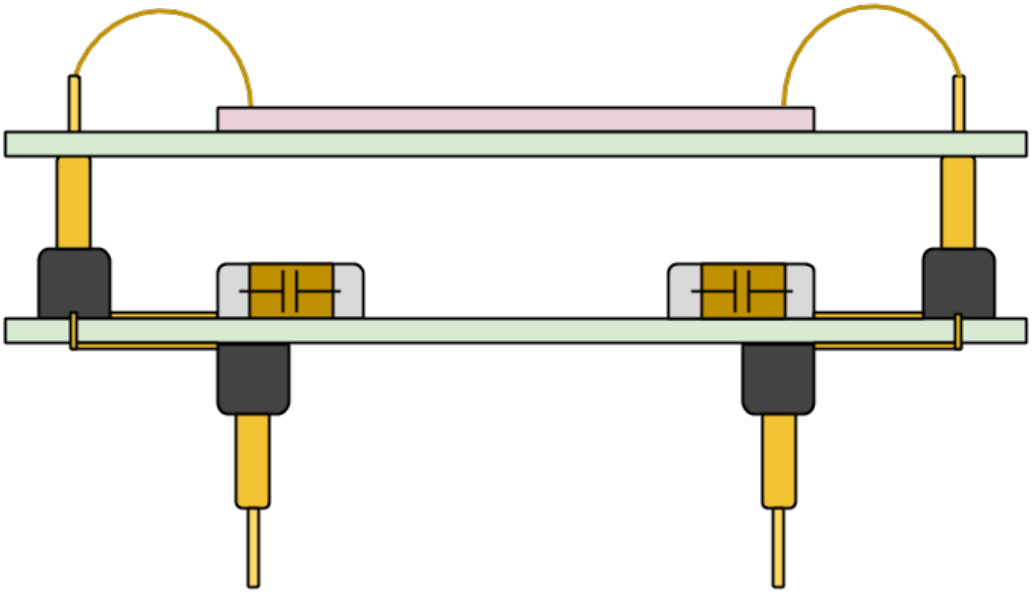

Figure 3.4.8: A diagram of the RC filtered sample holder. Each pin has a 1 uF capacitor connecting it to ground which provides the filtering.

In conjunction with the measurement circuit, this filter has a theoretical performance

shown in figure 3.4.9. This filter has a $-3dB$ point at $37Hz$. This is a very low cutoff frequency, but since the low temperature will significantly reduce the capacitance, its expected that the filter will end up with a cutoff point well above the measurement range.

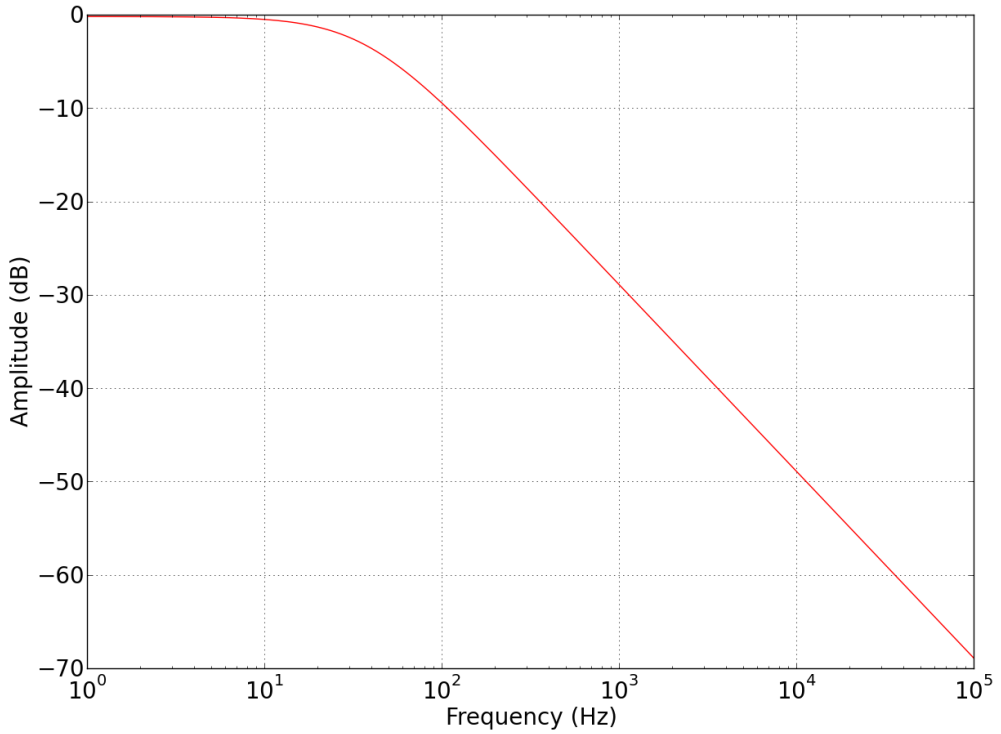

Figure 3.4.9: The theoretical response of the RC filter.

3.4.3 PCB Sample Holders

Making good electrical connections to mesoscopic conductors is a major challenge in experiments. For example, some contacts will tend to give better signals when used as voltage probes and some contacts will work better as current sources. These discrepancies in behavior are due to the microscopic environment near the contact which effects how the contact couple to the $+k$ and $-k$ states. Often contact performance isn't even consistent between cooldowns. Thus, for most measurements and devices there is a level of redundancy. For example during FQHE experiments in the lab, the sample will be cooled with

eight contacts even though only four are required. This allows for some contacts which simply do not work or are non-ideal. Also, generally different configurations of contacts can be tested to find the best results.

In the case of the quantum wire samples however, we are much less flexible. To mount a sample on the dilution fridge we are limited to eight contacts. Four contacts are reserved for ohmics so that we can measure the conductance and four are left to apply voltage to the gates. Each quantum wire requires two electrical contacts - one for each gate. If one of these contacts doesn't work, its impossible to operate the quantum wire. Similarly, the loss of any ohmic contact prevents four-point measurements. We can still make less precise two-point measurements if only one contact is lost, however if three of the contacts are lost, or two on a single side, measurement becomes impossible. Thus, we can see the difficulty. In an experimental environment where there is contact issues on virtually every cooldown, we have a very small margin of error and the result in many unsuccessful cooldowns.

Another concern was the way in which contacts were made. While most semiconductor devices are electrically connected using wire bonding, this process can damage delicate 2DEG if it punches through the contact. For this reason, it is common practice to use indium solder to make electrical contacts on the samples. While it is considered a more gentle process, it does have some effect on the samples. This is partly due to the fact that indium solder is difficult to work with; often many attempts must be made to create a single contact and contacts often need repair resulting. This means a great deal of sample handling and a hot soldering iron tip being repeatedly applied to the sample. Generally, applying indium solder does not greatly damage the sample, but repeated application and sample handling does have a gradually negative effect on samples. During experiments it was found that samples degraded and generally failed in rough correlation to handling and its severity.

Thus our problem is twofold: we require a contacting method that is more reliable when brought to low temperature and requires minimal handling and treatment of the samples. It was decided to pursue a method of contacting that would place metal directly in contact with the semiconductor, designated as the "flip chip" technique.

The idea is to pattern a small PCB in a way that matches the contacts on the quantum wire device and then place the device directly in contact with the PCB as illustrated in figure 3.4.10.

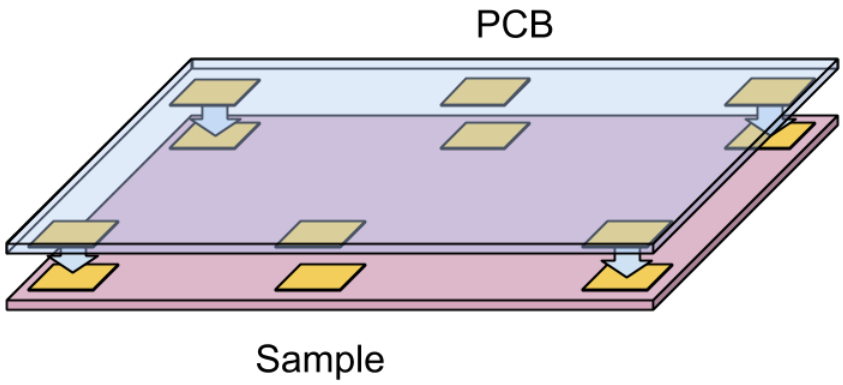

Figure 3.4.10: The PCB is patterned with metal matching the lithography on the device. The two are then put into direct contact to establish an electrical connection.

Naturally though, no two surfaces are completely flat and only three points of contact are required to be in stable contact between two surfaces. With pressure, more points of contact could likely be achieved, but not with the reliability we require. Thus a third piece is included in the sample holder, called the matrix. The matrix is a polymer material which has minuscule gold wires spaced every $50\mu m$. The result is that it creates a squishy layer which conducts only vertically. This allows the PCB and sample to achieve mechanical contact at all points without affecting the electrical characteristics.

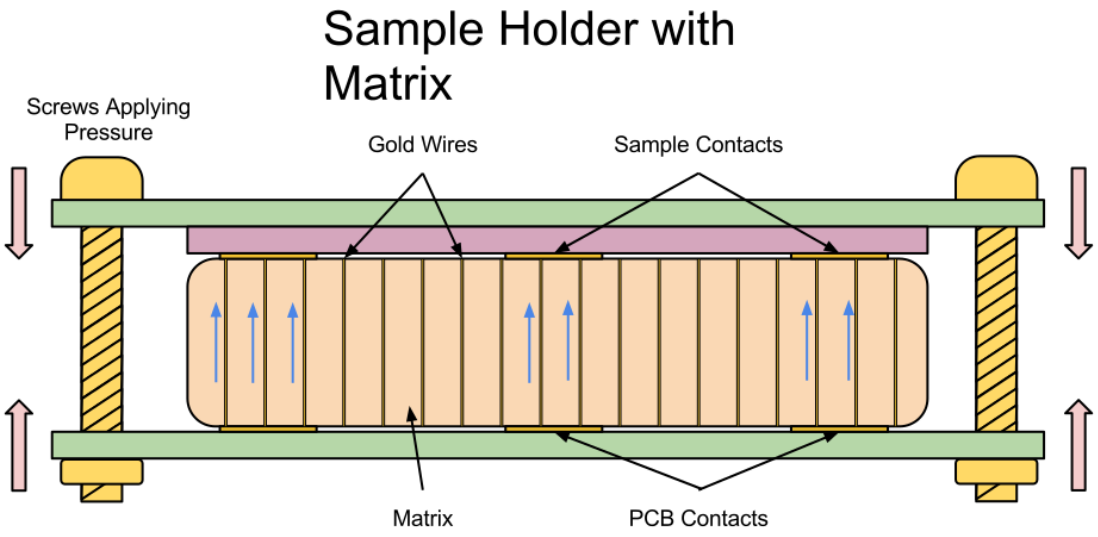

Figure 3.4.11: The sample holder with the matrix is shown in this diagram. A set of screws applies pressure to the matrix, which is made of a flexible polymer. This ensures contact between all sets of contacts. The PCB contacts are connected to intricate traces which lead to pins (not shown).

The downside of the this technique is the very tricky process of getting the alignment right. The PCB must be perfectly lined up with the sample to achieve good contact. To facilitate this process a sample mounting procedure was created.

Sample Mounting Process

The press plate (the PCB on which the sample is mounted) is created with alignment marks, showing where the sample should be located (see figure 3.4.12).

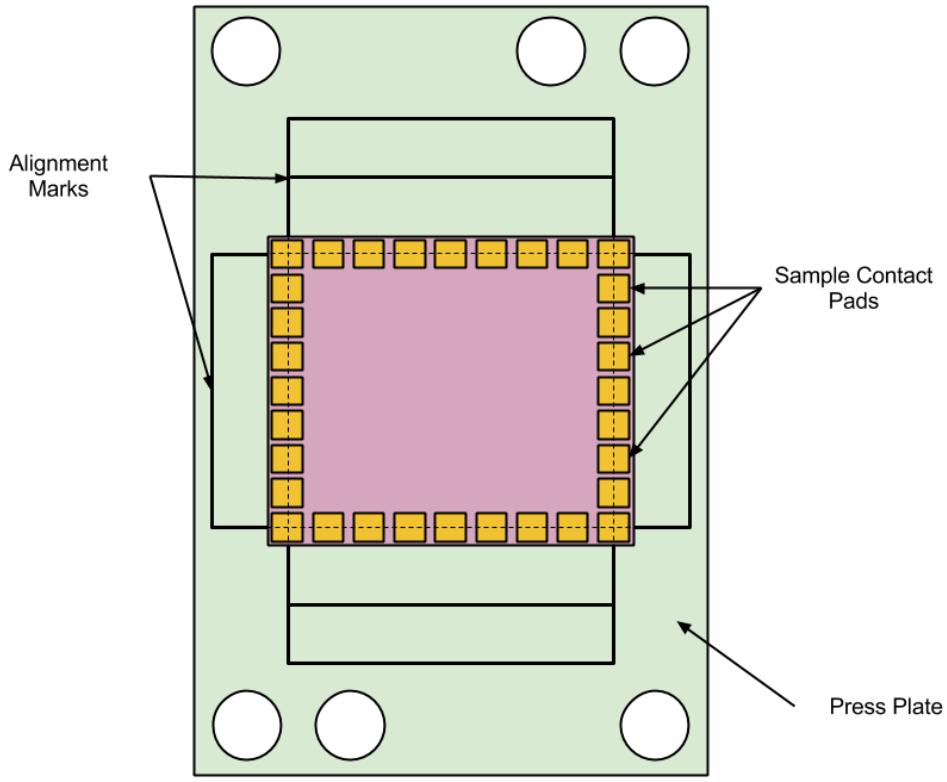

Figure 3.4.12: Diagram showing how the contacts of the sample align with marks on the press plate.

A vacuum tweezer mounted on a 3-axis stage is used to position the sample on the press plate and vacuum grease is used as a minor adhesive on the back of the sample. This is done under a usb microscope which is capable of 20x zoom. Software on the computer also allows for measurements on the image, so relatively precise alignments can be made. With the sample placed exactly on the press plate, the matrix can be placed on the sample using the vacuum tweezer. Alignment of the matrix is not critical, but it should cover all of the contacts as well as leave a gap where the quantum wires are located (see figure 3.4.13).

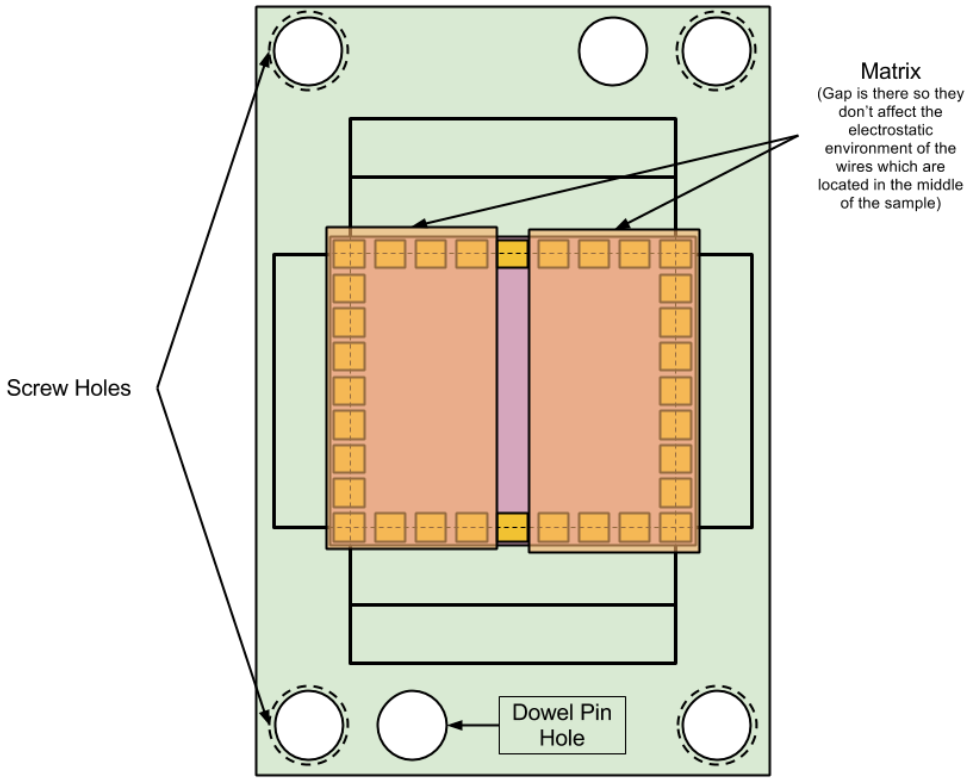

Figure 3.4.13: Diagram showing the proper placement of the matrix. The screw holes and dowel holes are specified.

The contact PCB can then be lowered onto the matrix, using two dowel pins to ensure alignment with the press plate as in figure 3.4.14.

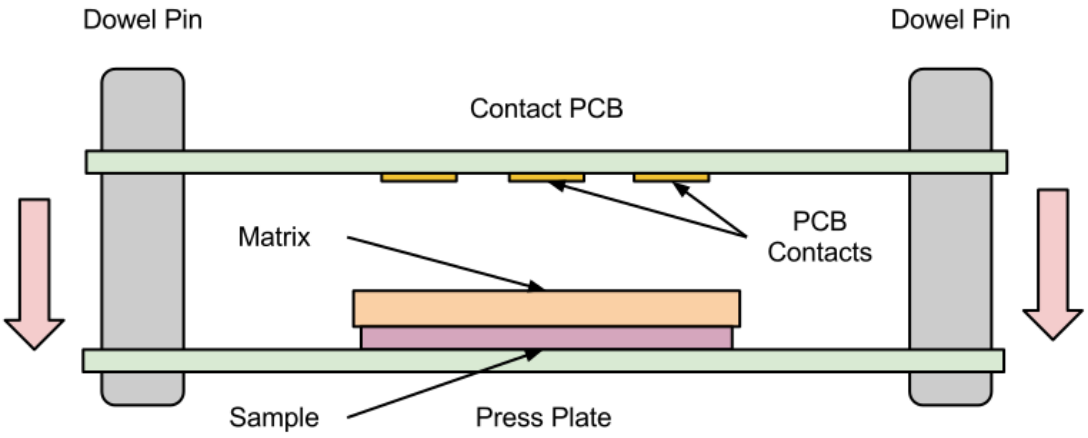

Figure 3.4.14: The contact PCB is lowered onto the press plate with the sample and matrix. This is the crucial stage, as slight misalignments will result in contacts not lining up.

Four tiny screws then apply pressure, to put the sample and PCB in contact as in figure 3.4.15.

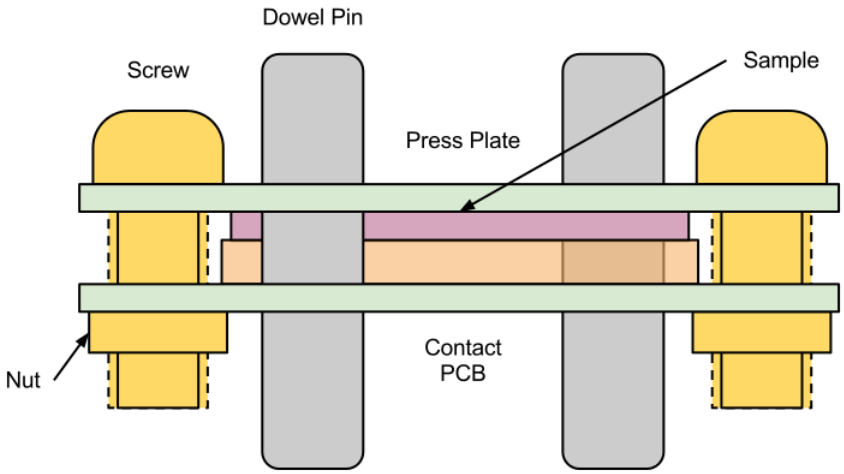

Figure 3.4.15: The final assembly of the sample holder is shown (from the side). The dowel pins stay in to ensure proper alignment, while four screws apply pressure to the matrix.

With the sample locked into place, electrical tests should be performed, to verify align-

ment. This can be done with a simple multimeter by testing the resistance of ohmic contacts with the meter on its lowest current mode (fixed highest resistance scale). Typical contact resistance is about $14k\Omega$. The sample holder is designed to be compatible with the filters discussed in the previous section. The sample can be inserted directly onto a filtered sample mount, or an adapter if filtering is not desired.

Issues with PCB sample holder

While this method successfully aligns samples with the contact PCB, maintaining contact at low temperature proved to be an issue. The same process is used for other samples in interferometry experiments with nearly 100% success, however the quantum wire samples proved to be troublesome. A brief outline of the remaining challenges will be given here.

The sample holders are extremely effective at high temperature, almost always achieving good contacts. However when cooled, it was found that many contacts were lost, or unreliable. The VTI fridge was used to investigate what was happening by slowly cooling the samples from 300K. It was found that contacts would work at room temperature, but when cooled to an arbitrary temperature, they would lose contact with the samples. What's more, the temperature at which a contact fails is not consistent. One contact was observed failing at $255K$, $170K$ and $90K$ on three separate trials, with no other variables adjusted. Other contacts displayed similar behavior, some even failed at high temperatures, only to work again at lower temperatures. We interpret these issues as relating to thermal contraction.

The sample holder is mechanically a rather complex device, containing five different materials all under some degree of stress. One possibility is electrical contact is lost because the screws reduce pressure. However, thermal contraction of the metal screws should result in increased pressure, not decreased. It could be the case that everything else is contracting more than the screws. This can also be dismissed though, as the screws are more susceptible to contraction than the other materials and nitrogen-temperature experiments confirmed that sufficient pressure was still being applied.

Its most likely the problem is that the gold wires in the matrix contract at low temperature, as do the gold contacts on the sample. This is supported by the fact that the interferometry samples on which this technique is used have a much greater metal thickness. This greater thickness would mitigate the effects of the contraction by pressing deeper into the matrix. This allows for greater margin of error when the wires in the matrix contract.

Additionally, it appears that repeated cooldowns fatigue the matrix, causing it to be less effective over time. It remains unclear what is causing these contact issues and it remains a subject of investigation.

References

[1] DG Schlom and LN Pfeiffer. "Oxide electronics: Upward mobility rocks!" In: *Nature materials* 9.November (2010), pp. 881–884. URL: http://www.nature.com/nmat/journal/v9/n11/nmat2888/metrics.

[2] Cory R Dean. "A Study of the Fractional Quantum Hall Energy Gap at Half Filling". PhD thesis. 2008.

[3] Seigo Tarucha, T Honda, and T Saku. "Reduction of quantized conductance at low temperatures observed in 2 to 10 μm-long quantum wires". In: *Solid state communications* 94.6 (1995). URL: http://www.sciencedirect.com/science/article/pii/0038109895001026.

[4] Frank Pobell and James Brooks. "Matter and methods at low temperatures". In: *Physics Today* 45.10 (1992), pp. 116–118. ISSN: 0031-9228.

[5] Soumen Mandal, Tobias Bautze, Rémi Blinder, Tristan Meunier, Laurent Saminadayar, and Christopher Bäuerle. "Efficient radio frequency filters for space constrained cryogenic setups." In: *The Review of scientific instruments* 82.2 (Feb. 2011), p. 024704. ISSN: 1089-7623. DOI: 10.1063/1.3543736. URL: http://www.ncbi.nlm.nih.gov/pubmed/21361623.

Chapter 4

Results

The results of the described experiments will be presented here. As discussed previously, the goal of the experiments was to observe a unique Luttinger liquid state. Any one dimensional electronic system (with no disorder) is expected to be in a Luttinger liquid state at T=0, but detecting the unique signatures is difficult. In the GaAs wire however, theoretical work from Daniel Loss [1] predicts that the nuclear spins of the wire will take on a helical nuclear spin-ordering. The interaction between the ordered nuclear spins and the electrons should create a feedback effect, resulting in a unique ordering at a relatively high temperature. This effect is expected to manifest at a critical temperature below $100\,mK$, which is within the experimental range of our dilution fridge. Below the crossover temperature, the unique ordering results in some testable experimental observations. The easiest to observe would be the pinning of half the electron modes, meaning that only electron channel is allowed rather than two. Therefore, the lowest plateau should be located at e^2/h rather than $2e^2/h$, a very clear prediction. If the observation was made, further evidence would be gathered by using radiation at the NMR frequency to disrupt the nuclear spin ordering, thereby and causing the conductance to return to $2e^2/h$.

We took a methodological approach to observing this state by starting with a variety of samples with varying parameters. The devices were first tested at $1.6\,K$ to ensure satisfactory operation and then at $300\,mK$ to identify devices with strong quantum behavior. Finally devices were tested at $23\,mK$ in hopes of observing the half-plateau indicative of the desired state. Unfortunately the half-plateau was not observed, as shown in figure 4.0.1, for a quantum wire cooled to $23\,mK$.

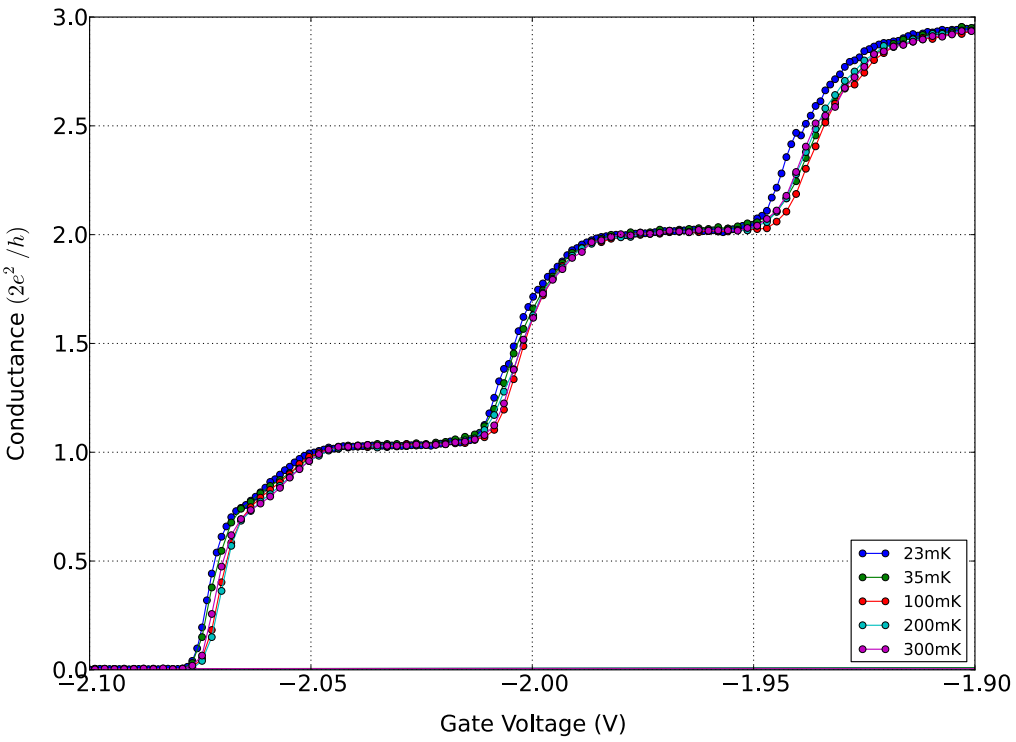

Figure 4.0.1: Results of cooling a quantum wire from $300mK$ to $23mK$. The expected plateau at e^2/h is not observed.

The absence of the half-plateau may be explained by many factors. The sample might not have been clean enough, or perhaps factors such as length, well-depth or even the gate design might have affected the sample. However, if we examine the temperature dependence, see figure 4.0.2, some possible clues emerge.

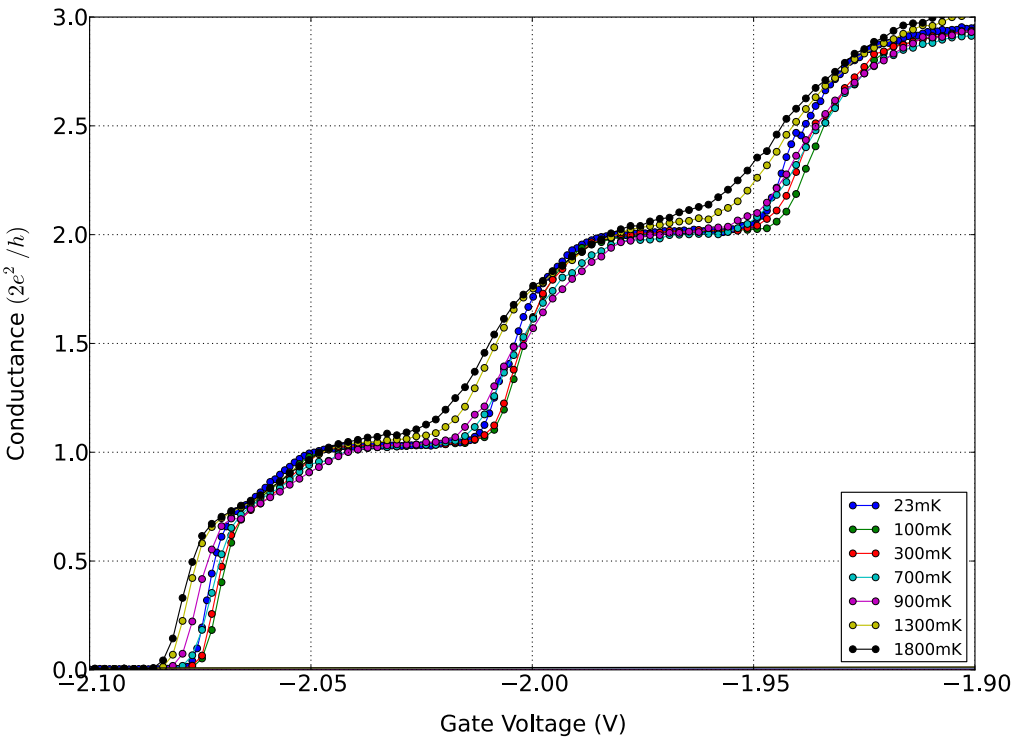

Figure 4.0.2: The quantum wire temperature dependence from $23\,mK$ to $1800\,mK$. While at the relatively high temperature of $1.8\,K$, the plateaus are visibly broadening, the conductance doesn't appear to change much at all below $900\,mK$.

Remarkably, in this measurement we observe plateaus at a temperatures as high as $1.8\,K$. In previous measurements near this temperature, there was no hint of plateaus. Additionally, it appears that the conductance traces are nearly identical below $900\,mK$. This is unexpected as QPCs generally display some kind of temperature dependence, especially around the 0.7 feature. Considering these two observations, it seems likely that the true electronic temperature was not the same as the fridge temperature. Rather, the electron temperature is probably somewhere in the hundreds of millikelvins and is being affected by some external source of heat. This would certainly explain the lack of temperature dependence below $900mK$ and the absence of the predicted effect.

After eliminating possible heat leaks from poor vacuum and radiation, it seemed likely that the electrons were being heated by high frequencies in the wires. Standard low temper-

ature procedure is to filter out these frequencies to prevent this effect, however, the wiring used on the dilution fridge was not sufficiently filtered and was identified as the most likely cause. For this reason, we decided to construct filters which would eliminate the electronic noise and cool our electrons to a lower base temperature. This was the motivation for the construction of filtered sample holders which could allow for lower electron temperatures.

4.1 Characterization of filters

Π filters at room Temperature

The room temperature Π filters used in experiment were previously discussed in section 3.4.1. Their performance was tested using both a dummy resistor and a sample on the 300mK ^{3}He system. This test was done using a lock-in amplifier whose frequency was swept from $1\,Hz$ to $100\,kHz$ and the resulting amplitude was measured using the four point technique. While the results were identical for the test resistor and the sample, only the resistor results will be shown here.

As seen, the filter's frequency response begins rolling off at approximately $100\,Hz$. Two resonance peaks can be seen near $10\,kHz$, owing to the fact that their is a Π filter both before and after the sample. Nonetheless, the resonance peaks never exceed $0\,dB$ and the response steeply rolls off beyond $10\,kHz$, reaching below $-140\,dB$ at $100\,kHz$. This is a highly favourable frequency response which effectively attenuates high frequency signals.

Π Filters at low temperature

While the characteristics of the room temperature Π filters were desirable, they remain at 300K, therefore allowing for the associated thermal noise to heat the samples. For this reason, we attempted to reproduce the filtering characteristics at low temperature. This required the use of different component values to account for the small amount of available space in the fridge. Specifically, $1\,mH$ inductors and $1\,\mu F$ capacitors, both available in surface mount form were used, and show similar filtering characteristics to the larger room temperature filters.

The filters display a $-3\,dB$ point at $\sim 10\,hz$ and a roll off of $-100\,dB$ per decade above $10\,kHz$. This filter is so low-pass that it would affect our measurements which are typically made between $10\,hz$ and $100\,hz$. However, at low temperature, component values are significantly affected, meaning the frequency response changes. The filters were tested

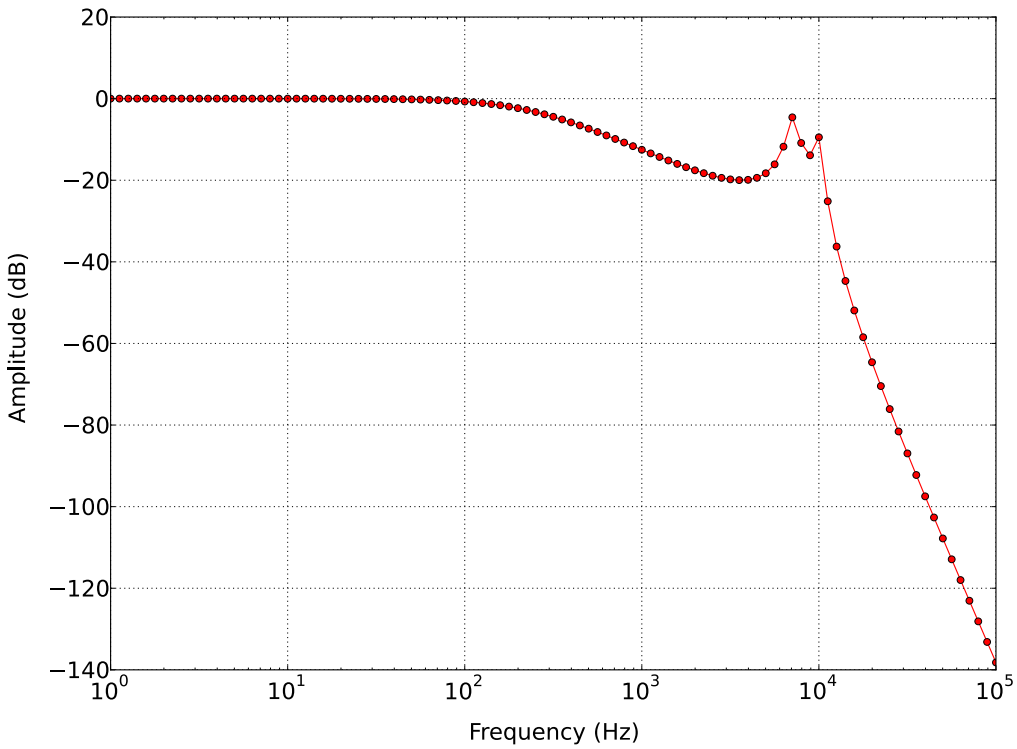

Figure 4.1.1: The frequency response of the Π filter at room temperature. Due to the fact that multiple filters are involved in the measurement, two resonance peaks are found. Nonetheless, the filter steeply drops off beyond 10,000hz, therefore eliminating the relevant frequencies.

at $1.6\,K$ to determine their low-temperature characteristics. Although the filters will be used at temperatures as low as $25\,mK$, ceramic capacitors of this type (class 2, ferroelectric X7R) display a roughly linear dependence on temperature, rather than exponential. Thus the difference between $25\,mK$ and $1.6\,K$ can be viewed as merely a degree, rather than two orders of magnitude and so the test should be indicative of the filter performance in all our systems. The $1.6\,K$ performance is shown in figure 4.1.3.

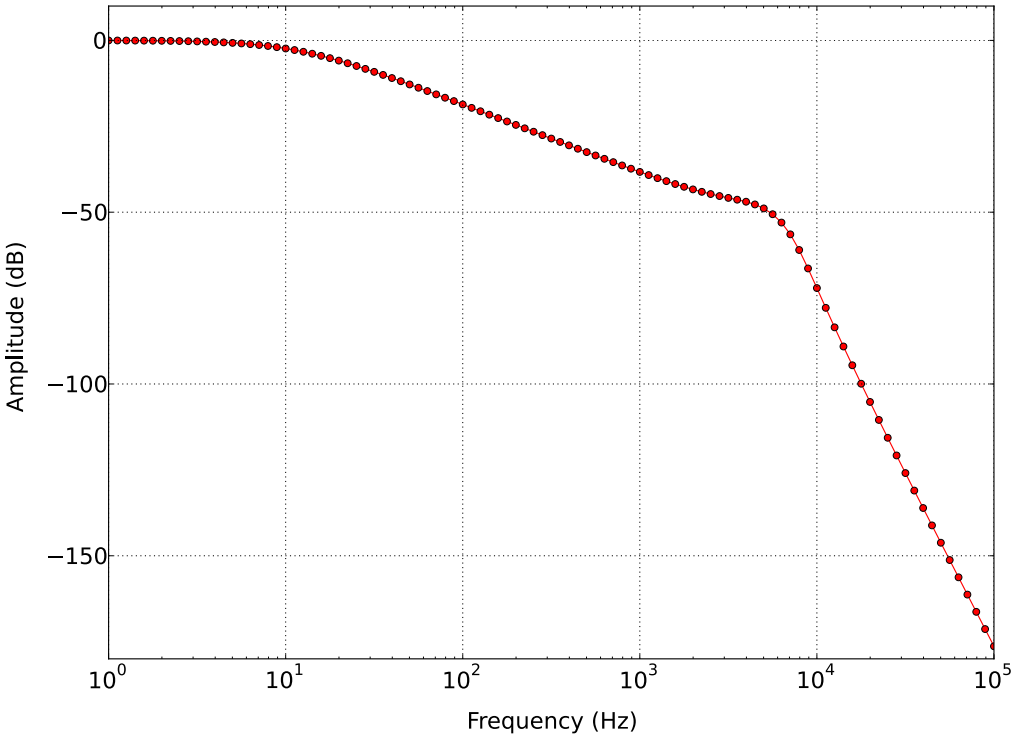

Figure 4.1.2: The frequency response of the miniature Π filter at room temperature.

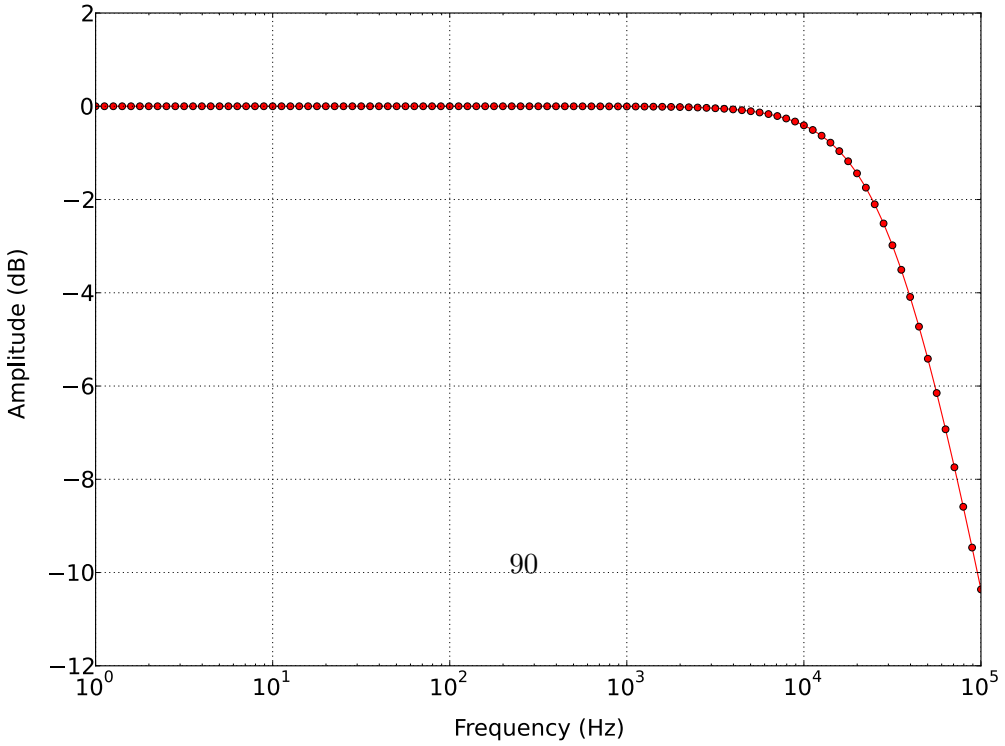

Figure 4.1.3: The performance of the miniature Π filter at 1.6K

The low temperature drastically effects the Π filters. The $-3\,dB$ is now found at $31\,kHz$ and the roll-off is not nearly as steep. Considering the weak performance, it was decided that this filter wasn't a particularly practical option for low temperature experiments. Additionally, thermal contraction proved a problem for this filter due to its rather complex construction. At low temperatures, contraction was found to cause contacts to become unreliable. Considering the weak performance and unreliability, we turned to simpler and easier to control RC filters.

RC filters at low temperature

The RC filters proved to be a much simpler design and also had much greater reliability. Additionally, having experience with the drastic effects of low temperature on component values, we were better able to select components which had desirable values at low temperature. Although it is unclear from the previous experiments how exactly the components changed, based on a physical understanding of the devices, the capacitors were the most suspect component. The inductors are, in principle, merely wire wrapped around a ferrite core. While the material parameters of the core may slightly change with temperature, as well as the conductance of the wire, these changes should have a relatively minor effect on the inductance and temperature dependence of inductors is rarely, if ever, reported on datasheets.

Capacitors on the other hand are sold with well specified temperature coefficients. Capacitors of the type used in these experiments contain a ceramic, usually some variation of barium titanate. Due to the wide range of applications for this type of capacitor, the temperature dependence is well studied and can be quite large ($\pm 15\%$), even over the standard operating range (-55^oC to 85^oC). Therefore, we selected very large capacitors ($1\,\mu F$) for our application, anticipating their values would be significantly reduced at low temperature. The RC filters were characterized at $300\,K$, $180\,K$ and $1.6\,K$.

As can be seen in figure 4.1.4, the filters are extremely low pass at $300\,K$, but the cutoff frequency increases as the temperature is lowered. The filters have a $-3\,dB$ point of $21\,hz$, $40\,hz$ and $540\,hz$ at $300\,K$, $180\,K$ and $1.6\,K$, respectively. They show a roll-off of $-19\,dB$ per decade regardless of temperature. The low temperature cut-off point of $\sim 500\,hz$ is superb for our application. Since measurements are typically performed between $10\,hz$ and $100\,hz$ the filter will leave these frequencies mostly untouched, but will cut off everything higher.

We also wished to establish exactly how much the low temperature was affecting the capacitor values. A circuit simulation was run with various capacitor values so as to reproduce the data, which were matched by eye. The results are shown below in figure 4.1.5.

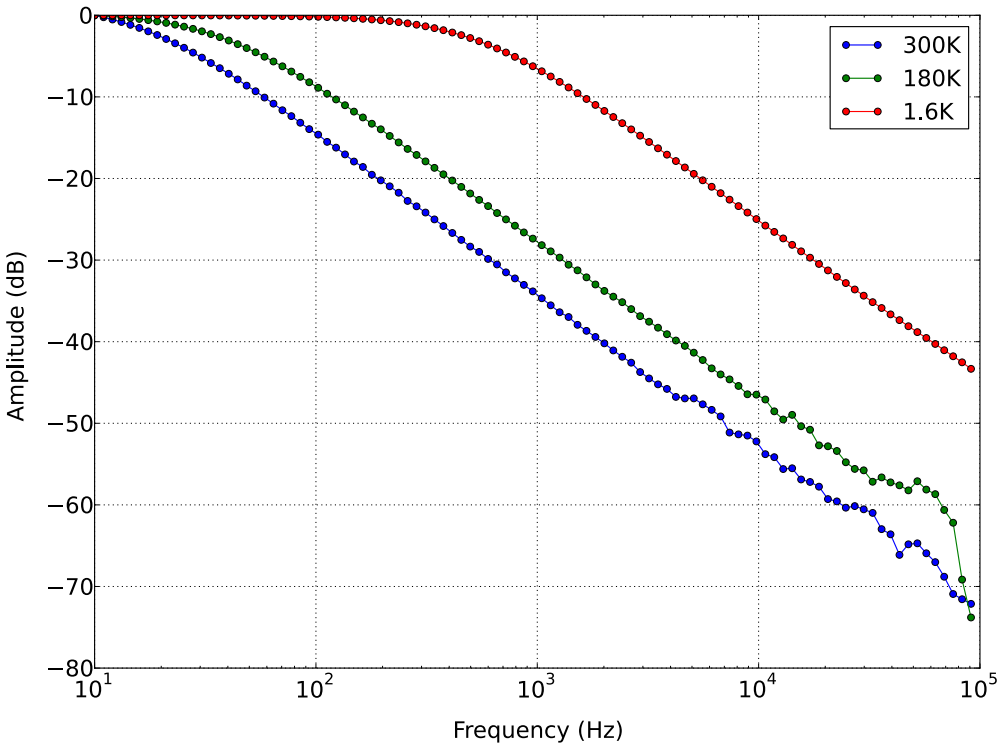

Figure 4.1.4: The performance of the RC filters at $300\,K$, $180\,K$ and $1.6\,K$

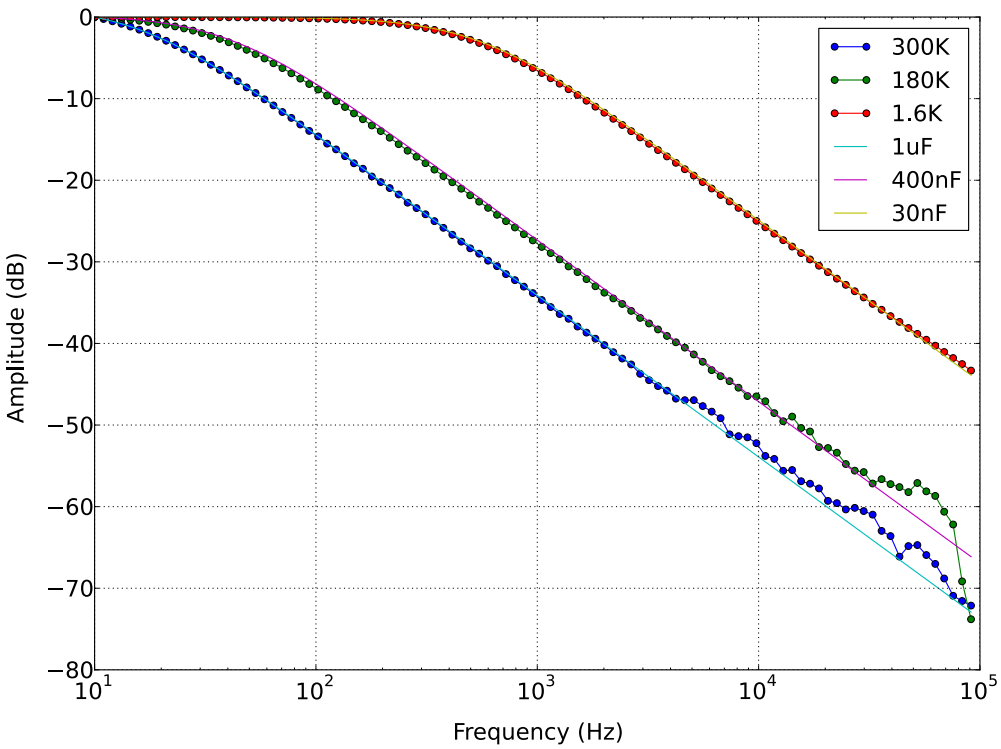

Figure 4.1.5: The experimental frequency response of the filters plotted against theoretical curves of different capacitor values

As can be seen, the theory and experiment are in extremely good agreement. While there is minor variations between the curves - likely do to the real capacitors not behaving ideally - the agreement suggests that these are accurate estimates for the capacitor values. At $300K$, the theoretical response of the $1\mu F$ capacitor is in extremely good agreement with the experimental. The $180K$ curve and $1.6K$ curve match up with theoretical capacitance values of $400nF$ and $30nF$. A crude linear fit suggests that the temperature coefficient is about $-30nF/K$, however from the data its clear that capacitance does not have a linear relationship with respect to temperature (see figure 4.1.6). It appears that the coefficient is lower near $0K$, meaning the capacitance will be more stable at the lower temperatures, which is of benefit to us.

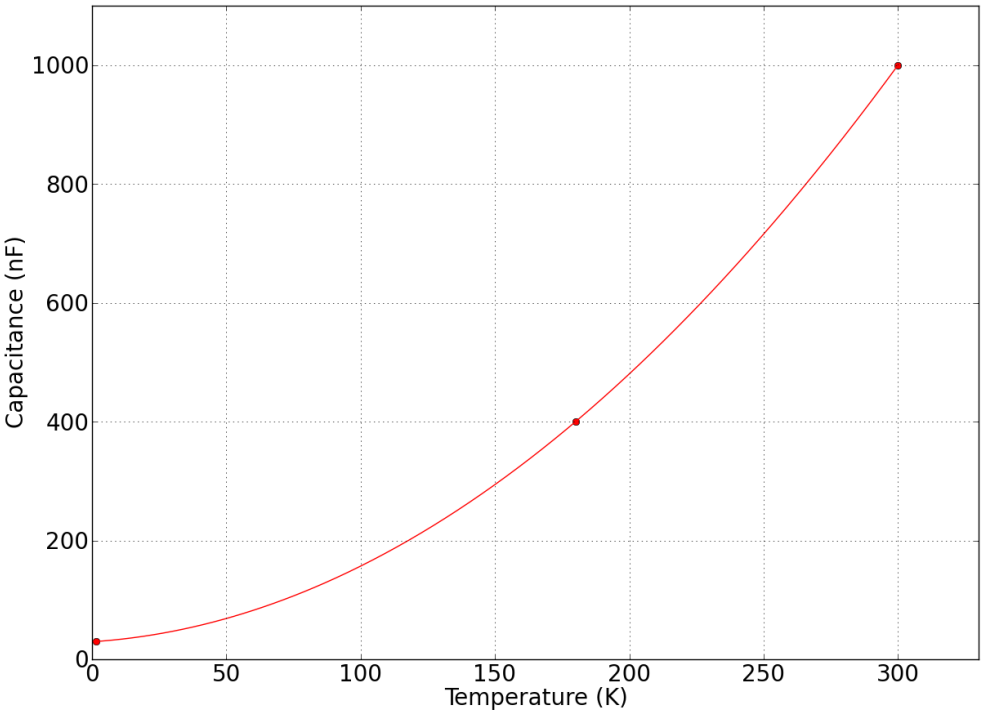

Figure 4.1.6: The temperature dependence of the capacitor

This concludes the characterization of the filters. The RC filters appear to effectively filter the desired frequencies at low temperature and were selected for use in our experiments.

Effect of Filters

The effect of the filters is difficult to judge, as a our sample does not offer a clear answer to what the electron temperature is. While the quantized conductance of the wire does have a temperature dependence, samples vary in characteristics between cooldowns on a scale far greater than the slight temperature dependence. Thus using the location of the plateaus or the pinch-off voltage as a temperature indicator is not an option.

This leaves us with the drawback of having to infer the effectiveness of low temperature filtering based on whether the samples are working or not. However, since samples

frequently fail or succeed for unclear reasons, it was difficult to isolate the effect of the filters. Nonetheless, some observations do support the effectiveness of filtering.

Specifically, we can look at a samples which were tested $300\,mK$, with and without the filters, and observe the difference between the conductance plots. While its not possible to directly extract the temperature from these plots, it is nonetheless clear that the quantum behavior is stronger with the filters than without as in figure 4.1.7 and figure 4.1.8. Because these are two different samples, on different cooldowns, it can't be conclusively stated that the filters are responsible for the enhancement of the plateaus. However, the failure of a large number of samples to show conductance plateaus, combined with the dramatic success of the first sample to use filtering is strong evidence that the filtering was resulting in lower electron temperatures.

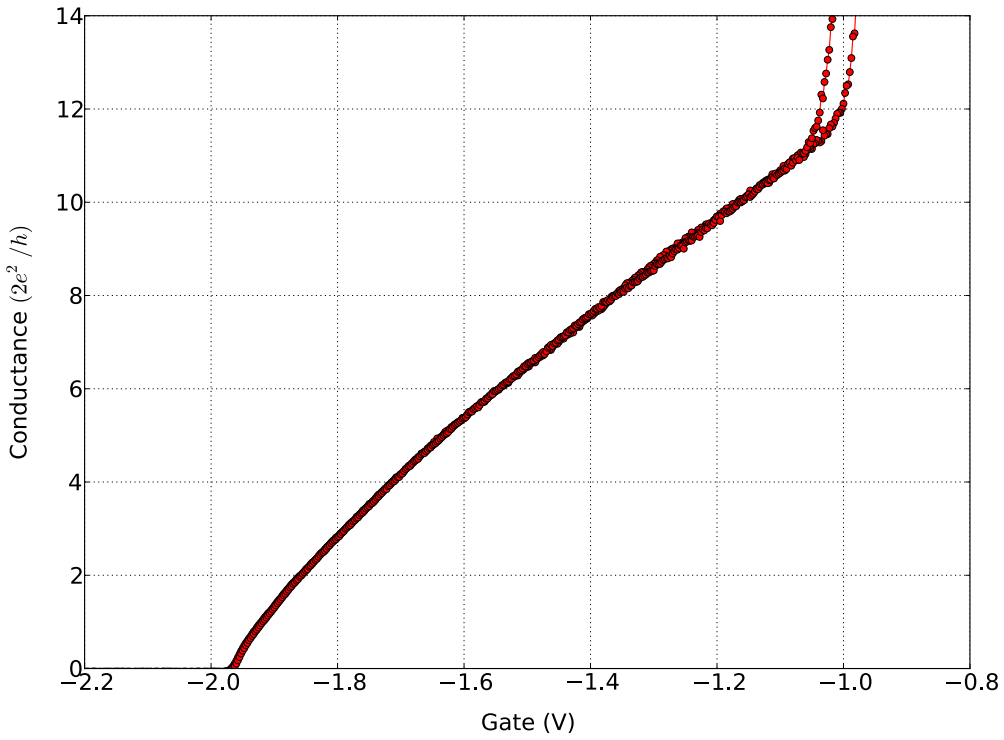

Figure 4.1.7: A $1\mu m$ wire from the sample VA150ALD2 tested at 300mK without filtering. Note the absence of conductance plateaus.

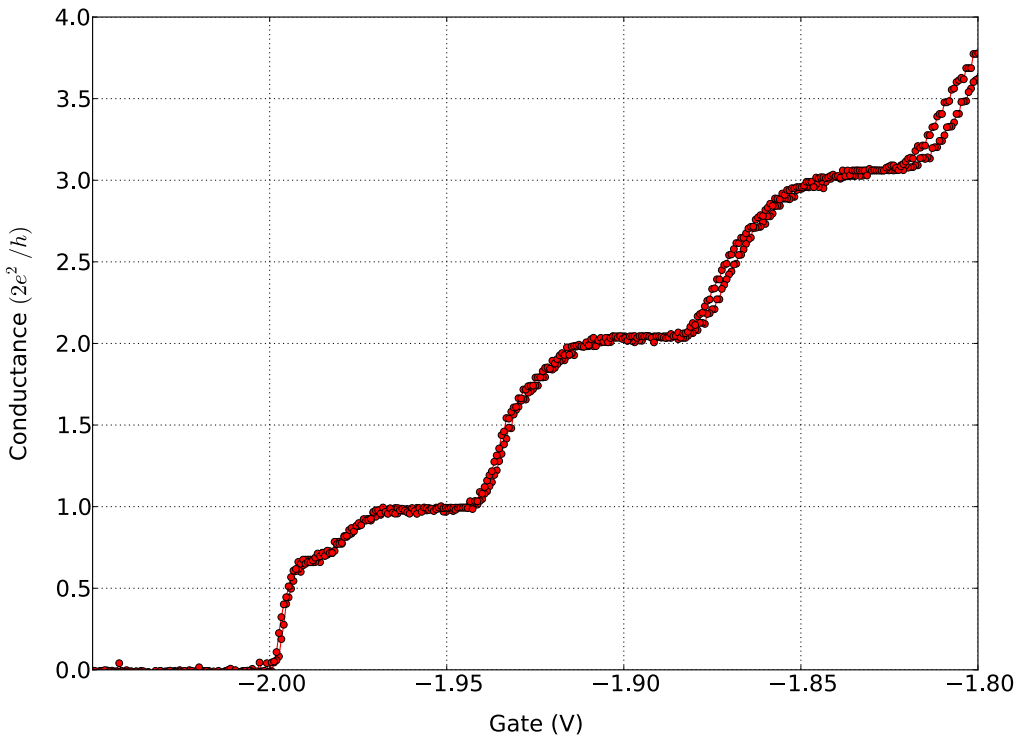

Figure 4.1.8: A $5\mu m$ wire from the sample VA150InSn1 tested at 300mK with filtering. This wire shows well-defined plateaus.

4.2 Quantization of Conductance

As mentioned in the methodology section, with such a large number of samples it was necessary to test at relatively high temperature (1.6K) to find the best candidates for further study. At this stage of the experiment, it was found that the wires displayed widely varying characteristics. While not all the results can be shown here, a few examples will be presented.

First, some examples of poorly performing wires will be shown, to give some sense of which characteristics were selected for.

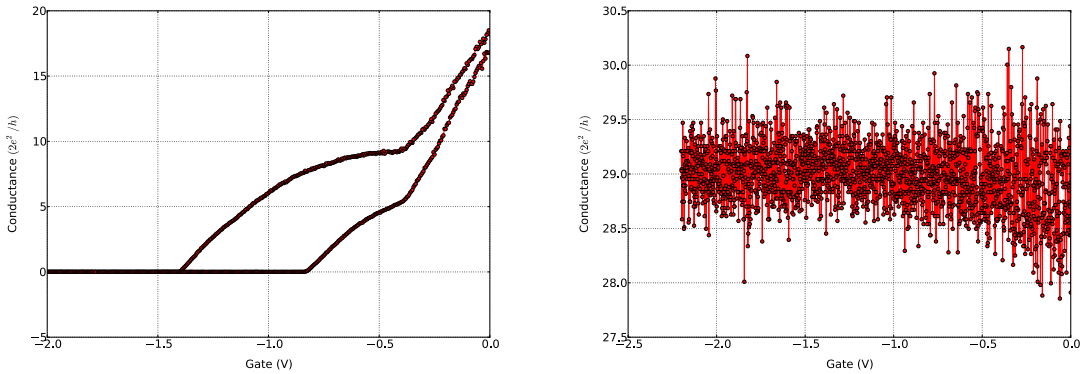

(a) (b)

Figure 4.2.1: In (a), a wire showing dramatic of hysteresis is shown. In (b) a wire which did not function when voltage was applied to the gates is shown.

The two conductance plots show the most common ways in which wires failed to function. In figure (b), it is clear that the gates did not function at all as no change in conductance of the 2DEG was measured. The causes of this were multiple. In some cases, there was a physically obvious problem, such as a wire becoming disconnected from the sample. In this case, the wire would be re-attached and the device retested. In other cases though, the reason was not clear and the wire would not be tested again in favour of more promising samples.

In (a), a wire showing significant hysteresis is shown. This is a more subtle problem than the non-functioning wire, but also suggests a poor candidate wire. The hysteresis is most likely due to fluctuations in the electrostatic environment near the wire. Since the state we wish to observe is extremely sensitive to disorder, this is a wire which we do not expect to display interesting behavior and would not be further investigated. Additionally, neither of these wires used and ALD layer, eliminating it as a possible factor.

Fortunately, there was no shortage of quantum wires showing good behavior. An example of an superb wire tested at $1.6\,K$ is shown below. This wire shows virtually no hysteresis, no unexplained fluctuations and pinches off steeply. This would be considered an ideal candidate for testing at lower temperature.

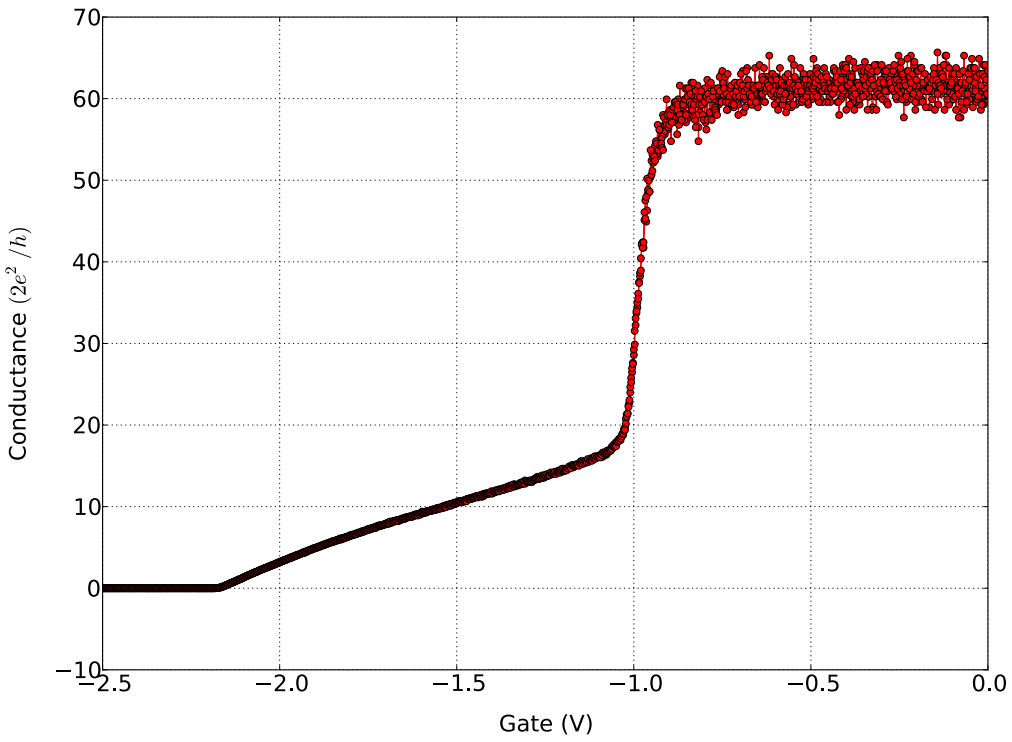

Figure 4.2.2: A $1\mu m$ quantum wire tested at $1.6K$ displaying proper behavior

Wires which performed well at $1.6\,K$ were selected for further cooling to $300\,mK$ or to $25\,mK$. At these temperatures, we can expect to observe the characteristic quantization of conductance associated with ballistic quantum transport. Although $300\,mK$ is likely too warm to observe the sought-after state, we are still able to select for wires which display particularly well-behaved quantum behavior. At $300\,mK$, quantization of conductance in some samples was observed. As mentioned, this quantization was strongly enhanced by the presence of filtering.

An example of conductance observed at $300\,mK$ is provided in figure 4.2.3.

As can be seen, the plateaus are very well-defined on this sample. We attribute this to both the lower temperature and the presence of filtering. Samples were also tested at $23\,mK$ in the dilution fridge, although without filtering. These samples also tended to produce excellent quantum characteristics as shown in figure 4.2.4.

Despite the successful reproduction of previously results for QPCs, these low tempera-

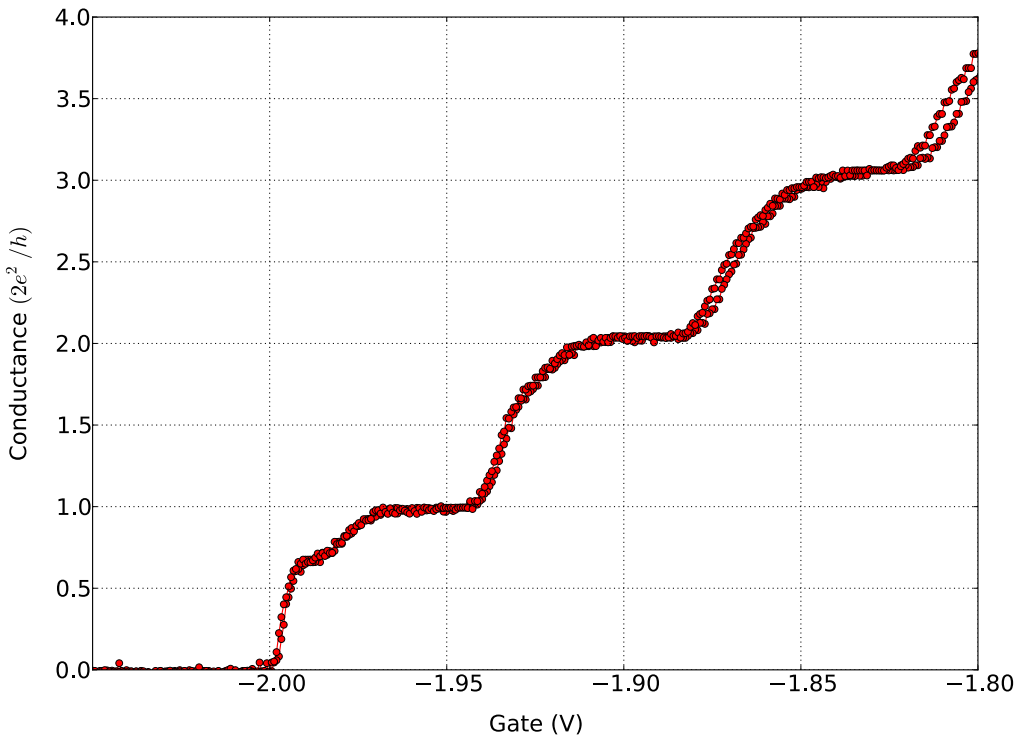

Figure 4.2.3: A $5\mu m$ wire from the sample VA150InSn1 tested at 300mK with filtering.

ture measurements failed to show the predicted half plateau, which would be indicative of the spin-ordered state. We believe this is due to the lack of filtering on this measurement which is resulting in an electron temperature above that reported by thermometers. It was these measurements which motivated the fabrication of low temperature filters. However, it was found during experiments that samples tended to degrade with each cooldown. Thus a sample such as the one shown in figure 4.2.4 which was cooled down six times has degraded to the point where no wires remain functional. This was similarly experienced with other samples as well. A particular difficulty which was encountered with many samples was an increase in hysteresis and a decrease in the pinch-off voltage. We consider this a sign of unwanted charge being present in the sample, affecting the electrostatic environment around the wire. This results in greatly increased fluctuations in conductance. The plateaus become poorly defined and conductance fluctuations become commonplace. This

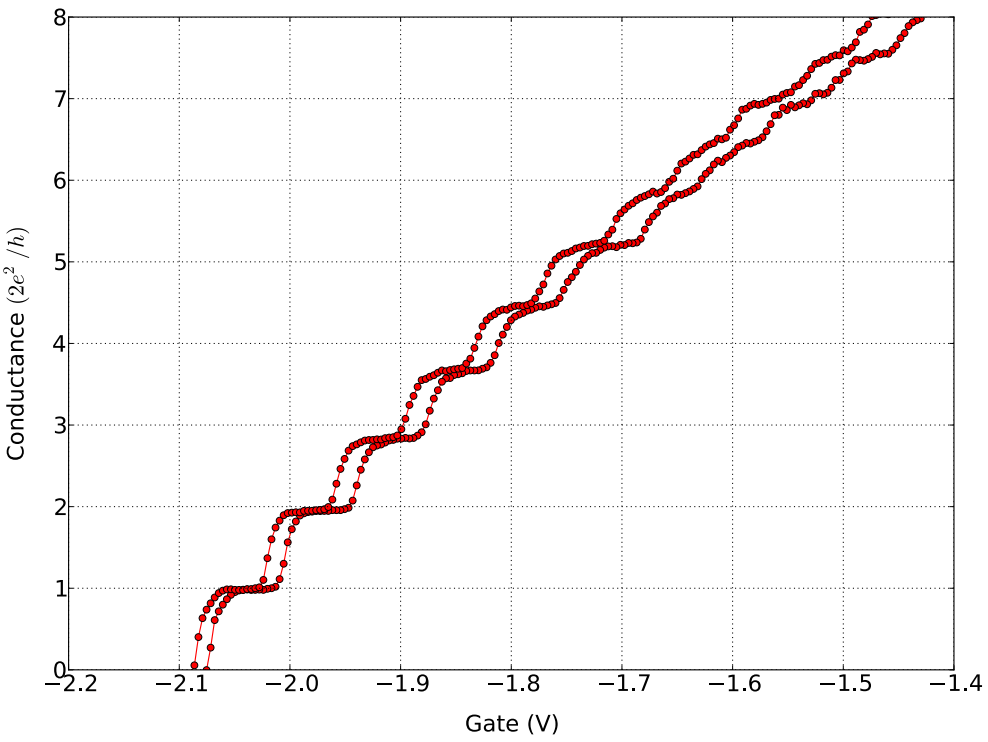

Figure 4.2.4: A quantum wire measured at $23mK$

would seem to indicate an unstable electrostatic environment in the vicinity of the wire which will surely prevent delicate quantum states from forming. For this reason, by the time low temperature filters were in place to ensure a low electron temperature, no samples were of sufficient quality to observe strong plateaus. An example of the degradation in performance is shown below for a $5\mu m$ wire on the sample VA150InSn1. The wire performed extremely well with filtering at $300\,mK$ as seen in figure 4.2.3. However, after significant handling and cooldowns, it's performance had significantly degraded, even when cooled to $23\,mK$.

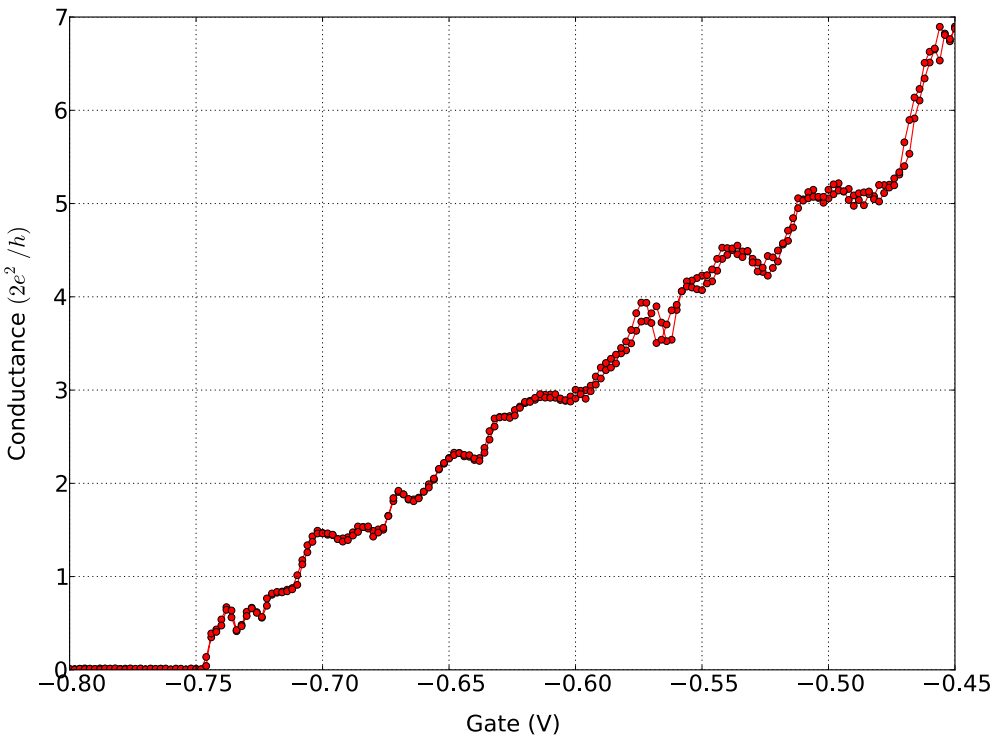

Figure 4.2.5: Quantum wire with degraded performance

While the quantization of conductance is clearly visible, fluctuations indicate severe disorder and an unstable electrostatic environment. Over time, and with repeated application of the magnetic field, it was found to improve somewhat.

4.3 Resistively-detected NMR

Following the lead of experiments from Dean [2] and Keane *et al* [3], we decided to investigate the response of the quantum wires to NMR stimulation. Additionally, in the case that the half plateau corresponding to the Loss prediction was observed, an easy way to verify it would be to disrupt the nuclear spins using an NMR coil. Thus the motivation for this experiment was twofold. First to gain insight into the state of our one-dimensional wires and second to achieve of proof of concept for disrupting nuclear spin ordering in future experiments. While previous experiments had used custom sample holders to provide a

precise source of NMR radiation, in this case we were primarily interested in simply observing a response. The radiation source used was a small copper wire coiled a few times around the sample.

To ensure the electron temperature was low, this sample used an RC filtered sample mount. Before searching for an NMR signal, it was necessary to characterize the magnetoresistance of the sample. The quantum Hall effect is shown in figure 4.3.1. The $\nu = 2$ level is visible centered around $2T$ and the $\nu = 3$ level around $4.7T$. Based on previous work, we selected a relatively high field between the $\nu = 2$ and $\nu = 3$ levels to search for the NMR signal. The field was set to $5.8T$, close the edge of the second landau level to ensure both spin species were present.

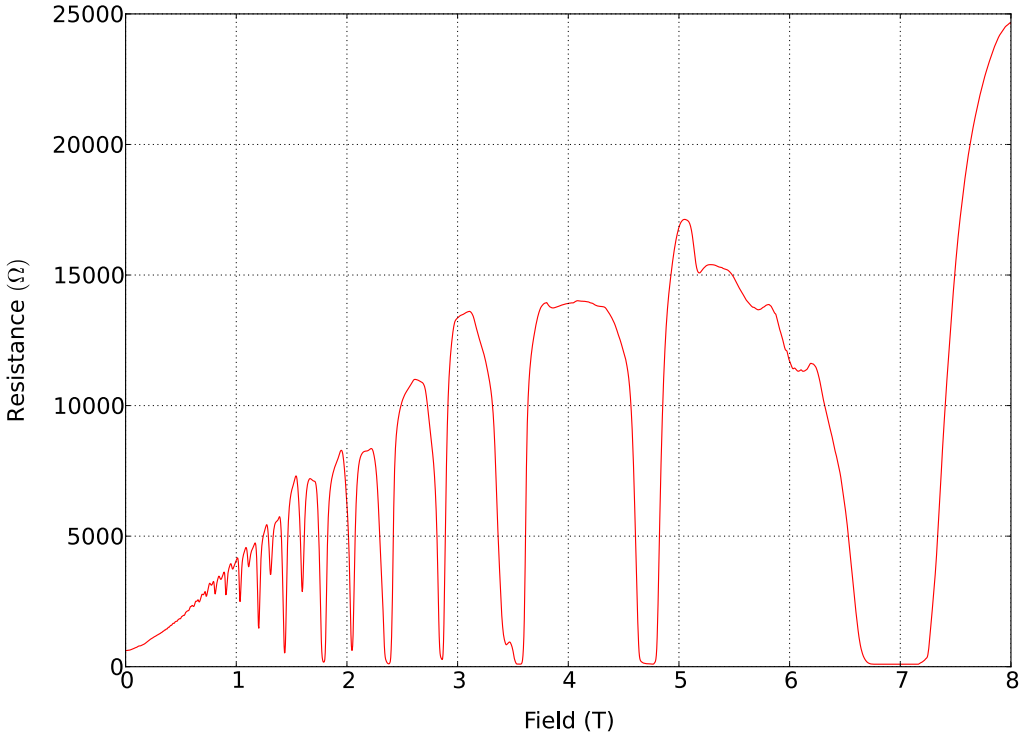

Figure 4.3.1: Longitudinal magnetoresistance vs field of the quantum wire sample (VA150InSn1).

To observe the quantized conductance, we found it necessary to select a field not within a Landau level, but somewhere with finite conductance. At high-field the Zeeman interaction

splits the energies or the spin-up and spin-down fermions, resulting in a lifting of the degeneracy of the conduction modes. Thus, at high field, plateaus are now found at levels of e^2/h as shown in figure 4.3.2.

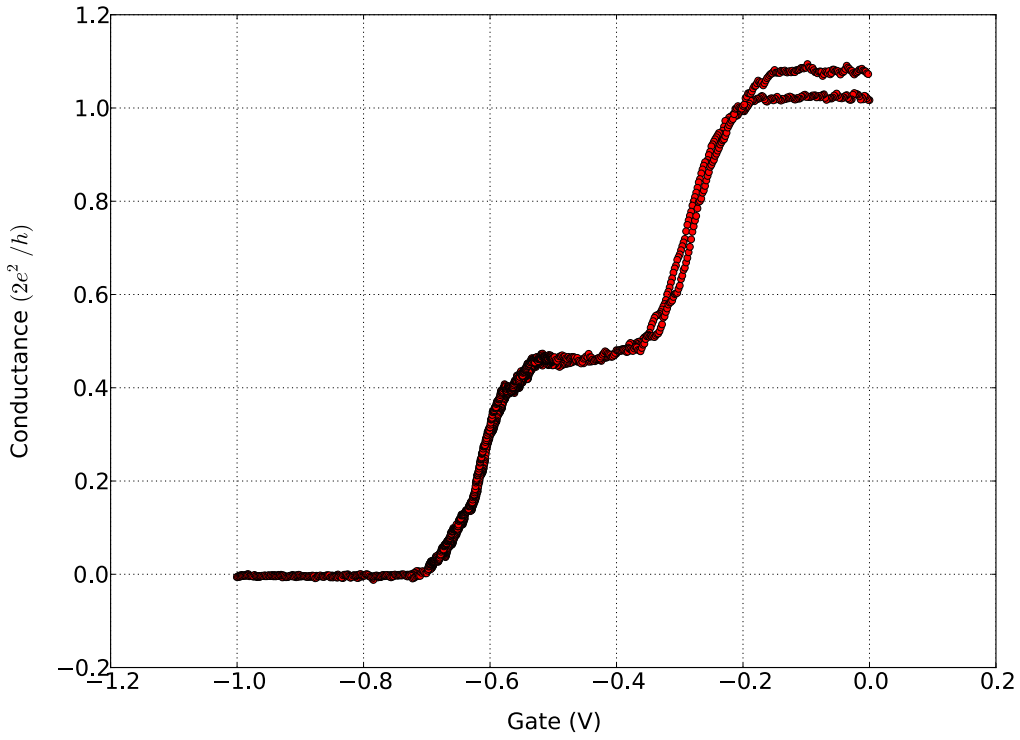

Figure 4.3.2: The conductance of the $1\mu m$ wire at $23mK$ and $5.8T$. Plateaus are evident at $1e^2/h$ and $2e^2/h$.

Despite the evident conductance fluctuations, the plateaus are relatively flat. This poses a problem for using changes in resistance to detect NMR as while in the plateau, the conductance will not change. For this reason, we must adjust the gate voltage such that the wire is on the edge of the plateau. At this point, the quantum wire can remain in its one-dimensional state, but allow conductance fluctuations.

Based on this theory, the points at which we expect to see RDNMR, would be the two edges of the plateau, at $\sim -0.55V$ and $\sim -0.35V$. As such the gates were adjusted to this voltage and the conductance given time to stabilize. It was found that over time, the

conductance fluctuations would subside allowing for more precise measurements. To apply the radiation to the quantum wires, an RF source was used to drive the coil wrapped around the sample. The frequency was selected based on measurements of the gyromagnetic ratio for ^{75}As[2], reported as $\gamma/2\pi = 7.3150 MHz/T$. For our field of $5.8T$, this predicts a NMR frequency of $42.42 MHz$. The frequency was swept around this value with the power set at $-18dB$, resulting in the following signal, found at $\sim 42.05 MHz$.

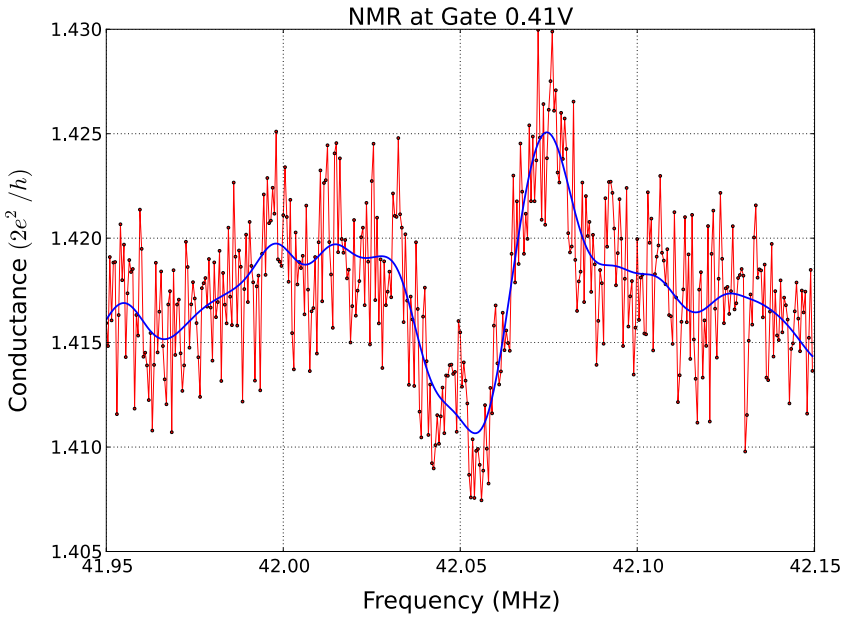

Figure 4.3.3: RDNMR signal found at $-0.41V$. The blue line is smoothed data, given as a guide to the eye

With the signal isolated, the gate was adjusted to determine how the NMR signal depended on the state of the quantum wire. At the back edge of the conductance plateau (less constricted) the gate was swept from the intermediate point between the first and second plateau into the first plateau and the change in the NMR signal was observed. We refer to figure 4.3.2 to see where these signals are found in terms of the quantum wire state. The figures below show the NMR signal at various gate voltages. The blue line is a statistical fit to provide a guide to the eye, while the connected red points are the raw data.

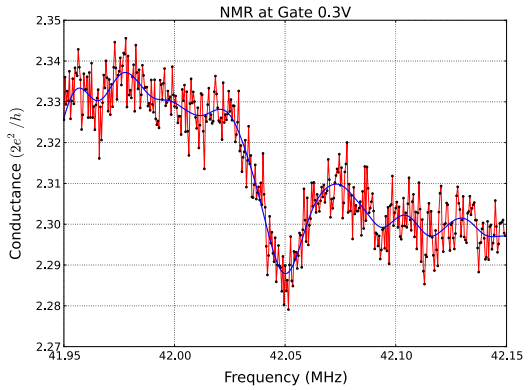

(a) RDNMR signal at $-0.3V$. The NMR has the effect of reducing the conductance here.

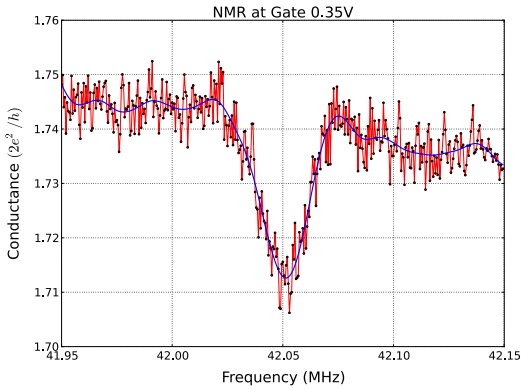

(b) RDNMR signal at $-0.35V$. The NMR has the effect of reducing the conductance here.

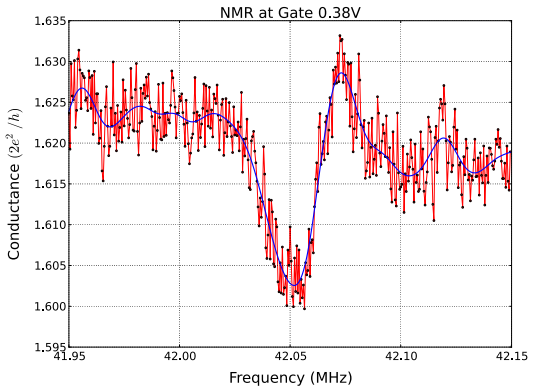

(c) RDNMR signal at $-0.38V$. The NMR has the effect of reducing the conductance followed by an increase in conductance.

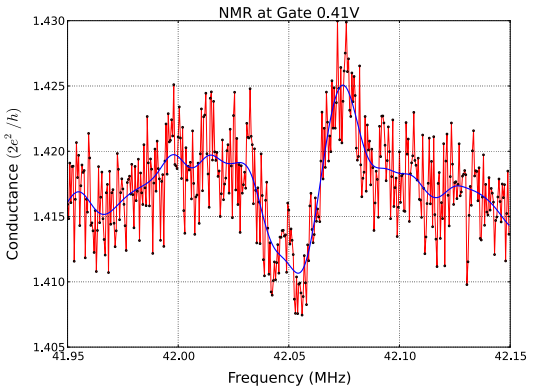

(d) RDNMR signal at $-0.41V$. The NMR has the effect of reducing the conductance here.

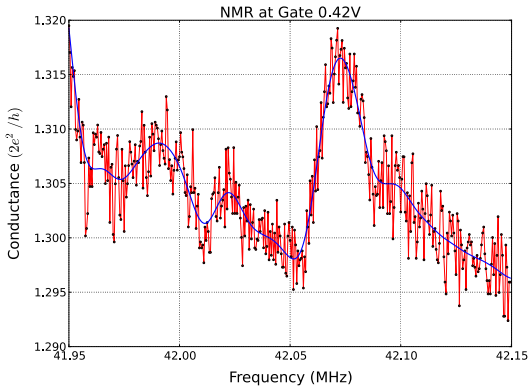

(e) RDNMR signal at $-0.42V$. The NMR has the effect of increasing the conductance

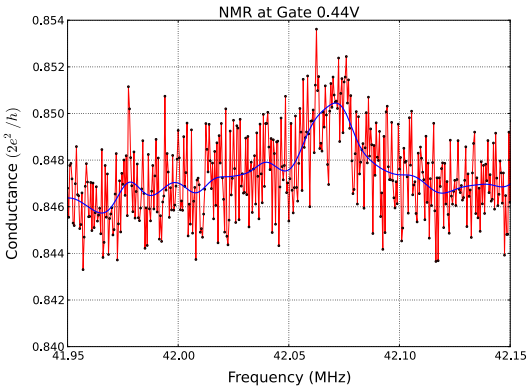

(f) RDNMR signal at $-0.44V$. The NMR has the effect of increasing the conductance

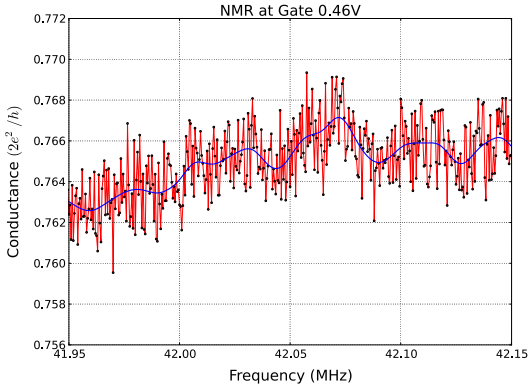

(g) RDNMR signal at $-0.46V$. There is no visible signal

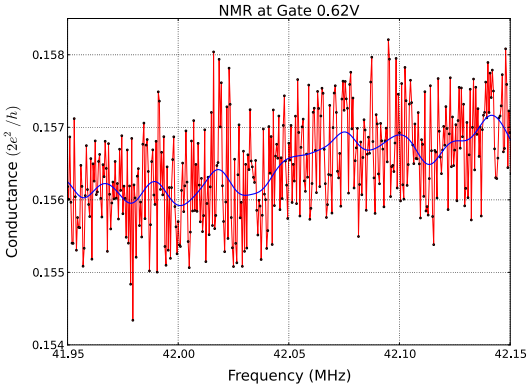

(h) RDNMR signal at $-0.62V$. A weak NMR signal appears. It is positive first, then negative and wider than the previous signals. The signal appears very weak due to high noise levels, but repeated runs verified its existence.

As the wire conductance is adjusted through the first plateau, the NMR signal is observed to begin as solely a reduction in conductance. Closer to the plateau however, it begins as a negative response and follows with an increase in conductance. The signal appears to vanish within the flatter part of the plateau but reappears at $-0.62V$ on the lower edge. The signal here is small, but this is also partly due to decreased conductivity and increased noise. It appears to be entirely positive on the lower edge and to have slightly increased in frequency. This is consistent with the observations closest to the plateau's upper edge as seen in figures 4.3.4e and 4.3.4f. These signals show the initial negative

part of the signal vanishing laving only the following positive signal and the frequency of the signal shifting up. It appears that as the wire is transitioning the single-mode state, the effect of randomizing the nuclear spins is exclusively increasing the conductance. The reason for this is unclear, but it suggests that the negative signal is related to one of the spin species, which vanishes as we transition to the first plateau, while the positive signal is related to the remaining species.

The results are now compared to previous results found by Keane *et al* [3] and Cory Dean [4] in the 2DEG. In the former study, they observed the NMR response in electron-based QPCs to be entirely negative. This is in contrast to our devices which exhibit the positive signal as well. Conversely, in the study of the bulk 2DEG a line shape similar to that observed here was found. Dean observed that the line shape was highly dependent on the magnetic field and filling fraction. For example at $8.2T$, a exclusively positive signal was observed while at $7.6T$ a negative, then positive signal was observed. This is strikingly similar to the transition we observed, suggesting an analogy between the mode number of our quantum wire and the filling fraction in quantum hall states. Additionally we note that in the transition of the line shape in the quantum hall states occurred as the state was moved close to the $\nu = 1$ filling fraction. This is again suggestive of the presence of spin species determining the line shape. Since the line shape is highly dependent on the field, the discrepancies between Keane's results and ours are likely the result of a slightly different field.

The width and location of the features can also be considered. While the accepted value of $\gamma_{^{75}As} = 7.3150\,MHz/T$[5], it was found in [4] to be $7.2653MHz/T$ and in [3] it is reported as $7.26\,MhZ/T$. Our measurement suggests a value of $\gamma_{^{75}As} = 42.07\,MHz/5.8\,T = 7.25\,MHz/T$ which is in close agreement with both sources.

The average peak width in our data is approximately $40\,kHz$. In the work of Keane et al[3], they found the width to be a bit wider, on the order of $60kHz$ while Dean[4] found a line width of approximately $40\,kHz$. While in the former source the width of the features is notably wider, judging widths is a inexact science and the results all appear to be in agreement, particularly when the variation in line shape is considered. Finally, Keane found the strength of the signal to be on the order of 1% of the conductance. This is similar to our data, which shows the NMR signal to be less than 1.5%.

The dependence of the signal on power was also observed. It was found that it was strongest at low powers while high powers eliminated it entirely. The gate was set to $-0.6\,V$ at the lower edge of the plateau.

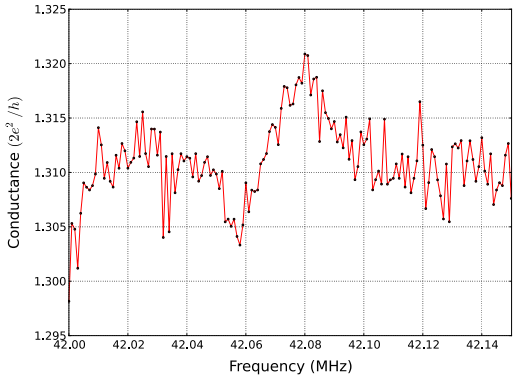

(i) NMR signal at -19dB

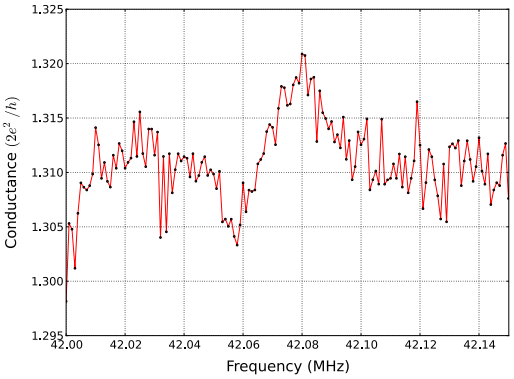

(j) NMR signal at -18dB

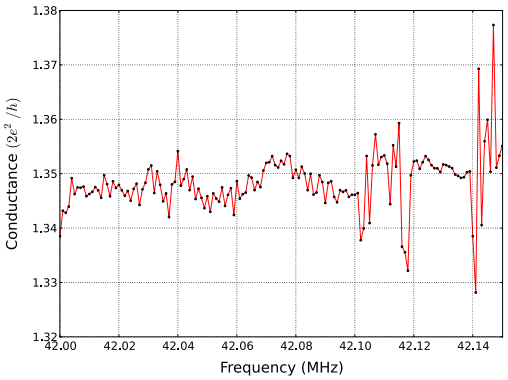

(k) NMR signal at -17dB

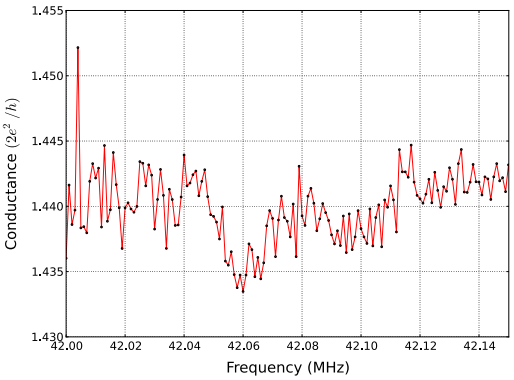

(l) NMR signal at -14dB

As seen in the plots, the signal was present at $-19\,dB$ and $-18\,dB$ but disappeared at powers larger than these. Thus the rest of the NMR data was taken at the best power, $-18\,dB$.

The RDNMR response indicates that the nuclear-spin and electron interaction does in fact exist in these devices and that it indeed affects the conductance. It is hoped that further study with a cleaner sample could provide more information to the response. Additionally, these results pave the way for the use of radiation at the Lamour frequency to effectively randomize the spin in a quantum wire. In the event that conduction states corresponding to predictions of nuclear spin ordering are observed, this RDNMR technique would provide a simply way to disrupt the ordering and verify the states existence.

References

[1] Bernd Braunecker, Pascal Simon, and Daniel Loss. "Nuclear magnetism and electron order in interacting one-dimensional conductors". In: *Physical Review B* 80.16 (Oct. 2009), pp. 1–28. ISSN: 1098-0121. DOI: 10.1103/PhysRevB.80.165119. URL: http://link.aps.org/doi/10.1103/PhysRevB.80.165119.

[2] C.R. Dean, B.a. Piot, L.N. Pfeiffer, K.W. West, and G. Gervais. "Resistively detected NMR in quantum Hall states: Investigation of the anomalous line shape near". In: *Physica E: Low-dimensional Systems and Nanostructures* 40.5 (Mar. 2008), pp. 990–994. ISSN: 13869477. DOI: 10.1016/j.physe.2007.08.101. URL: http://linkinghub.elsevier.com/retrieve/pii/S1386947707003001.

[3] Z K Keane, M C Godfrey, J C H Chen, S Fricke, O Klochan, A M Burke, A P Micolich, H E Beere, D A Ritchie, K V Trunov, D Reuter, A D Wieck, and A R Hamilton. "Resistively detected nuclear magnetic resonance in n- and p-type GaAs quantum point contacts." In: *Nano letters* 11.8 (Aug. 2011), pp. 3147–50. ISSN: 1530-6992. DOI: 10.1021/nl201211d. URL: http://www.ncbi.nlm.nih.gov/pubmed/21714512.

[4] Cory R Dean. "A Study of the Fractional Quantum Hall Energy Gap at Half Filling". PhD thesis. 2008.

[5] David R. Lide. "NUCLEAR SPINS, MOMENTS, AND OTHER DATA RELATED TO NMR SPECTROSCOPY". In: *CRC Handbook of Chemistry and Physics*. 2013, pp. 38–40.

Chapter 5

Conclusion

A number of quantum wire samples were studied at low temperature, in hopes of observing new quantum states of matter. The quantum wires operated as expected, showing quantized conductance plateaus at temperatures lower than 300 mk. The expected half-plateau however, failed to be observed, likely due to an electron temperature higher than the bulk. Several solutions were attempted to achieve lower electron temperatures, and ultimately, it was determined that portable low temperature filters were designed. The filters were constructed and characterized, showing promising filtering characteristics and the hope that lower electron temperatures could be achieved. Unfortunately, a degradation in the quality of the samples meant even filtered samples no longer displayed clear quantized conductance. It was unlikely that we could observe delicate new quantum states in a non-clean electrostatic environment so we decided to pursue the study of resistively detected NMR, as both a proof of concept and a measurement to provide information about the nuclear-spin interaction. These experiments were successful, with the quantum wire showing RDNMR signals at the expected location.

5.1 Future Work

The techniques developed and used in these experiments are expected to be useful in future work. With the experimental infrastructure in place, new quantum wires can be studied at low temperature very easily and could display the sought after state described by Braunecker *et al*[1]. The RDNMR technique used here could be useful in the detection of this state as proven way to disrupt nuclear spin ordering. Additionally, further RDNMR

on cleaner samples could provide useful information about the nuclear spin behavior in GaAs quantum wires.

Some specific steps that could be taken to follow up on these experiments is the measurement of a new batch of quantum wire samples. Rather than repeated measurements in multiple fridges which have been observed to degrade performance, a sample should be immediately placed in the dilution fridge with filtering. While not all wires are likely to give good results due to imperfections beyond our control, this gives the best chance of observing at least one clean state which could definitively show new physics. The use of the custom sample holders in particular, as well as the NMR coils make it possible to do excellent measurements in the first attempt, provided a suitable sample is found. Beyond the discovery of the spin-ordered state, the NMR response could be better characterized. While the relatively poor SNR was an issue with this data, better samples and repeated measurements could do a lot to achieve a cleaner signal. This would allow detailed probing of the nuclear spins, including relaxation time measurements.

In the longer term, future device designs could incorporate variable-length wires, wire networks or superconducting junctions in pursuit of the Majorana. It is hoped that this work will lead to some of these experiments in the future, and some fascinating new results.

References

[1] Bernd Braunecker, Pascal Simon, and Daniel Loss. "Nuclear magnetism and electron order in interacting one-dimensional conductors". In: *Physical Review B* 80.16 (Oct. 2009), pp. 1–28. ISSN: 1098-0121. DOI: 10.1103/PhysRevB.80.165119. URL: http://link.aps.org/doi/10.1103/PhysRevB.80.165119.